ELECTROCHEMICAL DETECTION OF METALS AT GOLD ULTRAMICROELECTRODES WITH APPLICATION TO CAPILLARY ELECTROPHORESIS

A thesis submitted to the
College of Graduate Studies and Research
in partial fulfillment of the requirements
for the degree of Master of Science
in the Department of Chemistry
University of Saskatchewan, Saskatoon

LANA JOHANNE NELSON

PERMISSION TO USE

As the author of this thesis, I agree that the Libraries of the University of Saskatchewan may make this thesis freely available for inspection. Furthermore, I agree that permission for copying of this thesis in any manner, in whole or in part, for scholarly purposes may be granted by the professor who supervised my thesis work, or, in his absence, by the Head of the Department or the Dean of the College in which this thesis work was done. It is understood that any copying or publication or use of this thesis or parts thereof for financial gain shall not be allowed without my written permission. It is also understood that due recognition shall be given to me and to the University of Saskatchewan in any scholarly use of any material in this thesis.

Requests for permission to copy or to make use of material in this thesis, in whole or in part, should be addressed to:

Head of the Department of Chemistry

Department of Chemistry, University of Saskatchewan
110 Science Place
Saskatoon, SK S7N 5C9
Canada

Tel: (306) 966-4655 Fax: (306) 966-4730

ABSTRACT

Electrochemical detection of metals can be done at polycrystalline gold ultramicroelectrodes using repetitive cyclic voltammetry (RCV), a detection method sharing some similarities with anodic stripping voltammetry (ASV). Each cycle of the potential waveform for RCV involves application of a negative preconcentration potential (for 50 to 300 ms) followed by a cyclic voltammetry (CV) scan at 20 to 1000 V/s. The response due to the metals is evident at potentials negative of the region for oxide formation in the resulting CVs. Metals are deposited at the Au surface by underpotential deposition (UPD) processes. Any metal that can be analyzed by RCV could potentially be quantified using UPD-ASV at Au (rather than by ASV at Hg).

The UPD kinetics of Pb and Cu at polycrystalline Au were examined by setting kinetic parameters (rate constant, symmetry factor, and electrosorption valency) within a simulation program used to generate simulated CVs. Reasonably good agreement between experimental and simulated CVs was possible using the simulation, with the same kinetic parameters used to generate simulated CVs to match experimental CVs over a range of sweep rates for each system. Using this method, the following rate constants (k_s) were estimated: for UPD of Cu in H_2SO_4 and $HClO_4$, $k_s \sim 3.6\times10^4$ s^{-1} and 1.1×10^4 s^{-1}, respectively, and for UPD of Pb in H_2SO_4, $k_s \sim 4.0\times10^5$ s^{-1}.

Repetitive cyclic voltammetry was applied to the detection of metals separated by capillary electrophoresis. Separation of Tl^+, Cd^{2+}, Cu^{2+}, Pb^{2+}, Zn^{2+}, Ni^{2+}, Co^{2+} and Mn^{2+} was demonstrated in 0.01 mol/L acetic acid and 0.01 mol/L ammonium acetate (pH ~ 4.6) using RCV. While stacking is commonly exploited for sensitivity enhancement during injection, it was shown that detection-end stacking is also useful.

A novel technique named electrophoretic extraction (EE) was developed for analysis of particle-containing solutions (e.g. soil extracts or other colloidal suspensions). EE involves application of backpressure during CE to prevent particles from entering the separation capillary: the applied pressure is regulated so analyte ions enter the capillary and migrate to the detector, whereas other particles are prevented from entering the capillary. The feasibility of this approach was demonstrated.

ACKNOWLEDGEMENTS

I would first like to acknowledge my supervisor, Dr. A. S. Baranski, for his unstinting encouragement, patience and humour throughout the inordinately long period of time that this thesis has taken, as well as his assistance with the technical and scientific aspects of this work. Thank you.

Thanks to the members of the advisory committee: Dr. Boison (Canadian Food Inspection Agency), Dr. Cassidy (Department of Chemistry), Dr. Huang (Department of Soil Science) and Dr. Waltz (Department of Chemistry) for the time expended on committee meetings. Dr. Cassidy was, besides being a committee member, an invaluable source of advice regarding capillary electrophoresis. Finally, thanks to Dr. Burgess (Chemistry) and Dr. Siciliano (Soil Science) for their comments and suggestions that have been incorporated into this thesis.

My former labmates Parviz Norouzi, Huaiguang (Lucy) Yang, Piotr Diakowski and Aliaksei Boika will be remembered for innumerable odd conversations in the electrochemistry lab, and are thanked for their support. Thanks also to colleagues Irina Zaharia, Samuel Gyepi-Garbrah and Shatha Qaqish for much-needed encouragement.

The financial assistance of the University of Saskatchewan in the form of a Graduate Teaching Fellowship is gratefully acknowledged.

DEDICATION

This thesis is dedicated to my husband, Russ, who supported me in this work even as it dragged on and took me away from him numerous times…

…and to my parents, Les and Delores Nelson, who not only financed my undergraduate education, but graciously allowed me to stay at home while finishing this degree.

Ecclesiastes 2:11

TABLE OF CONTENTS

PERMISSION TO USE i
ABSTRACT ii
ACKNOWLEDGEMENTS iii
DEDICATION iv
TABLE OF CONTENTS v
LIST OF TABLES viii
LIST OF FIGURES ix
LIST OF ABBREVIATIONS xii
PREFACE 1
CHAPTER 1: INTRODUCTION 4
1.1 ELECTROCHEMICAL DETECTION 4
1.1.1 Ultramicroelectrodes (UMEs) 4
1.1.2 Anodic Stripping Voltammetry 5
1.1.3 High-Speed Repetitive Cyclic Voltammetry 7
1.2 UNDERPOTENTIAL DEPOSITION 10
1.2.1 Underpotential Deposition Processes 10
1.2.2 Kinetics of Underpotential Deposition of Metals 12
1.3 CAPILLARY ELECTROPHORESIS 12
1.3.1 Principles of CE Separations 13
1.3.2 Sample Injection and Preconcentration 17
1.3.3 Detection in Capillary Electrophoresis 19
1.3.4 Capillary Electrophoresis/Electrochemical Detection (CE-ECD) 20
1.3.4.1 Practical Considerations 23
1.3.4.1.1 Electrode Positioning 23
1.3.4.1.2 Off-Column vs. End-Column Detection 24
1.3.5 CE-ECD of Metals 27
CHAPTER 2: EXPERIMENTAL 30
2.1 FOREWORD 30
2.2 REAGENTS 30
2.3 DATA ACQUISITION 30

2.3.1 Electrochemical Data Acquisition System 30
2.3.2 Software for Data Acquisition and Analysis 32
2.3.3 Cyclic Voltammetry / Fast Cyclic Voltammetry 32
2.3.4 Repetitive Cyclic Voltammetry / Fast Repetitive Cyclic Voltammetry 33
2.3.5 Repetitive Cyclic Voltammetry Stripping Analysis 34
2.4 FABRICATION OF ELECTRODES 34
2.4.1 Working Electrodes 34
2.4.2 Reference and Auxiliary Electrodes 35
2.5 FLOW-INJECTION ANALYSIS 36
2.5.1 Setup for Flow-Injection Analysis 36
2.5.2 Electrode Stability Experiments 36
2.6 KINETICS 39
2.6.1 Electrodes for Kinetics Measurements 39
2.6.2 Kinetics Experiments 39
2.6.2.1 Simulation for Determination of Kinetic Parameters 40
2.7 CAPILLARY ELECTROPHORESIS EXPERIMENTS 40
2.7.1 General Considerations 40
2.7.2 Control of High Voltage Power Supply 41
2.7.3 Injection 42
2.7.4 Detection Cell for CE / ECD 42
2.7.5 Electrode Positioning 44
2.7.6 Determination of Offset Potential 44
2.7.7 Detection for Capillary Electrophoresis Experiments 45
2.8 ELECTROPHORETIC EXTRACTION / PRECONCENTRATION 45
CHAPTER 3: INVESTIGATION AND OPTIMIZATION OF THE RCV DETECTION OF METALS AT GOLD ELECTRODES 48
3.1 FORWARD 48
3.2 ELECTRODE STABILITY 49
3.2.1 Underpotential Deposition of Cu at Au 49
3.2.2 Stability of Electrode Response under Scanning Conditions 49
3.2.3 Electrode Stability with and without Conditioning 60
3.3 SCOPE OF REPETITIVE CYCLIC VOLTAMMETRY DETECTION OF METALS AT AU 64

3.3.1 Detection of Various Metals at Gold using RCV 64
3.3.2 Calibration Curves and Detection Limits Metals at Au using Flow-Injection Analysis (FIA) and RCV Detection 67
3.4 UNDERPOTENTIAL DEPOSITION – ANODIC STRIPPING VOLTAMMETRY 74
3.4.1 Gold as a Substrate for Anodic Stripping Voltammetry 74
3.4.2 Effect of Sweep Rate on Determination of Metals at Gold by ASV 77
3.5 CONCLUSIONS 81
CHAPTER 4: KINETICS OF UPD PROCESSES 82
4.1 FORWARD 82
4.2 DETERMINATION OF THE KINETICS OF UPD OF METALS AT POLYCRYSTALLINE GOLD ELECTRODES 83
4.2.1 Treatment of Data and Experimental Considerations 83
4.2.2 Variation in Peak Separation with Sweep Rate 85
4.2.3 Summary of Kinetic Parameters for the UPD of Cu and Pb at Au 89
4.2.4 Discrepancies in Electrosorption Valency 91
4.3 CONCLUSION 92
CHAPTER 5: CAPILLARY ELECTROPHORESIS & ELECTROPHORETIC EXTRACTION 94
5.1 FORWARD 94
5.2 CAPILLARY ELECTROPHORESIS EXPERIMENTS 95
5.2.1 CE of Metals with Detection by RCV 95
5.2.2 Enhancement of Sensitivity in CE 98
5.2.2.1 Detection-End Stacking 98
5.3 ELECTROPHORETIC EXTRACTION 102
5.3.1 Initial Experimentation 104
5.3.2 Electrophoretic Extraction with Preconcentration by Stacking 105
5.3.3 Possible Modifications of Electrophoretic Extraction 113
5.4 CONCLUSIONS 115
CHAPTER 6: CONCLUSIONS AND FUTURE WORK 117
6.1 SUMMARY 117
6.2 FUTURE WORK 119
APPENDIX A: CONTROL OF HIGH VOLTAGE POWER SUPPLY 121
REFERENCES 125

LIST OF TABLES

3.1 Comparision of results for repetitive cyclic voltammetry with and without electrode conditioning. 63

4.1 Summary of kinetic parameters for various metal/electrolyte combinations obtained from matching of experimental curves with simulated data. 90

LIST OF FIGURES

CHAPTER 1

1.1 An example of the potential waveform used for repetitive cyclic detection of metals. 8

CHAPTER 2

2.1 Electrochemical data acquisition system. 31

2.2 Cell used for flow-injection analysis experiments. 37

2.3 Evaluation of peak height and peak area as a function of injection time for flow-injection cell used in experiments. 38

2.4 Schematic of detection cell for capillary electrophoresis. 43

2.5 Electrophoretic extraction/preconcentration. 47

CHAPTER 3

3.1 Underpotential deposition of Cu at Au: cyclic voltammograms of Cu^{2+} [5×10^{-4} mol/L Cu^{2+} in 0.1 mol/L H_2SO_4] at a 25-μm Au electrode. 50

3.2 Variation in area of Cu UPD peak with vertex potential. 51

3.3 Individual cyclic voltammograms from a repetitive cyclic voltammetry experiment, showing possible potential ranges for metal detection. 52

3.4 Changes in the Cu UPD peak area with time for electrodes subjected to scanning under different electrolyte/potential waveform conditions. 54

3.5 Changes in the peak area of the Cu UPD peak and capacitance with time for a 25-μm Au electrode in 0.5 mol/L sodium borate solution. 57

3.6 Change in double-layer capacitance with time for a 25-μm Au electrode in sulfuric acid and sodium borate. 59

3.7 Potential waveforms for repetitive cyclic voltammetry with and without electrode conditioning. 61

3.8 Repeated injections of 10^{-5} mol/L Pb^{2+} under flow injection conditions in 1 mol/L CH_3COOH. 62

3.9 Results for the detection of metals by RCV using flow-injection analysis in 1 mol/L CH_3COOH at Au. A: 4×10^{-5} mol/L Cu^{2+}; B: 6×10^{-6} mol/L Ni^{2+}; C: 5×10^{-5} mol/L Zn^{2+}; D: 1×10^{-5} mol/L Pb^{2+}. 65

3.10 Results for the detection of metals by RCV using flow-injection analysis in 0.5 mol/L CH_3COOH and 0.5 mol/L CH_3COONa at Au. A: 5×10^{-5} mol/L Co^{2+}; B: 1.5×10^{-4} mol/L Co^{2+}; C: 7×10^{-5} mol/L Mn^{2+}; D: 1×10^{-4} mol/L Ni^{2+}. 66

3.11 Results for detection of AsO_2^- by RCV (under flow-injection conditions).....68

3.12 Calibration curves for Ni^{2+} in 1 mol/L CH_3COOH at Au showing two different integration regions. 69

3.13 Calibration curves for (A–E): Mn^{2+}, Co^{2+}, Pb^{2+}, Cu^{2+} and AsO_2^- at Au. 72

3.14 A single continuous cyclic voltammetry stripping experiment for 5×10^{-8} mol/L Pb^{2+} in 1 mol/L CH_3COOH at an Au UME (25 μm diameter). 75

3.15 Calibration curve for Pb^{2+} in 1 M CH_3COOH under flow-injection conditions, using continuous cyclic voltammetry stripping detection at an Au ultramicroelectrode. 76

3.16 Variation of stripping peaks with sweep rate: a series of cyclic voltammograms at a 25-μm Au electrode of 5×10^{-7} mol/L Pb^{2+},Cu^{2+} and Cd^{2+} in 1 mol/L CH_3COOH. 78

3.17 Negative log of response (peak current, μA) vs. log of sweep rate for stripping experiments of 2×10^{-7} mol/L Pb^{2+} in 1 mol/L CH_3COOH. 79

3.18 Continuous cyclic voltammetry stripping experiments for 2×10^{-7} mol/L Pb^{2+} in 1 mol/L CH_3COOH at Au. 80

CHAPTER 4

4.1 Removal of noise in cyclic voltammograms used for the determination of kinetics. 84

4.2 Fit between experimental (background-subtracted) and simulated cyclic voltammograms. 86

4.3 Cyclic voltammograms of 2×10^{-5} mol/L Cd^{2+} in 1 M $HClO_4$ with different deposition potentials. 87

4.4 Comparison of experimental and simulated data for the variation of peak separation with log of sweep rate for different surface coverages. 88

CHAPTER 5

5.1 Electropherogram of 2×10^{-5} mol/L Pb^{2+}, Cu^{2+} and Cd^{2+} in CH_3COOH. 96

5.2 Electropherogram resulting from the separation of Tl^+, Cd^{2+}, Cu^{2+}, Pb^{2+}, Zn^{2+}, Ni^{2+}, Mn^{2+} and Co^{2+} in 0.01 mol/L acetic acid and 0.01 mol/L ammonium acetate (pH ~ 4.6). 97

5.3 Detection-end stacking: a series of experiments showing the enhanced response associated with increasing the concentration of background electrolyte of the solution at the detection end of the capillary. 99

5.4 Peak height vs. concentration of H_3PO_4 and KH_2PO_4 at detection end for Tl^+, Ni^{2+}, and Cd^{2+} (inset shows peak area). 100

5.5 Peak area vs. the square root of the total concentration of H_3PO_4 and KH_2PO_4 at the detection end of the capillary.....101

5.6 Reciprocal migration time of 1×10^{-5} mol/L Pb^{2+} injected from 1 mol/L CH_3COOH as a function of applied voltage for various capillary internal diameters. 106

5.7 The negative intercept of the linear relationships in Figure 5.6, plotted as a function of the square of the capillary internal radius. 107

5.8 Electrophoretic extraction experiment (no particles), with detection of Pb^{2+} using repetitive cyclic voltammetry at a 25 μm Au electrode (sweep rate 200 V/s). 108

5.9 Electrophoretic extraction experiment, with alumina particles (2×10^{-6} mol/L Pb^{2+}). 109

5.10 Plot of the reciprocal response versus square root of concentration of CH_3COOH. 112

5.11 Schematic of electrophoretic extraction and injection using a T-junction. 114

APPENDIX A

A.1 The layout of the pins of the Spellman CZE1000R high-voltage power supply. 123

A.2 A diagram of the interface between the high voltage power supply and the computer. 123

A.3 The graphical user interface for MicroVoltammetry and control of the high-voltage power supply. 124

LIST OF ABBREVIATIONS

API	atmospheric pressure ionization
ASV	anodic stripping voltammetry
BGE	background electrolyte
CE	capillary electrophoresis
CEC	capillary electrochromatography
CE/ECD	capillary electrophoresis with electrochemical detection
CGE	capillary gel electrophoresis
CL	chemiluminescence
CMC	critical micelle concentration
CZE	capillary zone electrophoresis
DNA	deoxyribonucleic acid
EC	electrochemical
ECD	electrochemical detection
EMD	electromigration dispersion
ESI	electrospray ionization
FCV	fast cyclic voltammetry
GC	gas chromatography
HIBA	α-hydroxyisobutyric acid
HMDE	hanging mercury drop electrode
HPLC	high-performance liquid chromatography
ID	internal diameter
iHp	inner Helmholtz plane
LIF	laser-induced fluorescence
MEKC (MECC)	micellar electrokinetic chromatography (micellar electrokinetic capillary chromatography)
MS	mass spectrometry
oHp	outer Helmholtz plane
PAD	pulsed amperometric detection
RCV	repetitive cyclic voltammetry
SASV	subtractive anodic stripping voltammetry
SWASV	square-wave anodic stripping voltammetry
UME; UMEs	ultramicroelectrode; ultramicroelectrodes
UPD	underpotential deposition
UPD/ASV; UPD/SV	underpotential deposition/anodic stripping voltammetry; underpotential deposition/stripping voltammetry
μTAS	micro total analysis system

PREFACE

The necessity of robust analytical methods for the quantitative determination of metals in environmental samples is obvious. Metals are ubiquitous in the environment, and play an important role in industry. Anthropogenic activities commonly release metals into the environment: a well-known example is the use of tetraethyl lead in gasoline [1]. Since many metals have demonstrable toxic effects on plants and higher life forms, careful monitoring and minimization of exposure to these metals is critical to maintaining a healthy environment.

While this is not a dissertation on metal toxicity, a few brief comments on the toxicity of certain metals (i.e. those appearing in this work) are appropriate here. Acute exposure to high amounts of metals is obviously detrimental to health and can be fatal, but there are also more insidious chronic effects (which may vary with route of exposure). Lead is notorious as a neurotoxin. The exposure of children to lead is of particular concern [2], resulting in deleterious neurological and developmental effects [3]. Arsenic is a known carcinogen; cadmium is another carcinogen, readily taken up by plants; and nickel is thought to be a respiratory tract carcinogen [3]. Thallium is highly toxic [3] although not overly common, and silver also has known effects [3]. Mercury – the traditional substrate for stripping analysis – has adverse effects on the central nervous system [3]. Other metals are essential to the body in small amounts, but toxic above certain levels. These include cobalt, copper, manganese and zinc [3].

Historically, electrochemical techniques have played a prominent role in the analysis of metals. Indeed, the need for sensitive determination of various metals has been the impetus behind the development of several electrochemically-based analytical techniques, particularly anodic stripping voltammetry (ASV). While there are numerous other methods suitable for the analysis of metals – including, for example, various forms of spectrophotometry, atomic absorption spectroscopy, atomic emission spectroscopy;

inductively coupled plasma atomic emission spectroscopy, inductively coupled plasma atomic emission–mass spectroscopy, neutron activation analysis and X-ray fluorescence spectroscopy [4-6] – electrochemical methods are perhaps underutilized in this context. The advantages of electrochemical methods in metal analysis include relatively inexpensive instrumentation, and the possibility of investigation of metal speciation and differentiation between ionic and bound forms of metals [7] – important because the degree of toxicity of a metal can vary significantly depending on its form. The use of ultramicroelectrodes of the dimensions of micrometers and even nanometers in combination with current positioning technologies allow for many interesting possibilities of generating spatially-resolved data related to, for instance, uptake of heavy metals by plant roots [8].

While there are many instances where electrochemical methods may be adapted for a particular analysis, the simultaneous determination of several metals may be impossible due to overlap of stripping peaks in the potential domain. The combination of a separation technique with electrochemical detection overcomes this limitation. Capillary electrophoresis (CE) is ideally suited to the separation of metals in solution. Previous work [9, 10] has demonstrated the feasibility of using capillary electrophoresis with electrochemical detection (CE/ECD) at gold ultramicroelectrodes for the determination of metals. This research further focuses on the use of CE/ECD for the analysis of various metals (as aqueous ions) – particularly Co, Cu, Zn, Ni, Cd, Tl, Mn and Pb. The end goal is the trace analysis of these metals in environmental samples, such as water samples and aqueous soil extracts. Several rather unusual techniques that would enable analysis or sampling of metals directly from slurries (particle-containing solutions) are also investigated.

The topics covered in the introduction may at first glance appear incongruous: however, all are related to this research. All work was done using ultramicroelectrodes (UMEs). The major electrochemical techniques used in this work (repetitive cyclic voltammetry and anodic stripping voltammetry) are described. Fundamental studies have been conducted regarding the underlying principles on which this particular method of electrochemical detection of metals is based, necessitating the discussion of underpotential deposition (UPD) processes and electrode kinetics. Finally, a summary of

the principles behind capillary electrophoresis with particular emphasis on detection and on-line sample preconcentration is also included in the introduction.

CHAPTER 1: INTRODUCTION

1.1 ELECTROCHEMICAL DETECTION

1.1.1 Ultramicroelectrodes (UMEs)

The term ultramicroelectrode (UME) is generally reserved for an electrode with at least one dimension that is extremely small [11], usually in the order of micrometers. Several unique properties of ultramicroelectrodes make them suitable for experiments not possible at larger electrodes. These properties include enhanced mass transport, decreased ohmic drop [11] and low time constants in comparison with macroelectrodes.

Due to the reduction in time constant and decreased effects of solution resistance with the use of ultramicroelectrodes, scan rates in excess of 10^5 Vs^{-1} [11-13] can be attained. This allows for the determination of the kinetics of electron transfer reactions that would be difficult to measure otherwise: for example, heterogeneous rate constants of the order of 10^{-2} ms^{-1} can be determined at UMEs with diameters from 0.05–5 μm [11]. In this work, the high scan rates accessible to UMEs are exploited for the sensitive detection of metals (Ch 3) and the determination of the kinetics of underpotential deposition (UPD) of metals on polycrystalline gold (Ch 4).

Despite their impressive credentials, a few pitfalls associated with the use of ultramicroelectrodes also should be noted. The enhanced mass transport of UMEs results in increased surface contamination [11] due to absorption of impurities at the electrode surface. Currents measured at ultramicroelectrodes are much smaller than at conventional electrodes and therefore more stringent demands are placed on instrumentation, both in terms of measurement of these small currents and the reduction of noise in the system. Finally, as the size is decreased, the difficulties associated with the process of electrode fabrication increase substantially. Ultramicroelectrodes with defects can exhibit odd behaviour [14], and therefore care must be taken to verify the quality of ultramicroelectrodes to be used in experiments (Section 2.4.1).

1.1.2 Anodic Stripping Voltammetry

Anodic stripping voltammetry (ASV) is the best-known variant of stripping analysis. In the most general sense, stripping analysis involves the accumulation of the analyte of interest on the electrode surface followed by voltammetric determination of the preconcentrated analyte. In anodic stripping voltammetry, metals are deposited by application of negative potential to an electrode (generally Hg) for a controlled period of time, followed by a stripping step, during which the deposited metal is stripped from the electrode. Stripping voltammetry of preadsorbed analytes is one of the most sensitive electrochemical techniques [15] with detection limits easily reaching 10^{-9} mol/L and lower.

The use of stripping voltammetry is closely associated with the development of the hanging mercury drop electrode (HMDE) [16]. The majority of measurements involving ASV are carried out at mercury electrodes, since the reproducibility of ASV experiments carried out on Hg is higher than for solid electrodes [16] and due to the comparative ease of rejuvenation of the electrode surface. The potential window accessible using Hg electrodes is also large due to the high overpotential of hydrogen evolution at Hg. In ASV carried out on Hg, metals are preconcentrated by formation of an amalgam with mercury during deposition. However, the preconcentration of metals on solid electrodes is also possible, with deposition occurring in the underpotential deposition region. It has been suggested that ASV on solid electrodes with deposition of metals by UPD during the preconcentration step could result in increased selectivity and a wider range of elements that can be analyzed [17].

Examples of the analytical applications of stripping voltammetry on solid electrodes were relatively sparse until recently. An example is the potentiometric stripping of Pb, Cd and Cu on carbon fiber and gold electrodes in the presence of Hg^{2+} [18]. Now, however, many examples of what is sometimes referred to in the literature as UPD-SV (underpotential deposition-stripping voltammetry) of metals on solid electrodes exist. A recent review of the subject is available [19]. Kirowa-Eisner *et al.* have published a series of papers detailing various studies of anodic stripping voltammetry at solid electrodes, including copper on gold [20]; mercury on gold [21]; lead and cadmium on silver and/or gold [22-24]; and lead, cadmium and thallium on silver-gold alloy

electrodes [25]. The determination of mercury and copper in seawater by SWASV (square-wave anodic stripping voltammetry) on an Au microwire electrode using background subtraction has also been described [26], and ASV on silver was used to determine lead and cadmium at silver in the presence of thallium [27]. There has also been work on a portable electroanalytical system for the stripping voltammetry of metals based on UPD-SV at Au [28], and the use of disorganized monolayer films on Au to prevent surfactant inhibition during detection of Cu [29].

The term subtractive anodic stripping voltammetry (SASV) also appears in the literature, and refers to anodic stripping voltammetry performed with the subtraction of the background current to isolate the signal (Faradaic current) from the (non-Faradaic) charging current. The background curve can be generated in several ways: among the most practical are the generation of a signal in the same solution with zero deposition time, or use of flow-injection analysis (FIA) to switch between background and analyte-containing solutions [30]. However, although initially SASV was used for background subtraction in ASV at Hg electrodes, several papers on stripping voltammetry with underpotential deposition at solid electrodes (from 1999 on) also use this terminology (i.e. SASV – see [20-23, 25, 27, 31-34]). In these cases, the original meaning seems to have been stretched to imply something like the previously discussed UPD-SV, although without conveying information about the deposition technique. The term UPD-SV is preferred in this work, because of the implication of a solid electrode and indication of the physical process exploited for deposition (although this name does not include information about background signal subtraction).

One potential drawback to ASV with preconcentration by underpotential deposition on solid electrodes is that it may not exhibit the high sensitivity typical of ASV at mercury. First, the background current at solid electrodes, including gold, is much greater than the background current at mercury. This can be expected to have a negative effect on the ratio of Faradiac current to background or charging current (i.e. signal-to-noise ratio). Furthermore, at polycrystalline gold, the stripping peaks of the metals will be much broader than at Hg for the same amount of analyte. This is due to the heterogeneity of the adsorption sites occupied by the deposited metal, and is also expected to have a negative effect on the sensitivity, since there is difficulty in

differentiating the signal from the background current at low concentrations. Another observation regarding the application of UPD-ASV to analysis of metals is that the upper limit of the linear range of the calibration curve will be determined by saturation of the adsorption sites during deposition (i.e. the formation of a full monolayer at the gold surface).

It should also be emphasized that UMEs are ideal for use in ASV for several reasons: the high mass transport at UMEs negates the need for forced convection during accumulation of the metals at the electrode. Also, in the case of Hg electrodes, the analyte is concentrated in a very small volume and is stripped completely during the anodic scan [11].

1.1.3 High-Speed Repetitive Cyclic Voltammetry

In the simplest possible form, amperometric detection can be performed with a fixed potential applied to the working electrode of an electrochemical cell. This constant-voltage amperometric detection, while being simple, has drawbacks in terms of the inevitable fouling of the electrode surface, due to the adsorption of impurities on the surface of the electrode. A more refined technique, pulsed amperometric detection (PAD), incorporates anodic and cathodic polarization in the potential waveform to clean and activate the electrode surface before each current measurement. This typically results in improved reproducibility of the electrode response. However, PAD gives little, if any, qualitative information regarding the analytes and has very little selectivity.

Instead of potential pulses, a triangular waveform (as in cyclic voltammetry) can be applied repeatedly, with a complete cyclic voltammogram collected during each cycle (voltammetric detection). This obviously is yet more complex; however, the cyclic voltammograms contain much more information about the analytes, as well as being useful for the purposes of quantification. The detection method primarily used in this work is a voltammetric technique which will be referred to as fast-scan repetitive cyclic voltammetry (RSV).

The potential waveform for repetitive cyclic voltammetry is depicted in Figure 1.1. First, the electrode is held at a negative potential (known as the preelectrolysis potential) in the UPD region to allow for deposition of the metal on the electrode surface. The preelectrolysis potential is applied for a set interval (the preelectrolysis time), which

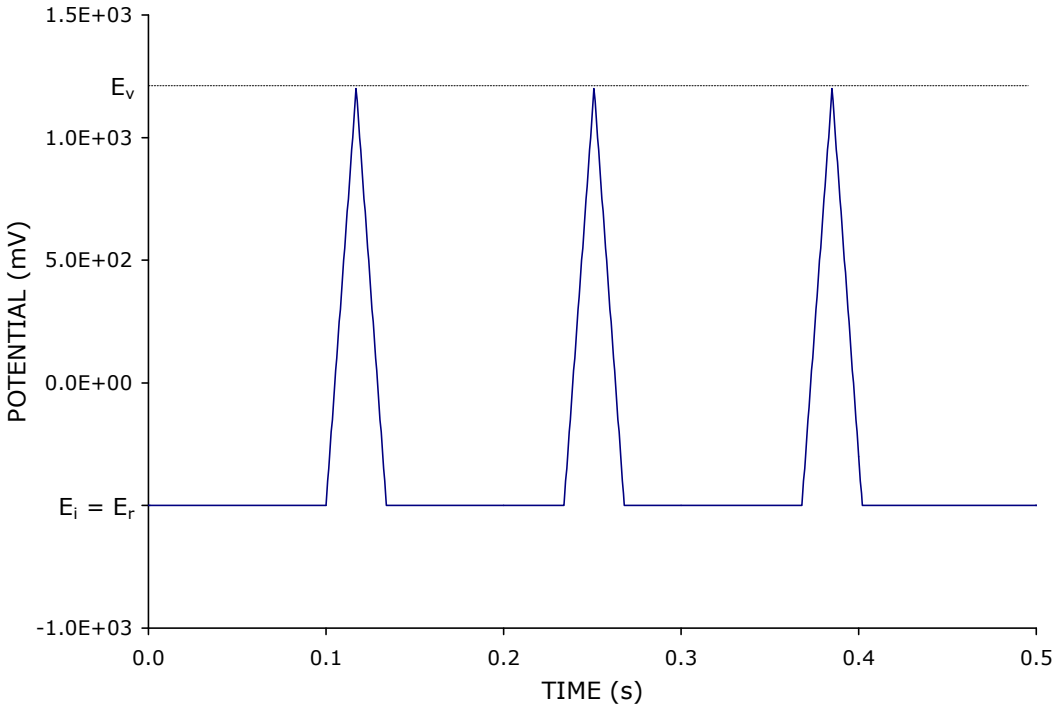

Figure 1.1 An example of the potential waveform used for detection of metals – in this case, the initial potential and the preelectrolysis, or rest, potential, $E_i = E_r =$ −500 mV, the vertex potential E_v = 1200 mV, the preelectrolysis time is 0.1 s and the scan rate is 100 V/s.

typically ranges from 100 to 2000 ms. After this, the electrode potential is scanned from the initial potential (usually the same as the preelectrolysis potential) to the vertex potential and back, with the current monitored during the scan. This cycle (preelectrolysis, followed by scanning) is repeated for the duration of the experiment. With each cycle of the waveform a complete cyclic voltammogram is collected: the response is generated by integration over the potential region where changes due to metal adsorption occur, and plotted as a function of time. Scan rates for RCV are generally in the range of several hundred volts per second.

This technique bears a remarkable resemblance to UPD-SV (Section 1.1.2). The potential waveforms for UPD-SV and RCV both involve a preconcentration step at negative potential, followed by a potential step, during which current is measured as the UPD layer is stripped from the electrode. However, the time scale of one cycle of repetitive cyclic voltammetry is considerably shorter than a typical UPD-SV experiment: for UPD-SV the preconcentration time is typically 60–90 s [19], whereas the preconcentration time for each cycle of repetitive cyclic voltammetry varies from 0.1 to 2 s. Thus (neglecting the possible choice of a different potential waveform for the stripping step of UPD-SV), each cycle of RCV could be construed as a time-compressed UPD-SV experiment at an ultramicroelectrode.

When adapting a technique such as RCV to detection of metals in CE, consideration must be given to the time of exposure of the detection electrode to the analyte band relative to the frequency of the potential waveform: enough data points are needed over the time of elution of the analyte to produce a well-defined peak in the electropherogram. This limits the time available for preconcentration of the metals at the electrode surface and ultimately the sensitivity, and also necessitates the use of relatively high scan rates. However, the use of RCV also has advantages such as the resolution of co-migrating species in the potential domain.

Finally, the high scan rates used (typically 20–1000 V/s) for RCV result in a relatively high background current. Background subtraction, however, is possible and very simple in methods such as flow-injection analysis or capillary electrophoresis, where a background response for the electrolyte solution without analyte is readily obtainable.

1.2 UNDERPOTENTIAL DEPOSITION

1.2.1 Underpotential Deposition Processes

The term underpotential deposition (UPD) refers to the deposition of less than a monolayer of metal onto a foreign metal substrate: this occurs at potentials more positive than the Nernstian potential for bulk deposition (of metal ions on the same metal) [35]. This positive overpotential is the result of the higher bonding energy of the deposited metal with the surface of the substrate than with itself [17].

The process of UPD of a metal on a foreign substrate has been described using the following equation [36]

$$S + M^{z+} + \gamma\ e^- \rightarrow SM_{ads}^{(z-\gamma)+} \tag{1.1}$$

where M is the metal, S is the substrate, γ is the electrosorption valency and z is the charge on the metal ion. The electrosorption valency (γ) is the charge necessary to adsorb the metal ion at constant potential: as such, the value of γ may be anywhere between 0 and the charge on the ion (z) [36]. If γ is equal to z, the ion is obviously completely discharged: however, for UPD the electrosorption valency can be substantially less than the charge on the ion, indicating partial charge transfer from the metal to the electrode.

Equation 1.1 is overly simplistic. Recalling the structure of the double layer, and taking into consideration the possibility of multi-step charge transfer between the adsorbed metal and the electrode, the following scheme could be proposed, as outlined in Equations 1.2 to 1.4:

$$M_{oHp}^{z+} \rightarrow M_{iHp}^{z+} \tag{1.2}$$

$$S + M_{ihp}^{z+} + \gamma_1 e^- \rightarrow SM_{ads}^{(z-\gamma_1)+} \tag{1.3}$$

$$SM_{ads}^{(z-\gamma_1)+} + \gamma_2 e^- \rightarrow SM_{ord}^{(z-\gamma_1-\gamma_2)+} \tag{1.4}$$

In this scheme, charge transfer is preceded by diffusion of the metal ion from the outer Helmholtz plane to the electrode surface (Equation 1.2). This is followed by partial charge transfer between the adsorbed metal and the electrode (1.3). In addition,

rearrangement of the adsorbed metal ions on the electrode surface, with further electron transfer, might occur after adsorption, as in Equation 1.4.

This idea of a multistep underpotential deposition process with initial adsorption of the metal at the electrode, followed by the (slower) complete discharge of the metal is discussed in Reference [37], where the authors found evidence for partial charge transfer in the UPD of Hg^{+}, Tl^{+}, Bi^{3+} and Cu^{2+} at polycrystalline gold electrodes. This scheme implies the existence of two forms of the metal (at equilibrium) on the electrode surface – i.e. partially and completely discharged metal species [37]. In addition, the overall (macroscopic) charge transfer coefficient ($\gamma_1 + \gamma_2$) of the completely discharged alloy deposit may differ from the initial charge transfer coefficient. Other authors, however, have found no evidence of partial charge transfer, including Lipkowski and Shi [38] (for Cu UPD in the presence of bromide, see Section 4.2.4 for further discussion).

The preceding discussion neglects the effects of adsorption of coions or rearrangement of ions in the double layer, both of which may contribute to the observed electrosorption valency. Furthermore, the metal must diffuse to the outer Helmholtz plane from the bulk solution before any reaction occurs. Finally, any metal in solution is a more complicated entity than a bare ion: it will at the very least be solvated[1] and may exist in the form of a complex with one or more of the other species present in solution.

As expected with a surface process, UPD is highly sensitive to the surface structure of the substrate. Thus, the study of UPD is simplified if well-defined single-crystal electrodes are used. Most of the literature actually consists of studies of UPD on single-crystal electrodes, although UPD has occasionally been examined at polycrystalline electrodes [36, 37]. For polycrystalline electrodes, the cyclic voltammograms for deposition and stripping of the metal monolayers show a series of current peaks, corresponding to deposition onto different crystal faces of the substrate [17, 36]. The effect of other species on the UPD process – e.g. the electrolyte [17], and the presence of counterions and/or specifically adsorbed anions [35] – is also strong, which is expected

[1] This is implied in Equation 1.2, since the outer Helmholtz plane is defined using the distance of closest approach between the electrode and a fully solvated ion. Similarly, the definition of the inner Helmholtz plane involves the distance between a desolvated ion and the electrode surface.

given that UPD always involves substitution (of one adsorbed species for another) at the interface.

1.2.2 Kinetics of Underpotential Deposition of Metals

As discussed previously (Section 1.2.1), the systems generally chosen for examining UPD employ single-crystal electrodes as the substrate. The same is true for kinetic studies of UPD, in the sense that it is single-crystal substrates for which the most data is available. However, a further complication is that there is little, if any, data in the literature for the adsorption or interfacial step of UPD (as given in Equation 1.3). Attempts to measure the kinetics of metal UPD have generally focused on the structural rearrangements of adsorbed metals [39, 40] or the overall rate rather than the actual adsorption step, presumably because of the difficulties associated with measurements on the time scale of adsorption (which, as an electron transfer reaction, is expected to be a very fast process).

Experiments attempting to measure the kinetics of UPD – even those involving longer time scales and on single crystal electrodes – are difficult to interpret. For example, the kinetics of the $(\sqrt{3}\times\sqrt{3})R30°$ to (1×1) phase transition of Cu^{2+} on Au(111) is reported to be dependent on the history of the sample [39]. To our knowledge, no determinations of the rate constant associated with the deposition of the metal at the electrode surface have been reported in the literature.

1.3 CAPILLARY ELECTROPHORESIS

Capillary electrophoresis exploits the differences in mobility of charged particles in an electric field to effect a separation. A summary of the historical origins of CE and overview of its subsequent development is available in Reference [41] and will not be discussed here in detail. Jorgenson and Lukacs were the first to use narrow bore fused-silica capillaries (75 μm inner diameter) for the electrophoretic separation of dansyl amino acids, fluorescamine-derivatized dipeptides and fluorescamine derivatives of amines with UV detection in 1981 [42]. The popularization of research in CE was ensured by the high separation efficiencies reported in this same paper (>400 000 theoretical plates) and also to commercial availability of fused-silica capillaries. The enhanced heat dissipation exhibited by these small internal diameter (ID) capillaries

facilitates the use of high potentials for separation [43]: these potentials would not otherwise be accessible, due to Joule heating (see Section 1.3.1), which is more prounounced in larger diameter capillaries.

The advantage of capillary electrophoresis over other separation techniques such as high-performance liquid chromatography (HPLC) and gas chromatography (GC) is the simplicity of the technique and its adaptability for the separation of a wide range of analytes using the same instrument and the same column, simply by choosing the appropriate background electrolyte [44]. CE is applicable to inorganic ions, organic molecules and biomolecules (including peptides and proteins, natural products and nucleic acids) [45] given the proper choice of conditions. In addition, the plug-shaped flow profile – in contrast to the laminar flow profile characteristic of hydrodynamic systems [41] – and minimal diffusion result in very efficient separations [43-45]. The amount of material needed for a separation is small (nL of sample and μL of buffer) [41, 44, 45] compared to other separation techniques. In addition, the waste produced in CE separations is small quantities of mostly aqueous solutions with some organic modifiers – in contrast to HPLC, where larger quantities of organic solvent waste are generated [44]. Finally, CE is amenable to miniaturization: the analysis of a sample from a single cell has been described [46], and many initiatives are focused on producing microfabricated CE systems [45] [lab-on-a-chip (LOC) devices or micro total analysis systems (μTAS)].

1.3.1 Principles of CE Separations

When a constant electric field E is applied to an electrolyte solution, the ions in solution experience a constant force proportional to the charge on each ionic species i and the strength of the electric field. This force is balanced by the frictional, or drag, force exerted by the environment of the ion, and thus all ions will move with a constant velocity, v_i, proportional to the electric field E (as in Equation 1.5).

$$v_i = \mu_{ep,i} E \tag{1.5}$$

The constant $\mu_{ep,i}$ (units of $m^2 V^{-1} s^{-1}$) is the electrophoretic mobility, defined by the following equation for the ionic species i (Equation 1.6):

$$\mu_{ep,i} = \frac{z_i e}{6\pi\eta r_i} \tag{1.6}$$

where z_i is the charge on the i^{th} ion, η is the viscosity, and r_i is the radius of ion i. The ion radius, r_i, is determined by the size and shape of the ion but also includes the solvation shell (i.e. the radius of the hydrodynamic equivalent sphere with the same transport properties as the ion being considered).

The movement of ions in capillary electrophoresis is not only due to the electrophoretic mobility of the ion, but also the bulk flow of the solution, which includes electroosmotic mobility (and hydrodynamic flow, if applicable). Electroosmotic mobility, or electroosmotic flow (EOF), arises as a consequence of the double layer formed at the capillary-electrolyte interface. The fused-silica capillary used for CE separations normally (under aqueous conditions) has an excess of negative charge, resulting from the ionization of the surface functional groups [43]. This negative charge is balanced by the cations present in the inner and outer Helmholtz planes of the double layer. The radial potential created due to this charge separation is known as the zeta potential, ζ, which is given by (Equation 1.7)

$$\zeta = \frac{4\pi\eta\mu_{eo}}{\varepsilon} \tag{1.7}$$

where η is the viscosity and ε the dielectric constant of the solution, and μ_{eo} is the electroosmotic mobility.

A rigorous mathematical treatment can be found in Reference [47]; however, for the purposes of this work it is enough to note one result (Equation 1.8)

$$\mu_{eo} = \frac{\sigma^*}{\kappa\eta} \tag{1.8}$$

where σ^* is the surface charge density and κ^{-1} is the double-layer thickness (see [47]).

The magnitude of the electroosmotic mobility is often large enough that positive and negative ions can be determined in a single CE separation, with detection at the cathode. From Equation 1.8 it is obvious that the electroosmotic mobility is strongly influenced by the extent of ionization at the capillary wall and thus dependant on the pH

of the solution. For acidic solutions, the excess of $H_3O^+_{(aq)}$ available to neutralize the silanol groups present on the capillary wall results in a relatively small EOF.

The actual magnitude of the EOF can be determined experimentally in CE, if needed, by the injection of a neutral marker that generates a detector response. Modification of EOF can be achieved by the use of wall-coated capillaries or inclusion of EOF modifiers in the run buffer. Surfactants added below the critical micelle concentration (CMC) can attenuate, eliminate or reverse the EOF by dynamic coating of the capillary walls [48].

An interesting aspect of the electroosmotic mobility is that the flow profile is flat, or plug-shaped (i.e. not dependent on radial position, except within a very short distance of the capillary wall). This is in contrast to laminar or pressure-driven flow (minimized in most CE separations, but significant in this work – see Section 5.3). The velocity, v_{lam}, of a fluid as a function of the radial position, r, is given by Equation 1.9 below [49].

$$v_{lam} = \frac{(p_1 - p_2)\left(r_c^{\,2} - r^2\right)}{4\eta l} \tag{1.9}$$

In the above equation, the term $(p_1 - p_2)$ is the pressure difference over a length, l of capillary with radius r_c, and η is (again) the viscosity: note that the flow profile across the capillary is parabolic.

The overall mobility of the ion i in an electrophoretic separation can be expressed (Equation 1.10) as the sum of its electrophoretic mobility and the electroosmotic mobility, assuming that hydrodynamic flow is neglected.

$$\mu_i = \mu_{ep,i} + \mu_{eo} \tag{1.10}$$

Joule heat is generated during capillary electrophoresis experiments as a result of the electric current that passes through the background electrolyte. This can have a negative effect on a CE separation in several ways. Since the electrophoretic mobility of an ion is strongly dependent on temperature, if the heat generated by the electric current is not dissipated, the temperature gradient within the capillary will result in a spatial dependence of the electrophoretic mobility of the ions, resulting in the degradation of the separation performance [47]. Furthermore, if the temperature gradients induced by Joule heating are steep enough, density gradients within the capillary can lead to natural

convection [47]. In the extreme case, the heat generated by passage of the separation current can also result in boiling of the background electrolyte solution filling the capillary. Joule heating can be minimized by limiting the current through the separation capillary. An obvious way of accomplishing this is the use of a lower applied separation voltage: however, this increases the length of time required for the separation.

The Rayleigh number (*Ra*, dimensionless) is a parameter that is useful for prediction of whether or not natural convection due to Joule heating (as discussed in the previous paragraph) will be significant [47]. This is defined as

$$Ra = \frac{r_c^{\,4} g}{\eta \alpha}\left(\frac{\Delta \rho}{\Delta r}\right) \tag{1.11}$$

where r_c is the radius of the capillary, g is the acceleration of gravity, α is the thermal diffusivity of the medium, and $\Delta\rho/\Delta r$ is the density change per unit of radial distance due to Joule heating [47]. If *Ra* is much less than one, convective flow is negligibly small. Perhaps the most significant result arising from consideration of Equation 1.11 is that electrophoresis performed in capillaries with small internal diameters allows the use of high electric fields without the negative effects of natural convection as a result of Joule heating.

Several variants or modes of CE exist and are indispensable for certain applications. Separations of neutral compounds are possible using micellar electrokinetic chromatography (MEKC – also often referred to as micellar electrokinetic capillary chromatography, or MECC). In MEKC, the addition of ionic surfactants to the background electrolyte at concentrations above the critical micelle concentration (CMC) results in two phases, an ionic phase and a micellar phase which acts as a sort of pseudostationary phase [43]. Neutral molecules are partitioned inside the micelles to various degrees, spending relatively more or less time in the ionic or "mobile" phase and are thus separated in the applied electric field. MEKC can be regarded as a sort of hybrid between chromatographic and electrophoretic techniques [48]. Another related technique is capillary electrochromatography (CEC), in which analytes are driven through a capillary column packed with a stationary phase by a combination of electroosmotic flow and an applied electric field [48]. Capillary gel electrophoresis (CGE) is a powerful analytical technique for the separation of nucleic acids, employing gel-filled capillaries

[48] (CGE in arrays is used for DNA sequencing [44]). Finally, chiral selectors such as cyclodextrins can be used as buffer additives for the separation of chiral analytes [48].

Despite the promise of CE, the narrow internal diameter of the capillaries used limits the amount of substance that can be introduced onto the capillary, hence the low concentration sensitivity [50]. Two possible solutions exist: the amount of analyte injected on to the capillary for separation must be increased and/or the sensitivity of the detection method must be increased. The topic of online sample preconcentration by stacking is discussed below (Section 1.3.2), followed by a survey of detection methods (Section 1.3.3).

As mentioned previously, CE is particularly suited to miniaturization. The concept of performing chip-based separations and detections (and also pre-separation sample preparation steps) on a single chip is under active investigation. These systems are known variously in the literature as the lab-on-a-chip (LOC) devices or micro total analysis systems (μTAS). Microfabricated CE devices are produced by etching or molding channels on a planar substrate (often glass or quartz in early applications; now plexiglass, low-temperature co-fired ceramics or polymer materials are also common) [51]. Performing microseparations on such a small scale leads to faster analysis, decreased cost and waste production, portability and disposability [51]. Other advantages are retention of the high separation efficiencies, minute sample and reagent consumption, high sample throughput and the ease of automation [53] characteristic of ordinary CE systems.

1.3.2 Sample Injection and Preconcentration

Sample injection in CE is done either hydrodynamically (using pressure) or electrokinetically (using an applied voltage) to introduce analyte ions from the sample into the capillary. To calculate the actual amount of analyte injected during electrokinetic or hydrodynamic injection, the appropriate parameters must be considered: these include the capillary internal diameter, buffer viscosity, total capillary length, buffer density, injection time, the applied voltage and the electrophoretic mobility of the analyte [44]. The use of electrokinetic injection gives a positive bias for those analytes with higher electrophoretic mobilities.

Inherent to capillary electrophoresis is the possibility of exploiting the applied electric field for sample preconcentration. Equation 1.12 presents a modified version of Ohm's law [53]. If E is the electric field strength, σ is the specific zone conductivity and j is the current density, then the relationship

$$E\sigma = j \tag{1.12}$$

is valid. The separation capillary has a constant cross-sectional area, and therefore j is constant for the whole electrophoretic system at any time. From this it follows that the local electric field strength is higher in a zone with a lower (local) conductivity. The specific zone conductivity σ (not to be confused with σ^* of Equation 1.8) can be obtained by a summation of the concentration c and mobility m of each ion of the system (F is the Faraday constant), as in Equation 1.13 [53].

$$\sigma = \sum_i c_i \left|\mu_{ep,i}\right| F \tag{1.13}$$

Again, the velocity of an ion i is given by Equation 1.5, restated here.

$$v_i = \mu_{ep,i} E \tag{1.5}$$

Consider a discontinuous buffer system composed of a zone of low conductivity (high electric field strength, E) followed by one high conductivity (low E), with minimal mixing between the two zones. The velocity of an analyte ion would, according to Equation 1.5, be high as it traveled through the low-conductivity zone, but the ion would slow as it entered the region with higher conductivity. The analyte ions thus have a tendency to stack at the boundary between the high- and low-conductivity zones.

On-line preconcentration methods based on the manipulation of the electric field differences in discontinuous electrolyte systems can provide significant sensitivity enhancement of analyte ions (by as much as two to three orders of magnitude). The generic term used for these preconcentration methods that lead to the compression of the analytes within a long sample plug into a much narrower band (with a correspondingly higher concentration of analytes) is stacking [50]. However, many other terms exist in the literature for the same or nearly the same procedures. To perform field-amplified sample stacking (FASS) the sample is prepared in background electrolyte of the same

composition, but different concentration [54]. Alternatively, field-amplified sample injection involves the introduction of a water plug in front of the sample zone [54] before injection. For samples in a low conductivity matrix, intrinsic sample stacking may occur, whereas for analyte preconcentration in samples with high conductivity, transient ITP stacking may be used [50] provided that the conditions are given careful consideration so that the sample and BGE contain both a leading and terminating electrolyte. A more complicated scheme is field-amplified polarity switching, which can be used to introduce both positive and negative ions into the capillary [54]. Each one of the techniques listed here, however, has the commonality of exploiting variation in the velocities of analyte ions in zones of varying conductivity (electric field strength) to result in the on-line preconcentration of analyte ions prior to separation. Similar preconcentration schemes also exist for MEKC (since these are based on chromatographic effects, the term sweeping is used [50]).

1.3.3 Detection in Capillary Electrophoresis

Historically, the most commonly-used detection techniques for CE have been based on UV absorbance, despite the relatively low sensitivities that can be achieved under CE conditions. Absorbance is widely used as the basis for detection in HPLC systems, thus the implementation of UV-absorbance for detection in CE systems was simplest from the perspective of instrumentation and its continued use is not surprising. For species which do not absorb in the UV region, indirect absorbance methods are employed, relying on the displacement of a UV-absorbing species by the analyte [55, 56]. Implementation is straightforward, involving the incorporation of a UV-absorbing ion (with the same charge as the analyte) in the operating buffer: the nonabsorbing analyte displaces the chromophore, resulting in a decrease in the absorbance signal due to this displacement [48]. However, absorption techniques exhibit relatively poor concentration detection limits (typically 10^{-5} to 10^{-6} M [57]). The application of UV absorbance (either direct or indirect) to CE is limited by the small path lengths of the capillaries used for the separations, typically <100 μm [56]. Efforts to improve sensitivity by overcoming the limitation of small path lengths across the separation capillaries – such as Z-shaped flow cells or multireflection cells [56] – have only partially succeeded.

Among the most sensitive detection techniques for CE is laser-induced fluorescence (LIF) [44]. LIF, while exhibiting very high sensitivity, is limited to analytes which fluoresce [56] – thus, derivitization may be required (pre- and post-capillary derivitization schemes are both used [48]). Indirect fluorescence detection (analogous to indirect UV detection) is also sometimes employed [48, 56] for CE separations to provide sensitive detection while eliminating the requirement for derivitization.

Other detection techniques for CE include thermooptical [48] and refractive index detection [48, 56]. Chemiluminescence (CL) detection has also been reported [48] (and has been used for the detection of metal ions separated by CE [58]). The combination of CE with mass spectroscopy is another possibility [48, 59]. While MS is an attractive option in terms of the qualitative information available, the interfaces required to couple CE with MS are complicated and limit the accessibility of this method.

Electrochemical detection is an attractive alternative for detection in CE. While implementation of CE-ECD is not without difficulties and is certainly not as simple as the use of UV-absorbance detection, CE-ECD combines high sensitivity (along with LIF, electrochemical detection provides the most sensitive detection for CE [44]) with good selectivity and low cost. Since CE-ECD is used extensively in this work, it is treated in much more detail in the following section.

1.3.4 Capillary Electrophoresis/Electrochemical Detection (CE-ECD)

Tanyanyiwa [55] has postulated two reasons to account for the relative neglect of electrochemical detection in capillary electrophoresis, which to some extent contradicts the patterns of the use of ECD in the more established technique of HPLC. These are as follows: (i) the early capillary electrophoresis instruments were designed for use in combination with existing UV detectors, and (ii) there is a perceived incompatibility between electrochemical detection and the high voltage required for CE separations [55]. While the lack of commercial instrumentation fitted for electrochemical detection is still an obstacle to its more widespread adoption, various approaches exist that at least partially mitigate the effects of separation voltage on electrochemical systems (these are discussed in Section 1.4.4.1.1 below).

Wallingford and Ewing first reported the combination of capillary electrophoresis and electrochemical detection in 1987 [60]. In this case, the separation of chatechol and

various catecholamines by CE with amperometric detection at a 10-μm carbon fiber electrode was achieved. Since then, conductimetric and potentiometric detection for CE have also been described. Conductimetric and potentiometric detection are somewhat simpler methods; however, amperometric detection imparts a degree of selectivity to the detection [56].

Conductimetric detection can be adapted for use in capillary electrophoresis, and is a universal method in that all ions elicit a response [55]: however, the background electrolyte for CE necessarily contains ionic species, leading to a high background signal. The conductivity response due to the analyte is based on the difference between the conductivity of the analyte ions and the electrolyte ions of the same charge displaced by the analyte, limiting the sensitivity. To maximize the sensitivity of conductivity detection, there should be a large conductivity difference between the analyte and buffer ions; however, this conflicts with the close match between conductivities needed to ensure lack of peak distortion (i.e. tailing or fronting of analyte peaks and the subsequent loss of resolution). Nevertheless, conductivity detection is inherently simple, versatile and relatively robust. Examples of the analysis of various species using capillary electrophoresis with conductivity detection are summarized in Reference [55] (potentiometric detection is also discussed). Suppression conductivity detection has also been employed for detection [56, 59].

A recent review of capillary electrophoresis with amperometric detection [61] summarizes the determination of a wide variety of analytes, including amino acids (at carbon, gold and copper electrodes); peptides and proteins (carbon or cuprous oxide-modified carbon composite electrodes); neurotransmitters (carbon, platinum and gold); phenolic compounds; carbohydrates (at copper); purine bases; inorganic ions; and various drugs (including antibiotics, β-blockers, β-agonists, NSAIDs, antivirals and illicit drugs). Amperometric detection is attractive in terms of simplicity and sensitivity: however, electrodes held at a constant potential are prone to contamination due to adsorption of impurities in the electrolyte and/or accumulation of reaction products at the electrode surface.

Electrochemical techniques more complicated than pulsed amperometric detection generally require customized potentiostats and data-acquisition systems, and thus are

less common. However, several examples of scanning electrochemical techniques do appear in the literature. Fast cyclic voltammetry detection has been used for the detection of metal ions in capillary electrophoresis [10] (since this pertains directly to the work discussed in this thesis, it is discussed in more detail in Section 1.4.5). Square-wave voltammetry detection (end-column) was investigated for detection of dopamine and epinephrine in CE [62]. The same authors report the application of adsorption-based detection of nonelectrochemically active analytes on Pt disc electrodes by square-wave voltammetry to the detection of sulfonamides, amino acids, β-agonists and a forensic drug mixture separated by CE [63].

Any scanning electrochemical technique could theoretically be adapted for use in capillary electrophoresis, provided that the sampling rate is high enough to provide proper quantification of the CE peaks. A sample rate of at least 5 Hz is needed for peaks of about 2 s duration [62]. Proper design of the instrumentation is necessary to achieve the frequencies and bandwidth required given such considerations. In the above example (SWV detection [62]) square-wave frequencies of 1 kHz or higher were required. Despite being more complicated than fixed-potential detection, one advantage of scanning electrochemical techniques is that they do in some instances provide qualitative information about the analytes.

Electrochemical detection is well-suited to the detection requirements of the capillary electrophoresis microchip devices now being developed, meeting the sensitivity requirements for low-volume detection while offering relatively simple implementation in comparison with other options such as laser-induced fluorescence (LIF) (for a discussion of a variety of detection methods for microchip separations, including electrochemical detection, see [64]). Microelectrodes can be fabricated using many of the same photolithographic techniques already in use to construct microchips: thus, the electrode can be fabricated directly on the chip, producing a fully integrated system [51, 65]. The considerations of isolating the detector from the electric field are identical to the discussion below with regards to capillary electrophoresis (Section 1.4.4.1.2), as are concerns about electrode positioning (Section 1.4.4.1.1). More discussion of the advantages of ECD for use in total analysis systems can be found in [53]. Several different applications of amperometric detection in microchip capillary

electrophoresis – for instance, the analysis of analytes such as neurotransmitters and carbohydrates – are summarized in Reference [51].

1.3.4.1 Practical Considerations

1.3.4.1.1 Electrode Positioning

A major issue related to the application of electrochemical detection to capillary electrophoresis is the necessity of a reproducible method for aligning the detection electrode with the capillary. The position of the electrode with respect to the capillary must be established and maintained over extended periods of time, and the positioning process must be reproducible. Even a relatively crude analysis is enough to reveal the importance of capillary/electrode alignment on detector response [66, 67]. Any misalignment of the electrode at the end of the capillary is obviously expected to have a negative effect on the sensitivity of the detection, and may also cause a decrease in the separation efficiency (due to convection and diffusional band broadening in the zone between the capillary and the electrode). Also, the electric field at the separation capillary is distance-dependant: thus, any shift in electrode position may cause a non-negligible shift in the potential of the detection electrode (as discussed in the next section). Alignment of the electrode and the capillary can be attained by using a detection cell specifically designed for reproducible capillary alignment, with integrated capillary/electrode systems, or by use of a micromanipulator [61]. These methods are discussed below.

Cells designed for reproducible capillary alignment generally reduce the problem of positioning the electrode in three dimensions to the rather simpler prospect of adjusting the distance between the separation capillary and detection electrode in one dimension. Generally, this requires fabrication of electrodes of the same external dimensions as the capillary. The fused-silica capillary used for CE separations is available in a wide variety of internal diameters, and most commonly has an outer diameter of 365 μm, so a simple method is to fabricate a working electrode from a piece of fused-silica capillary with a rather large internal diameter. Examples are given in [68] and [69]. However, these electrodes are rather fragile and their fabrication demands skill and patience.

Several integrated capillary/electrode systems have been proposed for use in CE. These include a configuration in which the working electrode was formed by placing

gold wire perpendicularly across the capillary outlet [67]. Another example is a system in which the working electrode was formed by sputtering a thin layer of Pt or Au onto the exit tip of the capillary [70]. These systems are slightly more rugged than those mentioned above: however, the care required to make such electrodes and/or need for specialized equipment are again considerations.

The final approach is the manual alignment of the capillary and electrode using a micropositioner, often under a microscope. This is the approach used throughout this work (the designs of the electrochemical cells and positioning technique used are described in Sections 2.7.4–2.7.6). While the use of a micropositioner to manually position the detection electrode is viewed as tedious and impractical (as well as time-consuming and non-reproducible), with practice a reasonable degree of competency ensues.

Two other attempts to simplify positioning of the electrode that do not fit into the above categories should also be noted. A conical capillary aperture can be obtained by etching in hydrofluoric acid to aid in electrode placement [71] (in this case, the electrode is cylindrical and placed inside the cone-shaped end of the capillary). In another approach, a normal-sized (>100 μm) disc electrode was positioned immediately in front of the capillary opening – the advantages of this being more rugged electrode construction and more reproducible alignment. This last system was used for the detection of carbohydrates at Cu and was found to give results similar to those obtained with the positioning of an ultramicroelectrode [72].

1.3.4.1.2 Off-Column vs. End-Column Detection

Electrical isolation of the electrochemical cell from the applied voltage to minimize detector noise (so-called “off-column” detection) was deemed necessary in the first CE-ECD system described (in 1987) [60], and discussion in the literature regarding the need for some form of decoupling of the separation voltage from the detection cell persists. Numerous designs for decouplers for use in off-column detection schemes have been reported. These designs include decouplers that make use of porous glass [60], an on-column frit, porous graphite tubing, Nafion tubing [73] and cast-Nafion [74].

Depending on the construction of such decouplers, some decrease in response is inevitable, since the analyte may diffuse through the assembly rather than reach the

detector. The Nafion used in some decouplers may also lead to band broadening, due to its interaction with cations. Finally, most decouplers require careful and labour-intensive construction, and the resulting structures are often rather fragile. In addition, it has been observed that in off-column detection, even with decoupling, increased detector noise was observed in systems with high electrophoretic currents [60] (in this case, the decoupler was a porous glass joint). These results suggest that the end of the capillary is not entirely isolated from the applied potential field even when decoupling is used (the use of high-resistance buffers was suggested to minimize these effects).

In end-column systems, the detection electrode is simply placed at the outlet of the separation capillary. End-column detection was not reported until 1991, when amperometric detection was performed at the end of 5-μm separation capillaries without decoupling [75] (end-column conductivity detection was reported in the same paper, with 80-μm capillaries). The rationale behind this approach was that for capillaries less than 5 μm, the separation current is small and thus electrical interference is minimized [75] – reduction of the internal diameter of the separation capillary from 75 μm to 5 μm results in a 200-fold decrease in electrophoretic current [27]. In practice, however, working with such small capillaries on a routine basis becomes impractical: extreme care must be taken due to the potential for capillary blockage. End-column detection was also investigated for capillaries between 10 and 25 μm [76]: again, the idea was that the rapid dispersion of the electric field at the end of the capillary would result in minimal interference from the applied separation voltage. For end-column detection, the separation voltage is grounded in the detection reservoir – thus, the working electrode is never completely immune to the electric field used for separation. A small but reproducible potential- and position-dependant shift in the potential of the working electrode is apparent when the separation voltage is applied.

Direct comparisons of end-column and on-column electrochemical detection are problematic in that the systems employed for such experiments (in particular potentiostats and decouplers) vary widely from laboratory to laboratory. However, the construction and performance of an electrical decoupler fabricated of Nafion deposited on a copper-plated tungsten wire was compared with the performance of the same system without grounding the separation voltage through this decoupler [74] (thus

performing electrochemical detection in both modes – end-column and off-column – using the same equipment). In this case, better results were obtained for end-column detection (that is, without decoupling).

The background noise in amperometric detection under CE conditions was also investigated using four different electrode materials (C, Pt, Au and Ag) and six background electrolytes in both grounded and ungrounded modes [76]. Again, this work is significant in that end-column and off-column detection were studied using the same system. The authors note that comparisons of electrochemical detection in end-column and off-column configurations are often based on isolated data obtained on equipment designs that vary from one group to another [76]. For ungrounded detection with the (cylindrical) electrodes placed inside the capillary, gas evolution was observed with a separation voltage as low as ~5 kV, indicative of the electrode being exposed to a considerable electric field (it should be noted that the capillary was not etched to give a conical aperture as in some other investigations; also, visual inspection of these electrodes revealed an obvious change in the electrode appearance).

It has also been suggested that the separation voltage has no significant effect on detection noise for end-column detection at 25 μm capillaries [76]. The response at a 25-μm Pt disc electrode placed within ~3 μm of the end of a series of capillaries with internal diameters of 10, 25, 50 and 75 μm exhibited an increase in background noise for capillaries with diameters greater than 25 μm [76]. However, the potential of the working electrode would have been shifted from the applied potential to a greater extent at the 75 μm capillary relative to the 10 μm capillary, so that the measurements were effectively taken at different working electrode potentials. Two applied electrode potentials were examined: +700 mV and −700 mV. While there was a slight increase observed in peak-to-peak noise levels for detection at +700 mV with increasing capillary diameter, the observed noise increase in the corresponding measurements at −700 mV were much more dramatic: from less than 0.5 pA for a 25 μm capillary to 50 pA at a 75 μm i.d. capillary – no measurement at +700 mV exceeded ~0.5 pA, even for a 75 μm capillary [76]. Two such widely different results are explicable if one considers that at +700 mV, a cyclic voltammogram for Pt (included in [76], although not for the same electrolyte – the results for different electrolytes were reported to be similar) exhibits a

relatively flat current-potential dependence, whereas at −700 mV, the current increases rapidly with decreasing potential. Any shift in the applied potential in this negative region would thus have a more dramatic effect on the observed current. In general, the measurements of peak-to-peak noise in this case should not be considered to have been measured at the same potentials, but at a positive (or negative) potential which shifted more or less according to the extent of the electric field that existed at the end of the capillary.

In our experience, it is possible to perform end-column electrochemical detection at disc-shaped ultramicroelectrodes without isolating the working electrode from the potential field generated by the separation voltage (see also [62]). The potential at the working electrode is dependant on a number of factors, including the internal diameter of the separation capillary, the applied separation voltage, the composition of the background electrolyte, and the position of the working electrode with respect to the end of the capillary, both longitudinally and radially. However, for a given set of conditions, assuming no shift in electrode position, the potential field at the end of the separation capillary should be relatively constant – in the absence of other effects such as Joule heating or instability in the voltage supply providing the separation voltage. Thus, the electrode will simply experience a slight potential shift or "offset potential" relative to the potential applied to the electrode. Provided that this shift is accounted for by a judicious choice of (for instance) detection potential in amperometric detection for each set of separation conditions, minimal degradation in noise levels as separation voltages are increased (within a moderate range) can be expected. Again, it should be noted that even in situations where the separation voltage was grounded before detection, the background noise of the system was often noted to increase with increasing separation voltage [60, 76, 77] indicating that true isolation of the detection circuit from the separation field was not achieved. Thus, it is important that whether end-column or off-column detection is chosen, the probable magnitude of the offset potential experienced by the working electrode in the separation field is taken into consideration.

1.3.5 CE-ECD of Metals

Lu and Cassidy have evaluated ultramicroelectrodes for the detection of metal ions in CE [9]. Carbon-fiber, gold and mercury films deposited on gold were used for constant-

voltage and pulsed-voltage amperometric detection. The pulsed waveform consisted of two steps: a potential of −800 mV was applied for 110 ms (to reduce analyte ions); followed by 200 mV (300 mV at carbon fiber) for 110 ms (to oxidize reduced metal and clean electrode surface): the current was sampled over last 55 ms. A detection limit of 5×10^{-7} mol/L was achieved for Pb^{2+} at a carbon-fiber electrode [9].

The research reported in this thesis builds on work done by Wen (previously at the Department of Chemistry, U of S). Fast cyclic voltammetry (FCV) detection was investigated for the detection of metal ions separated by CE at sweep rates from 20–1000 V/s at 10- and 25-μm Au disk electrodes (in an end-column configuration) [10]. The electrolyte used for separation contained α-hydroxyisobutyric acid (HIBA) and creatinine, as reported earlier for separations of metals. The potential waveform included a preconcentration period (55–300 ms) followed by cyclic voltammetry (the duration of which depended on the sweep rate but ranged from 2–100 ms). Response was taken to be either the CV current (maximum current in each voltammogram) or the integrated current over a selected portion of the CV (in units of coulombs), known as the CV charge response. The effect of preconcentration time on electrode response and peak shape was evaluated (under CE conditions). As expected, the electrode response was found to increase with preconcentration time [10]. The preconcentration time can be increased only to the extent that it does not interfere with the necessity of collecting enough points over the time of peak elution to result in well-defined peaks. In addition, peak broadening was observed when the preconcentration time was >250 ms, due to incomplete removal of analyte during the potential scan.

The dependence of electrode response on sweep rate (25–1000 V/s) was also examined for Tl^{+}, Co^{2+}, Ni^{2+}, Zn^{2+}, Cd^{2+}, and Pb^{2+} at 10- and 25-μm Au disc electrodes, also under CE conditions [10]. A linear increase in CV current with sweep rate was observed for Tl^{+}, Zn^{2+}, Cd^{2+}, and Pb^{2+} (at a 25-μm Au electrode; similar results were obtained for Co^{2+} and Ni^{2+} at a 10 μm Au electrode). However, the relationship between CV charge (integrated CV current) and sweep rate was more complicated. The maximum S/N for CV charge was obtained at sweep rates of between 150–350 V/s for Tl^{+} and Pb^{2+} (both analytes with fast charge-transfer kinectics); for other analytes, the sweep rate had only a slight effect on the S/N.

Detection limits for this technique under optimized conditions were also reported [10]. These were as follows: Tl^{+}, 5×10^{-9} mol/L; Pb^{2+}, 8×10^{-9} mol/L; Ni^{2+} and Co^{2+}, 1×10^{-8} mol/L; Zn^{2+} and Cd^{2+}, $(2–4)\times10^{-8}$ mol/L. Detection was performed at a 25-μm Au disc electrode with a sweep rate of 400 V/s (250 V/s at 10-μm Au). Another interesting aspect of this detection method was demonstrated by the resolution of two comigrating analytes (Zn^{2+} and Pb^{2+}) in the potential domain.

CHAPTER 2: EXPERIMENTAL

2.1 FOREWORD

The wide variety of experiments conducted in this work – some of them rather unusual – necessitates detailed explanations specific to each type of experiment conducted. It may be useful to read only the general aspects of the experimental work (Sections 2.2–2.4) at this time, deferring the remaining parts of this chapter until they are specifically referred to at later points in the thesis.

2.2 REAGENTS

All solutions were prepared using doubly-distilled deionized water (Corning Mega-Pure System, MP-6A and D-2). Supporting electrolyte solutions were made by dilution of the concentrated acid: acetic acid, nitric acid, hydrochloric acid and orthophosphoric acid (all from BDH Assurance) were used. Stock solutions of metals (usually 0.01 mol/L) were prepared from nickel chloride, cadmium acetate, zinc acetate, manganese(II) chloride tetrahydrate and cobaltous chloride (BDH Analar); lead nitrate, lead acetate, ferric chloride and silver nitrate (BDH Assurance); ferrous chloride (BDH reagent grade); and thallium(I) nitrate and copper(II) nitrate hydrate (Aldrich). Sodium acetate (BDH Assurance) and potassium chloride (BDH reagent grade) were also used. Experiments were carried out without removal of dissolved oxygen.

2.3 DATA ACQUISITION

2.3.1 Electrochemical Data Acquisition System

A custom-built system was used for data acquisition. A schematic of this system is presented in Figure 2.1.

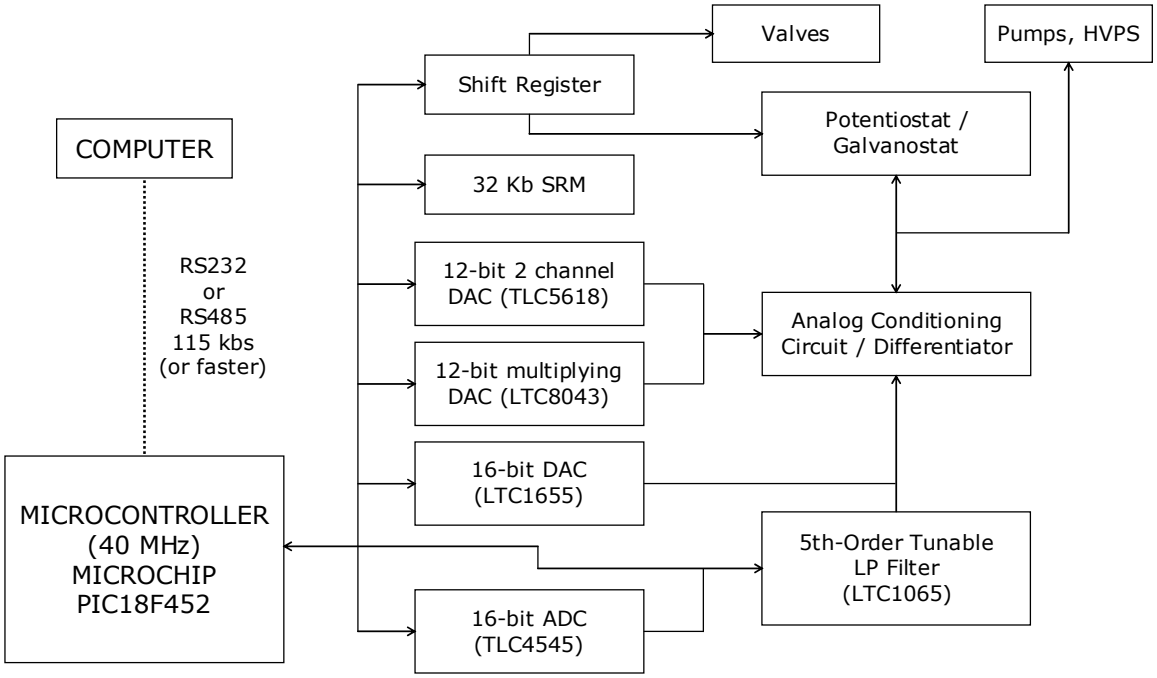

Figure 2.1 Electrochemical data acquisition system.

2.3.2 Software for Data Acquisition and Analysis

In-house software was used for all data acquisition and initial data analysis. The program, developed by Dr. A. S. Baranski, is called MicroVoltammetry. This software can be run in numerous modes, allowing for many electrochemical experiments to be conducted: however, for the purposes of this work, the software was most commonly used in the Cyclic Voltammetry and CV Monitor modes (standard experiments), the Fast Cyclic Voltammetry and Fast CV Monitor modes (fast techniques) and Continuous Cyclic Voltammetry Stripping mode. Various simulations (including the one used for determination of kinetic parameters, Sections 4.2.1–4.2.4) can also be run using this software.

The version of MicroVoltammetry used was updated during the course of this work as the capabilities of the software were expanded: however, the subroutines used for data acquisition when running various experiments (e.g. Cyclic Voltammetry, CV Monitor) remained the same, or with only very minor alterations that in no way affected the validity of previous data.

Analysis done in MicroVoltammetry (determination of peak area, peak height, etc.) can be made available to any standard spreadsheet program using a copy command which dumps data to the clipboard. Another function also exists in the software for saving entire curves (e.g. cyclic voltammograms or the response over the course of a CV monitor experiment) in a format compatible with Microsoft Excel. Any analysis done in addition to that done within MicroVoltammetry, as well as the plotting of graphs, was done using Microsoft Office Excel 2003.

2.3.3 Cyclic Voltammetry / Fast Cyclic Voltammetry

The Cyclic Voltammetry mode of the software was used to run standard cyclic voltammetry experiments (with sweep rates up to 10^3 V/s). The Fast Cyclic Voltammetry experiment was used for cyclic voltammetry with sweep rates up to 10^5 V/s, in particular for acquisition of the experimental cyclic voltammograms for determination of kinetic parameters (Sections 4.2.1–4.2.4).

2.3.4 Repetitive Cyclic Voltammetry / Fast Repetitive Cyclic Voltammetry

Repetitive cyclic voltammetry experiments were run using the CV Monitor option in the MicroVoltammetry software. This experiment involves continuous monitoring of the electrode response using cyclic voltammetry. One cycle of the RCV experiment proceeds as follows: the electrode is held at a specified potential (known as the rest potential) for a set interval (the delay or preconcentration time). After this, the potential is cycled (as in any cyclic voltammetry experiment) from the initial to the vertex potential and back, to complete the cycle. This is followed by an immediate return of the electrode to the rest potential, and this is repeated throughout the experiment. The current was sampled only during the potential scan. Typically the scan rates for repetitive cyclic voltammetry experiments are between 10 and 10^3 V/s; and the delay time is 0.05 to 3 s. The same experiment could be run at higher sweep rates using Fast CV Monitor (in MicroVoltammetry).

For both RCV and fast-RCV experiments, the quantity ΔQ is generated by integrating the change in electrode response over a user-defined potential range (E_1 to E_2) and expressing the result as electrical charge [78]. Since CV curves are actually recorded by sampling current in equal time intervals, this is accomplished using the following summation (Equation 2.1)

$$\Delta Q(k\tau) = \frac{\Delta E}{\nu}\left(\sum_{j=a}^{b} I(k,j) - \sum_{j=a}^{b} I(k_{ref},j)\right) \qquad (2.1)$$

where ΔE is the potential difference between two subsequent points on the CV curves, k is the scan number, τ is the time between subsequent scans, v is the scan rate, a and b correspond to the potentials E_1 and E_2, $I(k, j)$ represents the CV curve recorded during the k^{th} scan and $I(k_{ref}, j)$ is the reference CV curve [78]. The first few CV curves recorded at the beginning of an experiment (after the CV had stabilized) are averaged to generate the reference CV curve. The result of an RCV experiment is displayed as a plot of ΔQ versus time (although the raw CV data is also saved for each experiment).

2.3.5 Repetitive Cyclic Voltammetry Stripping Analysis

Repetitive cyclic voltammetry experiments were run using CCV Stripping (in MicroVoltammetry, version 9.2). This experiment is similar to the CV Monitor (RCV) experiment in that the applied potential waveform is the same. The delay time between cyclic voltammograms is, as in RCV experiments, between 0.055–3 s: however, the RCV waveform is stopped and a negative preelectrolysis potential pulse lasting up to 3000 s is applied mid-experiment to allow for accumulation of the metal at the electrode surface. After the preelectrolysis time, application of the RCV waveform resumes. The analyte is stripped from the surface within the next several scans. The response, ΔQ, is calculated in the same way as for the CV Monitor experiment (Equation 2.1).

2.4 FABRICATION OF ELECTRODES

2.4.1 Working Electrodes

For the purposes of this work, electrodes were prepared as described below. Gold wire, generally 25 μm in diameter (obtained from Alfa Aesar – Ward Hill, MA), was threaded through a piece of patch clamp capillary glass about 5 cm long (PG52150-4; World Precision Instruments – Sarasota, FL). A short section (about 0.5 cm) of the wire was sealed in the capillary at one end using a Bunsen burner flame. Extreme care was necessary to achieve a seal between the microwire and the glass without actually melting the gold. After cooling, electrical contact was made between the microwire and the exposed end of the connecting wire using silver conductive adhesive paste (Alfa Aesar). The adhesive was cured in an oven for a minimum of two hours.

For increased durability, the upper part of the electrode was sealed in heat-shrink tubing. The sealed end of the electrode was examined optically (using 10× magnification) and – if no defects in the seal were observed – was then cut perpendicular to the length of the capillary to expose a disk-shaped gold surface. Electrodes prepared in this way were polished with 400- and 600-grade carborundum paper and rinsed several times with distilled water to remove any particles from the polishing. Further polishing was done using alumina lapping films (World Precision Instruments).

The electrodes were screened for any erratic behaviour by observation of the oxide formation/dissolution peaks in acidic solution; or, in some experiments, the peaks due to

the underpotential deposition of Cu. Any aberrations resulted in the electrode being examined optically for defects (10× magnification) and repolished (if no defects were observed). If after repeated testing the CV curve generated was not normal, the electrode was discarded.

The first stripping peak for Cu^{2+} underpotential deposition (see Fig. 3.1, peak maximum at ~150 mV) – corresponding to monolayer coverage of the electrode – was used to approximate the actual (microscopic) surface area and surface roughness factor of the Au electrodes. The surface roughness factor, ρ, was determined from

$$\rho = \frac{A_m}{A_g} \tag{2.2}$$

where A_m is the microscopic electrode area and A_g is the geometric area [79]. The electrosorption valency for Cu^{2+} used for calculation of the surface area was 1.4, the value determined in Reference [36] for Cu^{2+} absorption at Au(111) (in perchloric acid), and the surface coverage of Cu (from the same source) was 2.2×10^{-9} mol/cm^2. Typical values for A_m – the calculated microscopic surface area of the electrodes – were from 6.1×10^{-6} to 1.0×10^{-5} cm^2. The geometric surface area for an electrode of 25 μm diameter is 4.9×10^{-6} cm^2. The corresponding values of the roughness factor ranged from approximately 1.4–2.1: the electrodes used in this work were those in the lower range.

2.4.2 Reference and Auxiliary Electrodes

A laboratory-made Ag|AgCl electrode was used as a reference electrode in many experiments, as specified (particularly for CE and flow-injection analysis experiments). The remaining experiments were done using tungsten wire as a pseudo-reference electrode. This was a convenient way of minimizing the contamination of electrolyte and/or sample solutions due to leakage of Ag^+ from the reference electrode. The potential of a tungsten pseudo-reference electrode in 1 mol/L CH_3COOH is .. vs. Ag|AgCl. There was no noticeable fluctuation in this potential.

Tungsten wire was used as an auxiliary electrode for CE and flow-injection analysis (FIA) experiments. A Pt foil electrode (~1 cm^2) was used as the auxiliary in stripping and kinetics experiments, as specified.

2.5 FLOW-INJECTION ANALYSIS

2.5.1 Setup for Flow-Injection Analysis

Many initial experiments were done using flow-injection analysis rather than CE experiments, which are more complicated and time-consuming. The flow-injection cell construction was similar to that described in Reference [78] (see Figure 2.2). A three-way solenoid valve (EW-01367-72, now discontinued; Cole-Parmer – Vernon Hills, IL) interfaced to the computer allowed for control of injection and solution switching. The flow-injection setup also included a dual-channel, variable-speed, compact peristaltic pump (six rollers, reversible; Masterflex C/L EW-77120-62; Cole-Parmer) which again was controlled by the computer. The recommended Tygon microbore tubing (various internal diameters, Cole Parmer) was used with this pump.

The variation in response – both peak area and peak height – with injection time (as specified by the user in the computer software) is shown in Figure 2.3. The peak area of the response increases with time, as expected: however, there is a leveling-off in the peak height observed at injection times of more than about 6 s. Injection times were typically between 2–6 s.

2.5.2 Electrode Stability Experiments

Experiments designed to examine the stability of the electrode response over time were done using flow-injection analysis. These experiments were performed with freshly polished 25-μm Au electrodes using a combination of experiments collected in the CV Monitor and Cyclic Voltammetry modes of MicroVoltammetry.

The data acquisition program allows the creation of a template file which specifies a series of experiments to be run with predetermined experimental parameters. These template files can include solution changes and changes in the type of experiment run, and also serve to define the parameters for each experiment sequentially. This completely automated data acquisition (after initial setup and checking of the system) allowed the experiments monitoring electrode stability to be carried out unattended over long periods of time (>40 hours, usually limited by the lifetime of the electrode), with all experiments saved in a file for future analysis. Analysis of the data was done manually and involved calculation of area of the Cu UPD peak or double-layer capacitance.

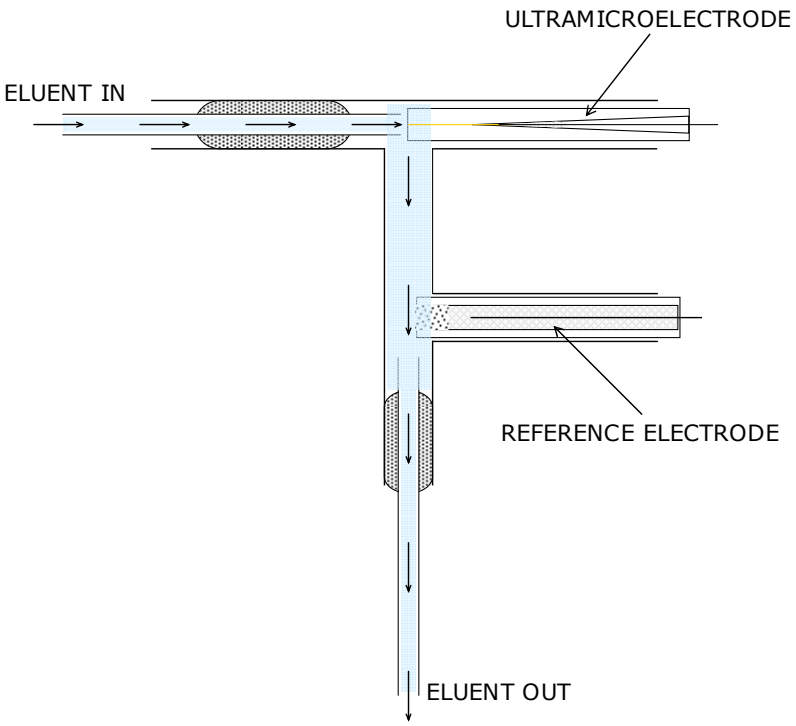

Figure 2.2 Schematic of cell used for flow-injection analysis experiments.

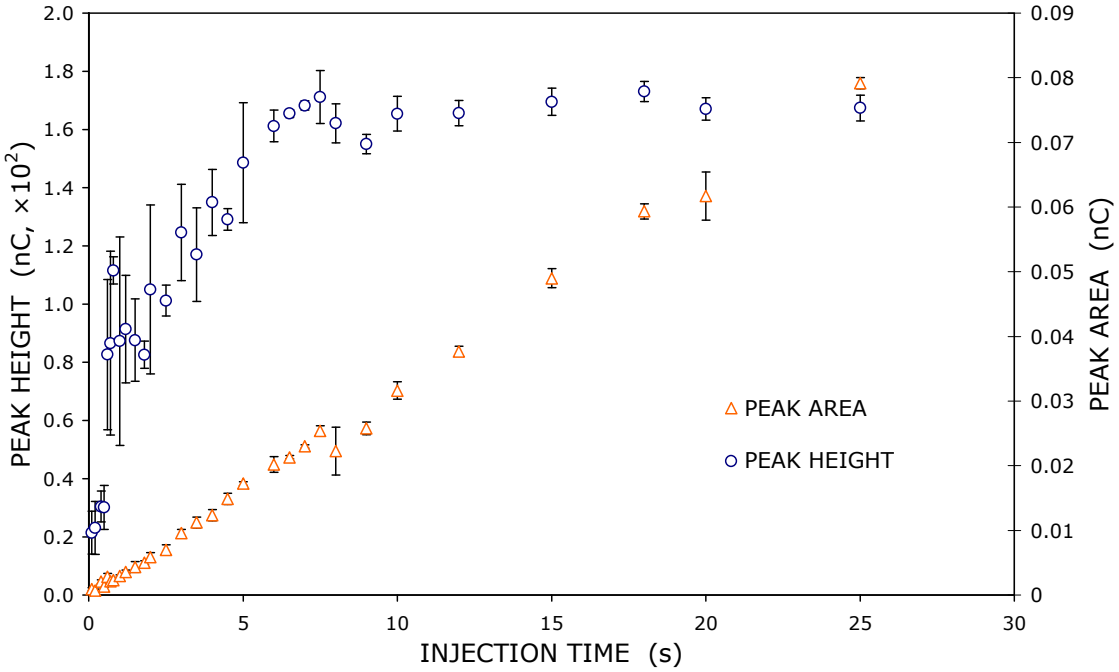

Figure 2.3 Evaluation of peak height and peak area as a function of injection time for repeated injection of 2×10^{-5} mol/L Zn^{2+} in 1 mol/L CH_3COOH under flow-injection conditions using repetitive cyclic voltammetry for detection. 25 μm Au working electrode, Ag|AgCl reference; sweep rate 98 V/s; preconcentration time 0.2 s; initial potential −300 mV, vertex potential 1600 mV, rest potential −300 mV. The flow rate was approximately 1 mL/min. The error bars represent the standard deviation of repeat injections.

2.6 KINETICS

2.6.1 Electrodes for Kinetics Measurements

Shielded electrodes were used for kinetics measurements. These were prepared as described in Section 2.4.1; however, electrical connection was made to the interior wire of a coaxial cable. The outside insulation of the coaxial cable was slit with a razor blade to expose the shielding. The mesh shielding material was then carefully slid back to allow for a connection to be made between the interior wire and the 25-μm Au microwire. After the connection was made, the shielding was eased back over the electrode to within 5–6 mm of the electrode tip. A bead of thermal glue was applied over the end of the shielding, and the whole assembly was slid into a piece of heat-shrink tubing before the thermal glue hardened. A heat gun was then used to shrink the tubing to cover the shielding and electrode.

Before performing any kinetics experiments, several scans of the electrode were done at a low sweep rate (0.1 V/s) in a solution of 0.1 mol/L sulfuric acid containing 5×10^{-4} mol/L Cu^{2+}. Any irregularities in the appearance of the cyclic voltammograms or discrepancies in the measured currents were taken as evidence of defects in the electrode. In such cases, the electrode was repolished and retested. If the irregularities persisted after repolishing, the electrode was discarded.

2.6.2 Kinetics Experiments

The fast cyclic voltammetry experiment in the MicroVoltammetry program (with sweep rates of up to 5×10^{4} V/s) was used for the collection of data to later serve as a reference or "target" for the simulation. These experiments were done using flow injection, switching the solution between the supporting electrolyte (1 mol/L H_2SO_4 or 1 mol/L $HClO_4$) and the metal ion solution (2×10^{-5} mol/L Cd^{2+}, Cu^{2+} or Pb^{2+} in the supporting electrolyte) using a computer-controlled valve. Cyclic voltammograms were recorded at several different sweep rates, and in some cases also for different surface coverages (by varying preelectrolysis time) at constant sweep rate. In each case, cyclic voltammograms were recorded under exactly the same experimental conditions for both the metal-containing solution and the background electrolyte to allow for subtraction of the

background current: these CVs were recorded with as little time between them as practically possible.

2.6.2.1 Simulation for Determination of Kinetic Parameters

The CV Adsorption (G) simulation (part of the MicroVoltammetry program developed by Dr. A.S. Baranski) was used to generate simulated cyclic voltammagrams to match background-subtracted experimental cyclic voltammograms recorded as described above. Certain simulation parameters – including the temperature, sweep rate, initial potential and final potentials, electrode radius and bulk concentration of metal in solution – were set to reflect as closely as possible the actual experimental parameters. Other parameters, such as the initial coverage, rate constant, alpha, and charge transfer coefficient, were changed according to what was necessary to match the experimental curves. This was done by modifying parameters in essentially a trial-and-error process: however, the same kinetic parameters were used to match the entire series of experimental curves for a metal over a wide range of sweep rates. For example, one set of data for Cu included experimental CVs at sweep rates of 7.9, 9.9, 13.9, 15.8, 19.8 and 25.7 kV/s: these CVs were all matched using the same parameters (i.e. rate constant, alpha, and charge transfer coefficient).

A more detailed explanation of the simulation program appears in Reference [80].

2.7 CAPILLARY ELECTROPHORESIS EXPERIMENTS

2.7.1 General Considerations

Fused-silica capillaries (various internal diameters, outer diameter 365 μm) with polyimide coating were obtained from PolyMicro Technologies, Inc. (Phoenix, AZ). The required length of capillary (usually 40-50 cm) was cut using a capillary cleaving tool (Chromatographic Specialities, Inc. – Brockville, Ontario) to give a clean perpendicular cut without any jagged edges. The ends of the capillary were examined with the aid of an eyepiece to determine whether or not the cut was satisfactory.

Capillary electrophoresis experiments were generally done under conditions of relatively low pH (the pH of a 1 mol/L solution of CH_3COOH, which was generally used as the background electrolyte, is ~2.4). Since the reproducibility of the electroosmotic flow in the experiments was not critical and EOF is minimal at low pH,

new capillaries were treated by rinsing with background electrolyte for at least one hour. Capillaries were also flushed with background electrolyte for half an hour before experiments were started for the day, and when there was a delay between experiments. Filling and rinsing of capillaries was accomplished by suction, using either a syringe coupled to the capillary by either a luer to CE capillary adapter (InnovaQuartz, Inc. – Phoenix, AZ) or an in-house assembly constructed of small internal diameter tubing (to fit snugly around the capillary) attached to a syringe needle using heat-shrink tubing and five minute epoxy.

Polyethylene sample vials (0.8 mL, Cole-Parmer Instrument Company – Vernon Hills, IL) were used to contain the background electrolyte and standard solutions. Electrolysis products due to the separation current may change the composition of the small volume of electrolyte in the CE-ECD cell. To minimize this possibility and achieve a stable baseline, the solution at both ends of the capillary was replaced every few runs. In addition, in all but the electrophoretic extraction experiments, care was taken to ensure that the injection and detection ends of the capillary were at the same level to eliminate any hydrodynamic flow. For all CE experiments, the detection cell and potentiostat were housed in a Faraday cage to minimize environmental noise.

2.7.2 Control of High Voltage Power Supply

Capillary electrophoresis experiments were performed using a CZE1000R high voltage power supply (Spellman High Voltage Electronics Corporation – Valhalla, NY) with a maximum output of ±30 kV. A Plexiglas box (produced in-house) with interlock switches on the door was used as a safety precaution.

Two modes of operation are possible with this instrument: it can be controlled manually or by use of a computer interface. Control of the high voltage power supply with the computer is attractive for several reasons. First, data acquisition for electrochemical detection is done entirely through the computer, and it is convenient to have the power supply controlled by the computer also. For instance, with computer control of data acquisition and separation voltage, detection can be started automatically a certain time after the voltage is applied. More importantly, the use of a computer to control the voltage allows for accurately timed electrokinetic injection, increasing the reproducibility. Finally, the interfacing of the high voltage power supply to the computer

also leads to the possibility (with further modifications) of a completely automated system for sampling, separation and detection. For these reasons, the Spellman unit was interfaced with the computer as described in Appendix A.

2.7.3 Injection

Both electrokinetic and hydrodynamic injection was used in capillary electrophoresis experiments. Electrokinetic injection was done using the high voltage power supply control program, which includes a subroutine for the timed application of a voltage set by the user; however, the injection end of the capillary was moved manually between the background electrolyte and analyte solutions. Hydrodynamic injection was done manually, holding the end of the capillary in the sample vial 15 cm above the detection end, and timing the injection with a stopwatch. This method was rather crude and obviously less accurate than electrokinetic injection, and thus was rarely used.

2.7.4 Detection Cell for Capillary Electrophoresis / Electrochemical Detection

The positioning of the electrode at the end of the capillary is of great importance in end-column detection for capillary electrophoresis, as discussed in Section 1.3.4.1.1. Two detection cells were used in this work, both of which allowed for the reproducibility and stability of electrode placement at the end of the detection capillary.

The first configuration is depicted in Figure 2.4. A tubular bell-shaped piece of glass (glass shop, University of Saskatchewan) is closed with a Teflon plug which has a small hole through which the separation capillary is threaded. The plug serves both as a watertight seal and to keep the capillary end in a fixed position. A custom-manufactured aluminum base (Physics Machine Shop, University of Saskatchewan) was fitted to hold the detection cell and the micropositioner, which had a plate to which the ultramicroelectrode could be secured. This base is not shown in Figure 2.4. A more compact detection cell developed by Gerhardt was used in later work and is described and pictured in Reference [62]. No appreciable difference was observed in the quality of the results obtained using either cell.

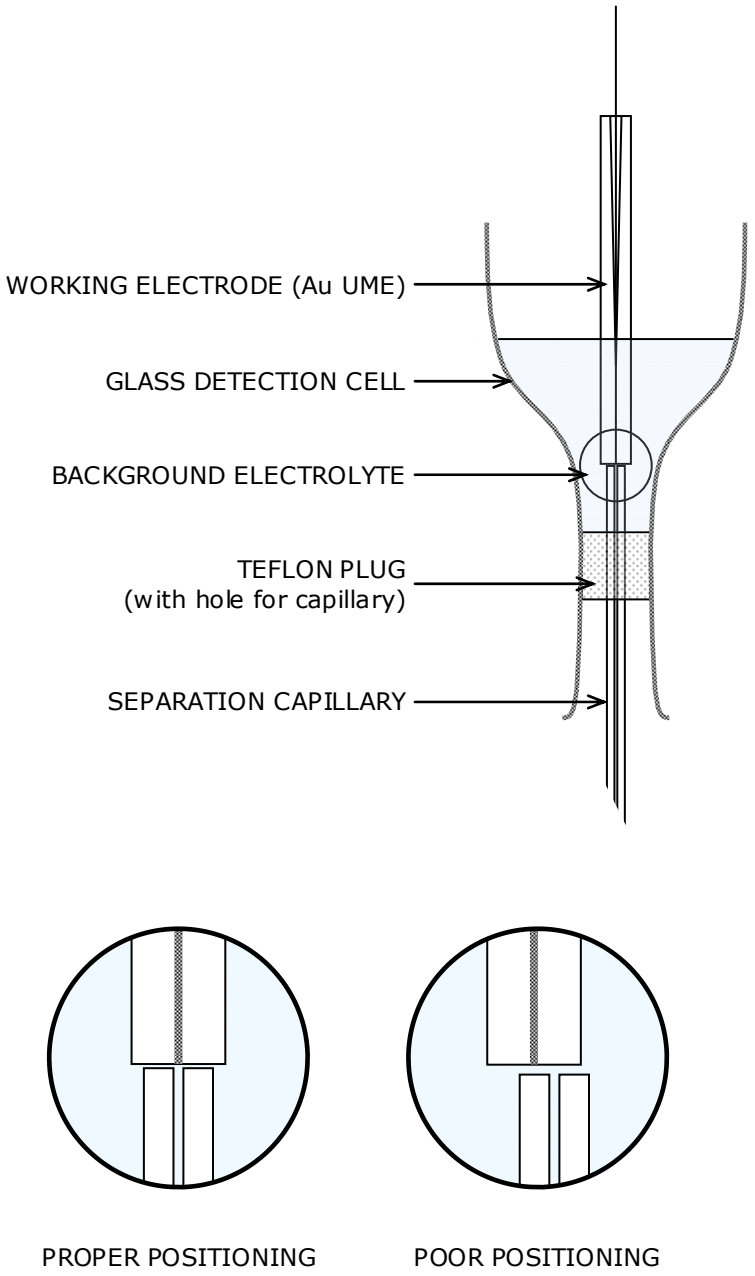

Figure 2.4 Schematic of detection cell for capillary electrophoresis. The working electrode is attached to a micropositioner fixed to a stage (not shown). The glass cell is mounted (by the bottom lip) to a platform on the same stage, underneath the micropositioner.

2.7.5 Electrode Positioning

Electrode positioning was done as follows: after polishing and testing (to avoid positioning a defective electrode) the working electrode was introduced and fixed into the detection cell described above. The separation capillary was threaded through the Teflon plug, and a rough alignment of the capillary and electrode was done. The assembly was then placed in front of a microscope which was used to view the capillary and the electrode, and the micropositioner was manipulated (in three dimensions) to align the electrode with the end of the capillary. Alternatively, electrode/capillary alignment was achieved by adjusting the screws in the second detection cell as described in Reference [62] (when the second detection cell was used).

Capillary alignment was checked by determination of the offset potential (see Section 2.7.6) and/or the injection of a standard solution (e.g. 2×10^{-6} mol/L Pb^{2+}) for which the magnitude of the response was well known.

After alignment of the electrode, it was usually not necessary to realign the working electrode unless the capillary was exchanged or the electrode required cleaning (by mechanical polishing). However, to ensure that some accidental movement did not result in misalignment of the electrode and capillary, any change in the magnitude of the offset potential (as described below in Section 2.7.6) was taken to be a sign of a change in the alignment, and the positioning procedure was repeated.

2.7.6 Determination of Offset Potential

The MicroVoltammetry program includes a subroutine for the simple determination of an "offset potential" used to correct for the potential shift. The appropriate initial and final potentials for a cyclic voltammetry experiment are set: the potential must be scanned over a range containing some significant feature, such as the peaks for oxide formation and reduction. Once the electrode is thought to be aligned properly, scanning of the potential between these values is started, with the high voltage off. The resulting cyclic voltammogram is displayed on the screen and after a certain amount of time (to allow for the CV to become stable) becomes fixed as a sort of target cyclic voltammogram. After this point, the separation voltage is switched on, with the potential still being scanned, and the resulting cyclic voltammogram is displayed on top of the target. The oxide formation/reduction peaks should now be shifted relative to the

original CV due to the potential field at the end of the capillary. The left and right arrow keys are then used to shift the CV curve until it overlaps with the original target cyclic voltammogram. The value of the offset potential – the potential shift applied to the electrode – is displayed at all times during this procedure. This potential is then entered as a parameter for the CV monitor experiment, and the potential waveform applied to the electrode during the CE separation is automatically offset according to the offset potential. Typically, the offset potential for a reasonably aligned electrode at the end of a 20-μm capillary (length 40 cm; 1 mol/L CH_3COOH background electrolyte) is about 270–300 mV.

2.7.7 Detection for Capillary Electrophoresis Experiments

Almost all detection for capillary electrophoresis was done using the CV Monitor experiment in the MicroVoltammetry software. This detection mode is referred to throughout this work as fast-scan repetitive cyclic voltammetry or RCV. Both the high voltage and the data acquisition are controlled completely by the computer (as discussed previously). The actual experiment began with the application of the separation voltage: this triggers the start of data collection after a short delay (of no more than 2 s). Both the CV and the response (generated as discussed in [78], see Section 2.3.4) are displayed throughout the experiment.

2.8 ELECTROPHORETIC EXTRACTION / PRECONCENTRATION

Due to the close relationship of this technique to capillary electrophoresis, many of the procedures followed in the original electrophoretic extraction experiments were the same as for normal CE experiments, including those discussed in Sections 2.7.1, 2.7.2, and 2.7.5–2.7.7 (i.e. electrode positioning, treatment of capillaries, determination of offset potential, control of high voltage power supply, etc.). The electrochemical cell described in Section 2.7.4 (see Figure 2.4) was suitable for these experiments. A hole was drilled in the bottom of the Faraday cage and through the top of the Plexiglas box housing the lead to the high voltage power supply to allow the capillary to be aligned vertically.

This setup allowed for the performance of what was essentially a quasi-CE experiment in a vertical configuration. There is no injection, the injection end of the capillary is simply placed in the sample solution, the separation voltage applied, and data acquisition started in the usual manner. A stepwise response is observed for each analyte arriving at the detector (rather than peaks as for CE). After each experiment, the capillary was rinsed with background electrolyte solution for at least 5 minutes.

Alumina particles (maximum particle size: 0.1 μm; Goodfellow – Oakdale, PA) were used as a convenient model system in place of soil particles for the initial experimentation.

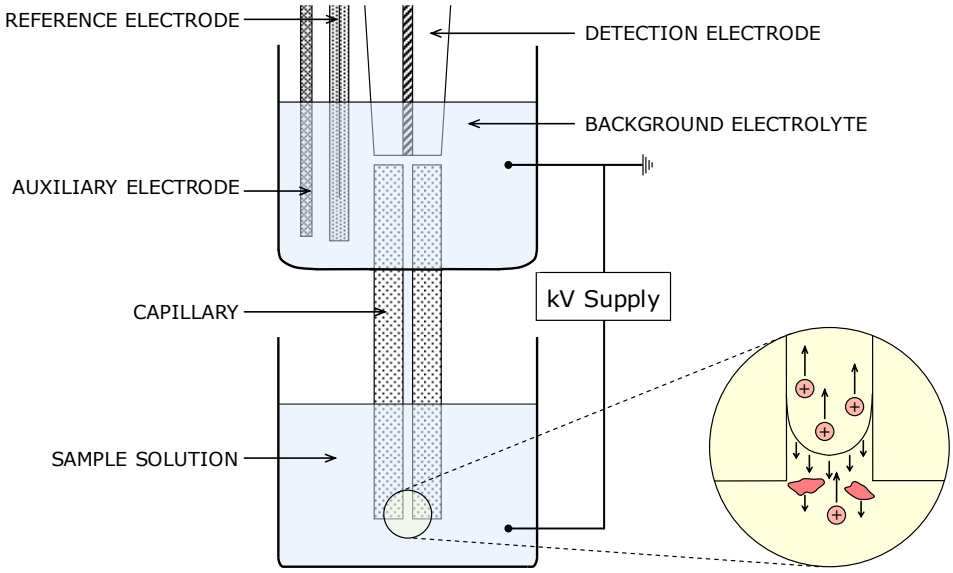

Figure 2.5 Electrophoretic extraction/preconcentration.

CHAPTER 3: INVESTIGATION AND OPTIMIZATION OF THE RCV DETECTION OF METALS AT GOLD ELECTRODES

3.1 FORWARD

The practical utility of any detection method depends to a large extent on the reproducibility of the response over time. At the same time, electrodes used for electrochemical detection have the tendency to change with time under normal experimental conditions: one example is electrode fouling by absorption of organic impurities or reaction products [81]. Electrodes must be reactivated periodically, either mechanically (by polishing) or electrochemically (by a series of potential pulses) to maintain a stable response.

In setups such as capillary electrophoresis, mechanical polishing of the electrode is not easily accomplished, requiring the removal of the electrode from the detection cell and realignment of the electrode at the detection end of the capillary. However, scanning or pulsing of the electrode potential during electrochemical detection can be accomplished without physical removal of the electrode and the accompanying time expenditure. With scanning or pulsing of the electrode potential during electrochemical detection, the difficulties associated with poisoning of the electrode surface are partially alleviated. For example, in the case of gold or platinum, application of positive potentials (in the oxide formation region) results in the oxidization and desorption of organic impurities [81].

Scanning into the oxide formation region is unnecessary for the detection of metals at gold, since the stripping peaks for the metals are at potentials more negative than the potentials for oxide formation [10]. However, it is not certain if scanning over a narrow potential range is as effective in keeping the electrode free of impurities. Thus, the inclusion of an electrode conditioning step – i.e. a series of potential pulses (positive

and/or negative) before the deposition step – should be investigated systematically, as it may improve the stability of the electrode response over time.

Some empirical knowledge regarding the limits (due to stability) of the electrode in various electrolytes has also been gained through previous work: however, these also require systematic experimentation.

3.2 ELECTRODE STABILITY

3.2.1 Underpotential Deposition of Cu at Au

The UPD of Cu on polycrystalline gold was briefly investigated (mainly for use in characterizing electrodes prior to kinetics experiments – see Chapter 4) although it is a well-studied system. Cyclic voltammograms recorded in a solution of 0.1 mol/L H_2SO_4 containing 1×10^{-5} mol/L Cu^{2+} are shown in Figure 3.1. The initial potential (positive of the region for Cu deposition) was always set to 600 mV, while the vertex potential was different for each CV curve (ranging from 100 mV to −350 mV in increments of 50 mV). A stripping peak – due to underpotential deposition of Cu – at approximately 150 mV in the reverse scan is evident in all cyclic voltammograms (see Figure 3.1, peak A). A second peak (at about −100 mV, see Figure 3.1, peak B), corresponding to bulk deposition, appears only as the vertex potential becomes more negative (at potentials less than −200 mV). These results agree qualitatively with other studies of Cu deposition on Au in the literature [36]. In addition, a gold wire was flame annealed and the tip of the wire was immediately touched to the copper deposition solution – cyclic voltammograms taken with this arrangement (not shown) also agreed with the results of Figure 3.1. Figure 3.2 illustrates the change in peak area of the Cu UPD peak with change in the vertex potential: the increase in CV charge levels off when the vertex potential becomes more negative than approximately −150 mV.

3.2.2 Stability of Electrode Response under Scanning Conditions

As mentioned previously, the potential region for metal UPD is negative of the region for oxide formation (see Section 3.3.1 for depictions of the response of various metals at Au). Two cyclic voltammograms at a gold electrode – one with a vertex potential before the region of oxide formation (A), and one over the entire potential region (B) – are shown in Figure 3.3. Scanning over a wide potential range (as in Figure 3.3 B) may

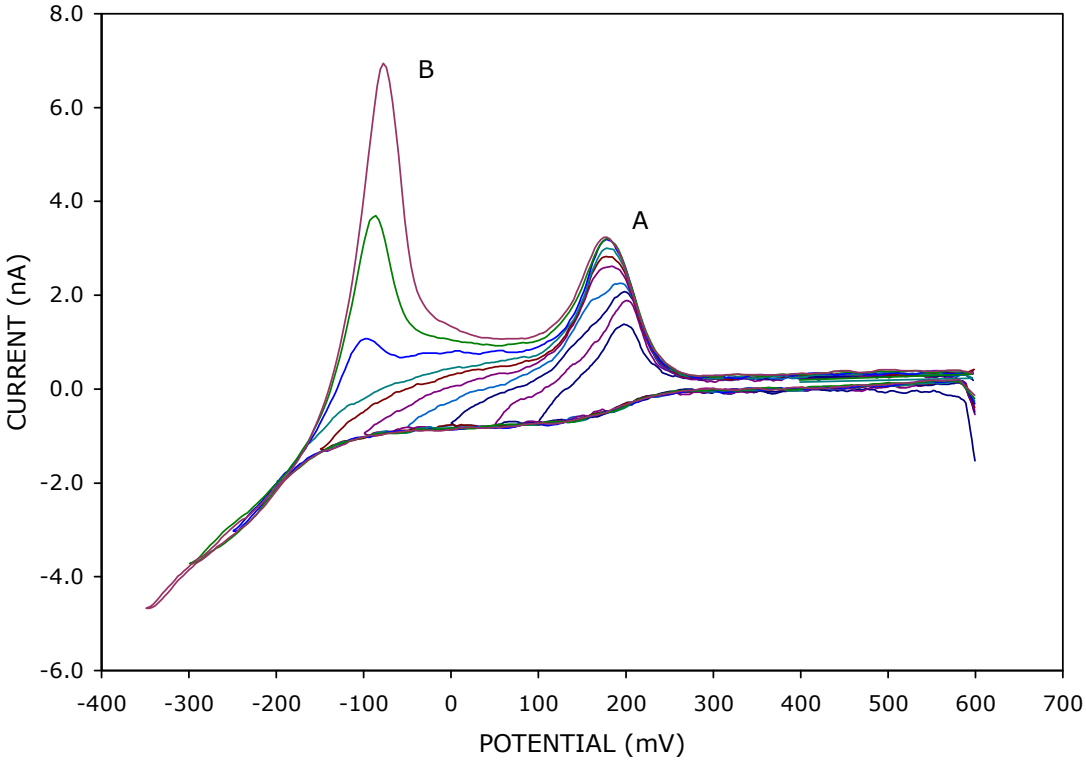

Figure 3.1 Cyclic voltammograms of Cu^{2+} [5×10^{-4} mol/L Cu^{2+} in 0.1 mol/L H_2SO_4] at a 25-μm Au electrode (Ag|AgCl reference, tungsten auxiliary). The sweep rate was 0.1 V/s, preelectrolysis time 0.5 s (at $E_{pc} = E_i = 600$ mV), and rest potential (applied between experiments) 800 mV. All scans began at positive potentials ($E_i = 600$ mV); however, vertex potentials of 100, 50, 0, −50, −100, −150, −200, −250, −300, −350, and −400 mV were used for the series of cyclic voltammograms shown. Each cyclic voltammogram in this graph (i.e. the cyclic voltammogram for each vertex potential) is the average of five separate cyclic voltammograms. Peak **A** is due to the underpotential deposition of Cu.

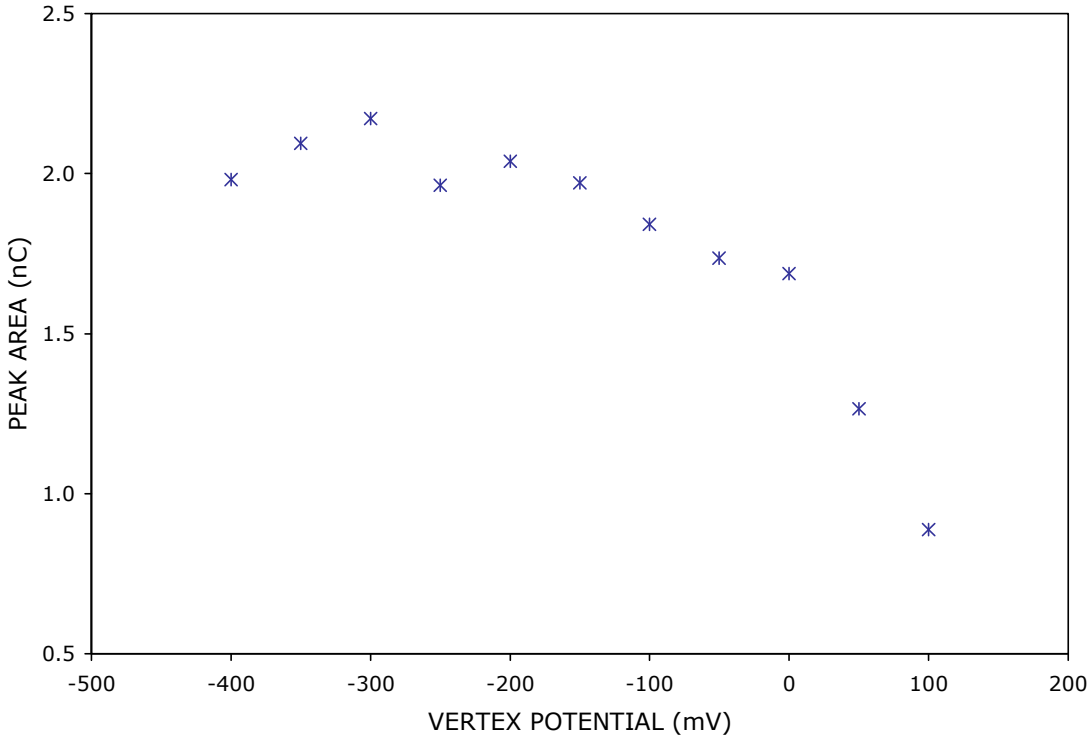

Figure 3.2 Variation in area of the Cu UPD peak (maximum at 150 mV, see Figure 3.1) with vertex potential, generated from the cyclic voltammograms shown in Figure 3.1.

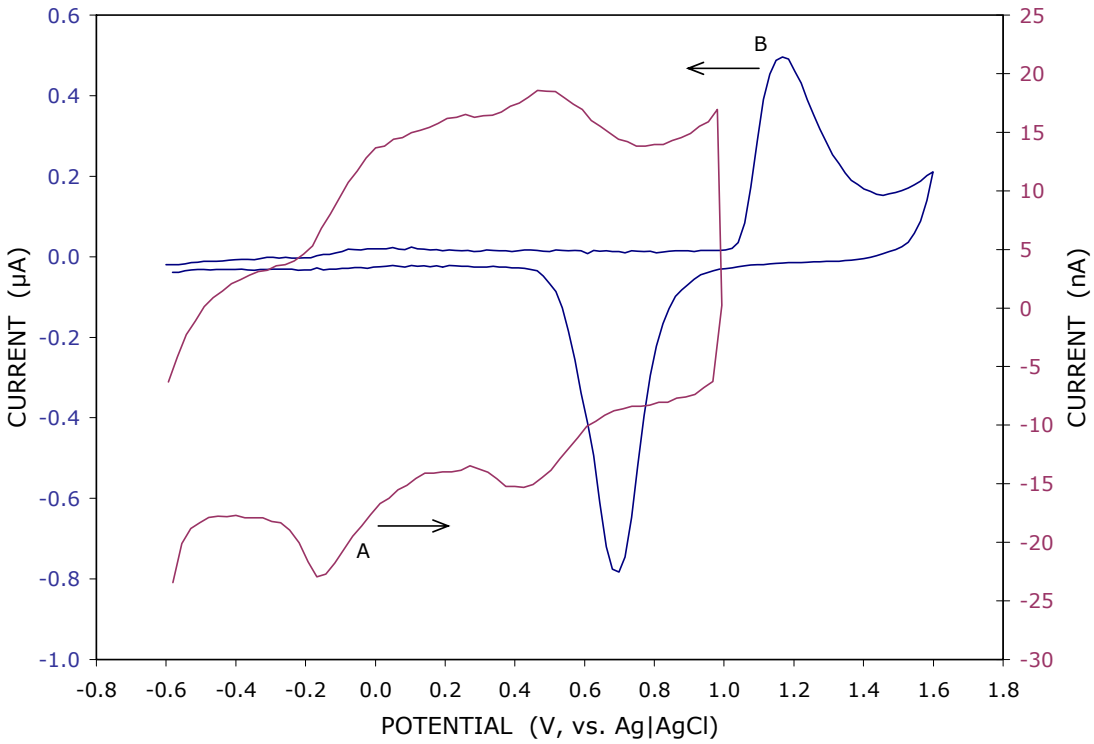

Figure 3.3 Individual cyclic voltammograms from one cycle of a repetitive cyclic voltammetry experiment. Both **A** and **B** were taken at a 25 μm Au electrode with an Ag|AgCl reference and tungsten auxiliary electrode in 0.1 mol/L H_2SO_4. The sweep rate for both CV curves was 20 V/s. **A** ("narrow" potential range): initial potential −600 mV, vertex potential 1000 mV; **B** ("wide" potential range): initial −600 mV, vertex 1600 mV. These cyclic voltammograms illustrate the potential ranges referred to in Figure 3.4. In **A**, the vertex potential is negative of the region in which oxide formation occurs, whereas in **B** the peaks for oxide formation and dissolution are included in the potential scan.

offer some improvement in electrode stability due to a decrease in electrode contamination by organic impurities; however, the response of most metals is confined to the potential region included in the narrow potential range (Figure 3.3 A). Furthermore, higher scan rates are accessible when scanning over the double layer region (Figure 3.3 A) due to the absence of the oxide formation/dissolution peaks (present in Figure 3.3 B) which are severely distorted at higher scan rates.

Figure 3.4 shows the results of three experiments in which a gold working electrode was subjected to different electrolyte/potential waveform conditions. The electrode was cycled for 1000 s intervals in either 0.1 mol/L sulfuric acid (top of Figure 3.4) or 0.5 mol/L sodium borate (bottom of Figure 3.4). In sulfuric acid, two different potential waveforms were investigated: cycling in the potential region before oxide formation (narrow potential range; initial potential −600 mV, final potential 1000 mV) or cycling over the entire potential range of the electrode, including the oxide formation region (wide potential range; initial potential −600 mV, final potential 1700 mV). Between these 1000 s (~17 min) periods of cycling, the solution was switched to 5×10^{-4} mol/L Cu^{2+} in 0.1 mol/L sulfuric acid to allow for scans to be used in the determination of the peak area associated with Cu UPD (as in Figure 3.1).

Analysis of the data presented for sulfuric acid in Figure 3.4 was done for the points indicated with either a cross (×) or plus (+) symbol superimposed on the data points. The relative standard deviation of the area of the Cu UPD peak was calculated by taking into account the deviation of each data point from the linear regression data (i.e. exactly as for a calculation of the relative standard deviation, but substituting the calculated peak area for the mean in the RSD equation). For the electrode which was cycled into the potential region of oxide formation (wide potential range) the RSD calculated in this manner was 9.3; whereas for the electrode which was cycled in a narrow potential range the RSD was 9.2. These results do not show any significant difference in performance. Thus, scanning exclusively in the region before oxide is entirely justified – there seems to be no advantage to using a wider potential range.

Although one would expect that scanning into the region of oxide formation would be beneficial in reducing electrode fouling due to adsorption of organic impurities, scanning the electrode continuously – over any reasonably wide potential region –

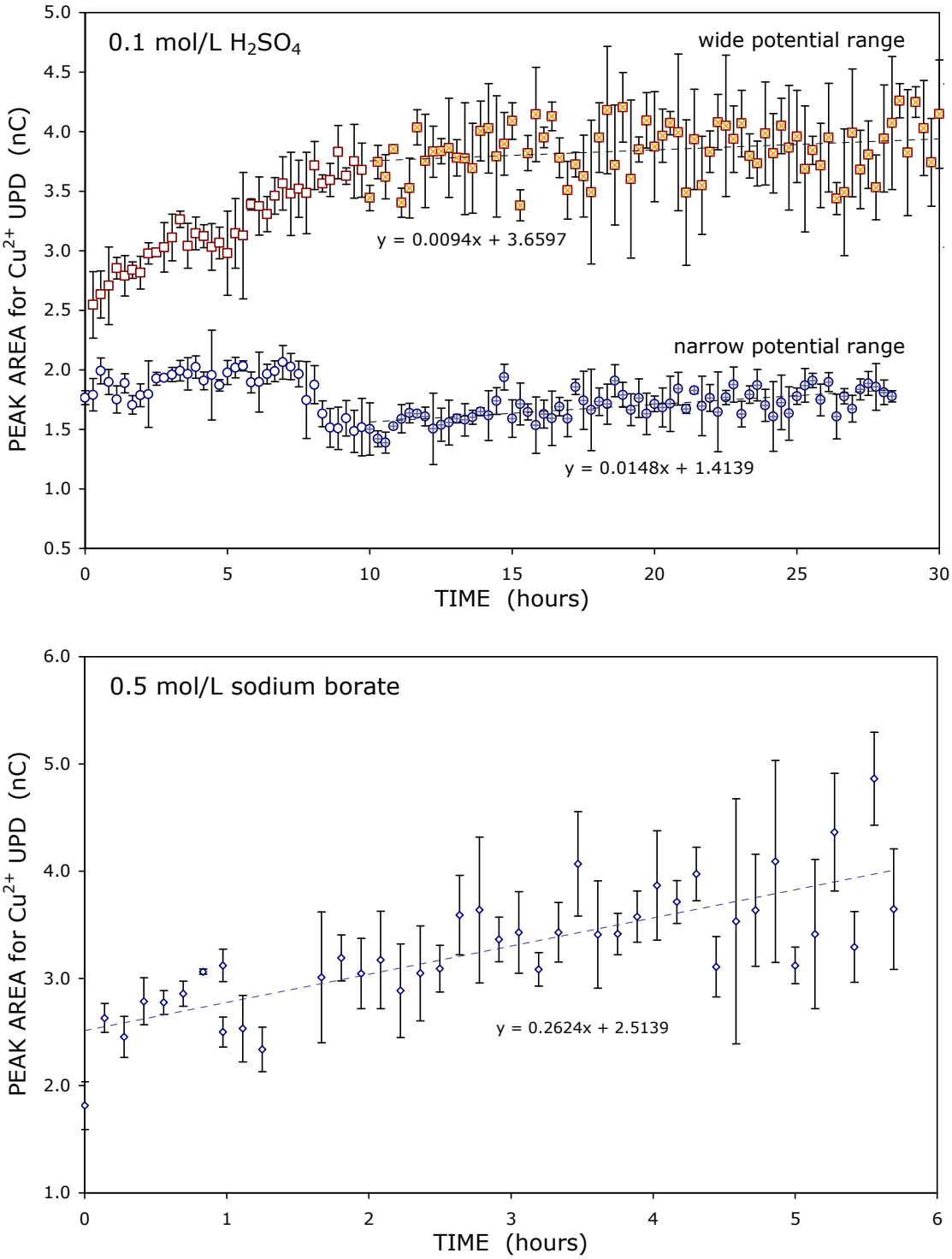

Figure 3.4 *(see legend next page)*

Figure 3.4 *(see previous page)*

Change in the Cu UPD peak area with time (measured from start of electrode scanning – i.e. continuous analysis) for three electrodes subject to scanning under different electrolyte/potential waveform conditions. In the top graph, the results in acidic solution are shown: ○ – 0.1 mol/L sulfuric acid, initial potential, $E_i = -600$ mV, vertex potential, $E_v = 1000$ mV (*before* region of oxide formation); □ – 0.1 mol/L sulfuric acid, $E_i = -600$ mV, $E_v = 1700$ mV (in region of oxide formation). In the bottom graph, the electrode was cycled in 0.5 mol/L sodium borate, $E_i = -1500$ mV, $E_v = 1250$ mV. In all cases, the working electrode was polycrystalline Au (25 μm) with an Ag|AgCl reference electrode, and the sweep rate was 20 V/s. The electrolyte was switched to a solution of 5×10^{-4} mol/L Cu^{2+} in 0.1 mol/L sulfuric acid between scanning for determination of the Cu UPD peak area. The error bars represent the standard deviation of the determination of peak area.

appears to be just as effective. Consider that a sample solution or even the supporting electrolyte may contain various surface active compounds which could contaminate the electrode. For each of these compounds, there are characteristic potential regions where the adsorption process is thermodynamically favourable or unfavourable. For example, negatively charged surfactants are most strongly adsorbed at potentials positive with respect to the zero charge potential (E_{pzc}), but are readily desorbed at negative potentials (when the electrode surface also has a negative charge). The opposite occurs for positively charged surfactants, but in the case of neutral surfactants, adsorption is spontaneous around E_{pzc} and desorption occurs at either positive or negative potentials (provided that the applied potential is sufficiently removed from the zero charge potential). When the electrode is cycled over a significantly large potential range, the electrode potential passes through regions where impurities would undergo spontaneous desorption (regardless of whether they are positive, negative or neutral), even if the electrode passes through this potential region favourable for spontaneous desorption for a very short time. This phenomenon is clearly illustrated by desorption of metals accumulated on the electrode surface by the UPD process (which is simply another form of adsorption): this will be discussed further in Section 3.4.1.

In the sodium borate electrolyte, the duration of the experiment shown in Figure 3.4 (bottom) was much shorter than in sulfuric acid, due to the short lifetime of the gold electrode in this solution. Further experimentation involved trials in which both the Cu UPD peak area and capacitance were monitored (in sodium borate): two of these experiments are shown in Figure 3.5. From this data, it can be seen that the double layer capacitance of the electrode follows the same trend as the area of the Cu UPD peak. This is easily explained if the upward drift in both the Cu UPD peak area and capacitance reflect an actual increase in the microscopic surface area of the electrode: both the Cu UPD peak area and the double-layer capacitance are expected to increase with surface area of the electrode. It is possible that with repeated cycling in the sodium borate solution, some etching or dissolution of the surface of the Au occurs.

Another experiment (not shown here) was carried out involving repeat determinations of Cu UPD peak area (as in the experiment described above) after intervals in which the solution was switched to sodium borate with constant electrode

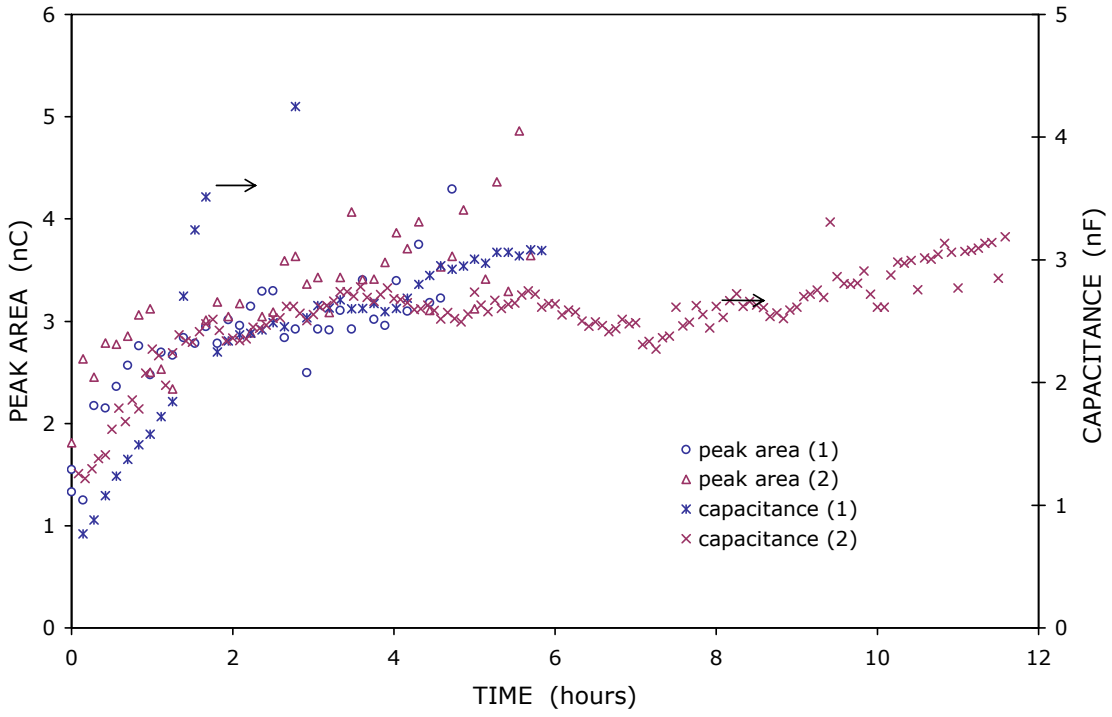

Figure 3.5 Changes in Cu UPD peak area and capacitance with time for two separate trials of a 25-μm Au electrode in 0.5 mol/L sodium borate solution, $E_i = -1500$ mV, $E_v = 1250$ mV. The electrolyte was switched to 5×10^{-4} mol/L Cu^{2+} in 0.1 mol/L sulfuric acid between scanning (500 s interval) for determination of the Cu UPD peak area. Capacitance was determined using the current in the double layer region of a cyclic voltammogram in 0.5 mol/L sodium borate.

potential applied – i.e. with no cycling. In this case there was no appreciable increase in the Cu UPD peak area over the course of the experiment, suggesting that the any changes in the Au electrode with time are due to the potential cycling in the sodium borate solution.

A final experiment involved scanning the Au electrode in either sodium borate or sulfuric acid, eliminating the switching between the electrolyte solution and the solution containing Cu^{2+}. Instead of using the Cu UPD peak area as an indicator of the changing electrode surface, the capacitance of the electrode was calculated from determination of the average current in the double-layer region of the cyclic voltammogram. Results are shown in Figure 3.6. The jump in the capacitance at about 25 hours in the sulfuric acid solution was due to an air bubble at the surface of the electrode that was subsequently dislodged.

According to these results it should be possible to use an Au electrode for detection for at least 24 hours in sulfuric acid solutions without significant degradation in the electrode performance. By comparison, the performance of the Au electrode is not stable in basic solution, where there is a marked variation in the response of the electrode over time, possibly due to gradual dissolution or pitting of the Au surface while scanning (as evident from the apparent increase in electrode area of Au in basic solutions, see Figure 3.5).

These observations were made under some slight variations of the experimental parameters for optimized RCV detection under CE conditions. For actual experiments involving CE/ECD, higher scan rates are applied to the electrodes. Furthermore, the electrode is exposed to various metals, not only Cu: although in CE this exposure is short and interrupted by long periods in which the only species present are those of the background electrolyte. Despite the shortcomings, these experiments should be somewhat indicative of the reasonably stable response of Au electrodes in acidic solutions over time for detection of metals by RCV.

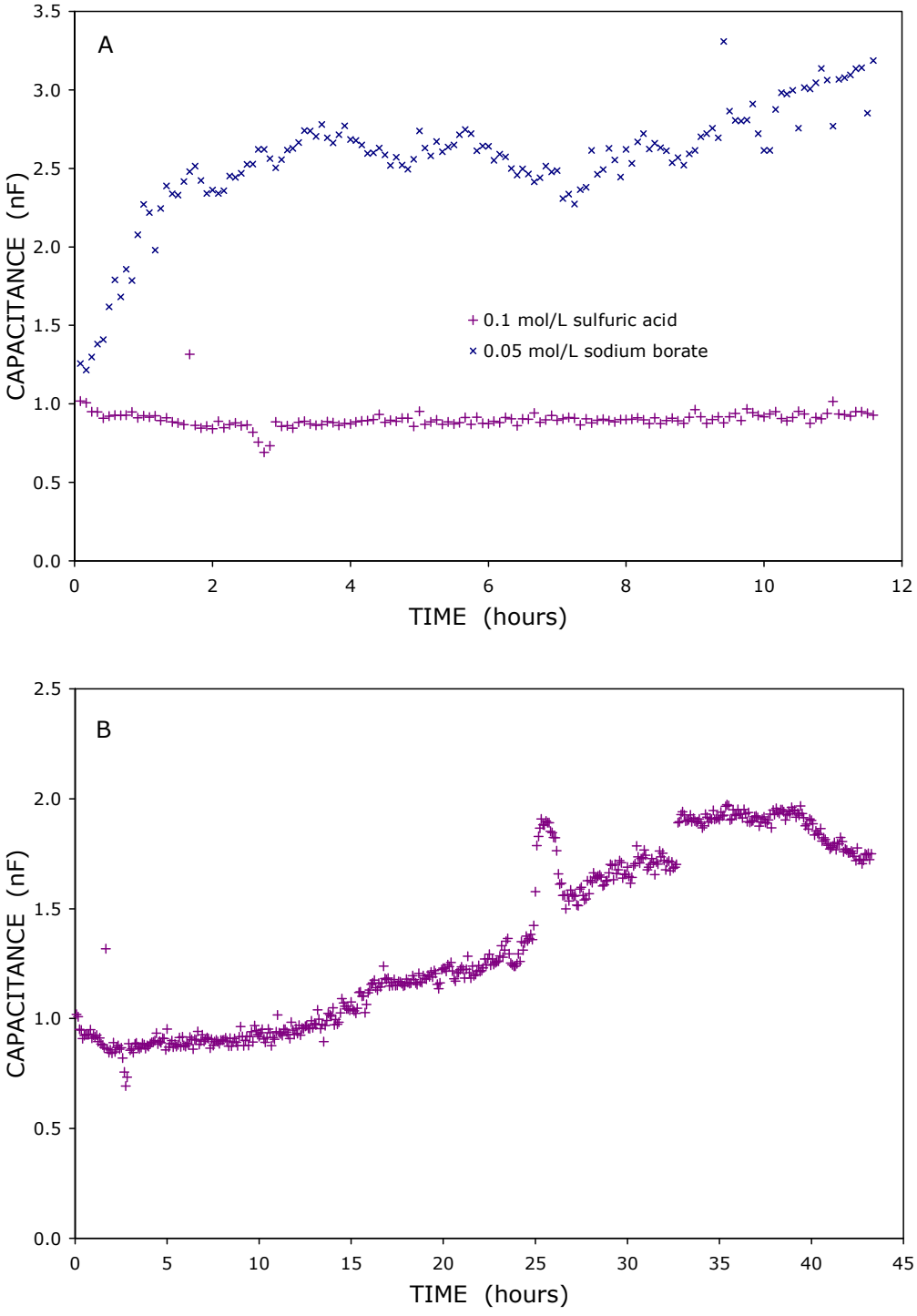

Figure 3.6 Change in double-layer capacitance with time for a 25-μm Au electrode in sulfuric acid and sodium borate. Experimental conditions: sulfuric acid, E_i = −500 mV, E_v = 1600 mV; sodium borate, E_i = −1500 mV, E_v = 1300 mV; Ag|AgCl reference electrode; sweep rate 20 V/s (for both trials). In B the full time scale of the experiment in sulfuric acid is shown (>40 hours).

3.2.3 Electrode Stability with and without Conditioning

An attempt was made to improve the stability of the electrode response by inclusion of a positive conditioning pulse before the CV scan. Figure 3.7 depicts two almost-equivalent generic potential waveforms: with (Figure 3.7 A) and without (B) an electrode conditioning step. With the inclusion of electrode conditioning, the triangular CV waveform and preconcentration step is preceded by up to three potential pulses ($E_{cond,\,1}$, $E_{cond,\,2}$, $E_{cond,\,3}$). In the potential waveform shown in Figure 3.7 A, the CV scan does not extend to the potential region where oxide formation occurs: however, a positive potential pulse (for conditioning) is set well into the region of oxide formation. This positive potential pulse should allow for desorption of organic impurities at the electrode surface before metal deposition (at a negative potential). Other combinations of potential pulses are also possible between CV scans: however, only the one illustrated in Figure 3.7 is investigated here.

Repeated injections (FIA) of 1×10^{-5} mol/L Pb^{2+} were done at a 50-μm Au electrode with and without a two-pulse electrode conditioning scheme applied. In both cases, the initial potential, E_i, was −500 mV and the vertex potential, E_v, was 1200 mV; however, electrode conditioning potential pulses were included [20 ms at 1700 mV ($E_{cond,\,1}$) followed by 20 ms at −600 mV ($E_{cond,\,2}$)] in the one set of experiments. Otherwise the potential waveforms were identical.

The results of these experiments are shown in Figure 3.8. There is a definite drift for the two sets of data obtained *with* electrode conditioning (slopes of 2×10^{-3} and -1×10^{-3} from linear regression data, compared to 2×10^{-4} and -3×10^{-4} without electrode conditioning). However, there is quite a lot of scatter in the data in all cases. Table 3.1 shows a comparison of the relative standard deviations of all four sets of data (over the first twenty-five injections as well as over the entire data range).

It should be noted that since the second conditioning potential applied to the electrode ($E_{cond,\,2}$) is in a region where the deposition of metals occurs, this increases the time available for metal deposition. However, since the preconcentration time is 300 ms and $E_{cond,\,2}$ is applied for only 20 ms, this represents an increase of less than 7 per cent, which is not expected to be of significance. Actually, in Figure 3.8 a slight decrease in

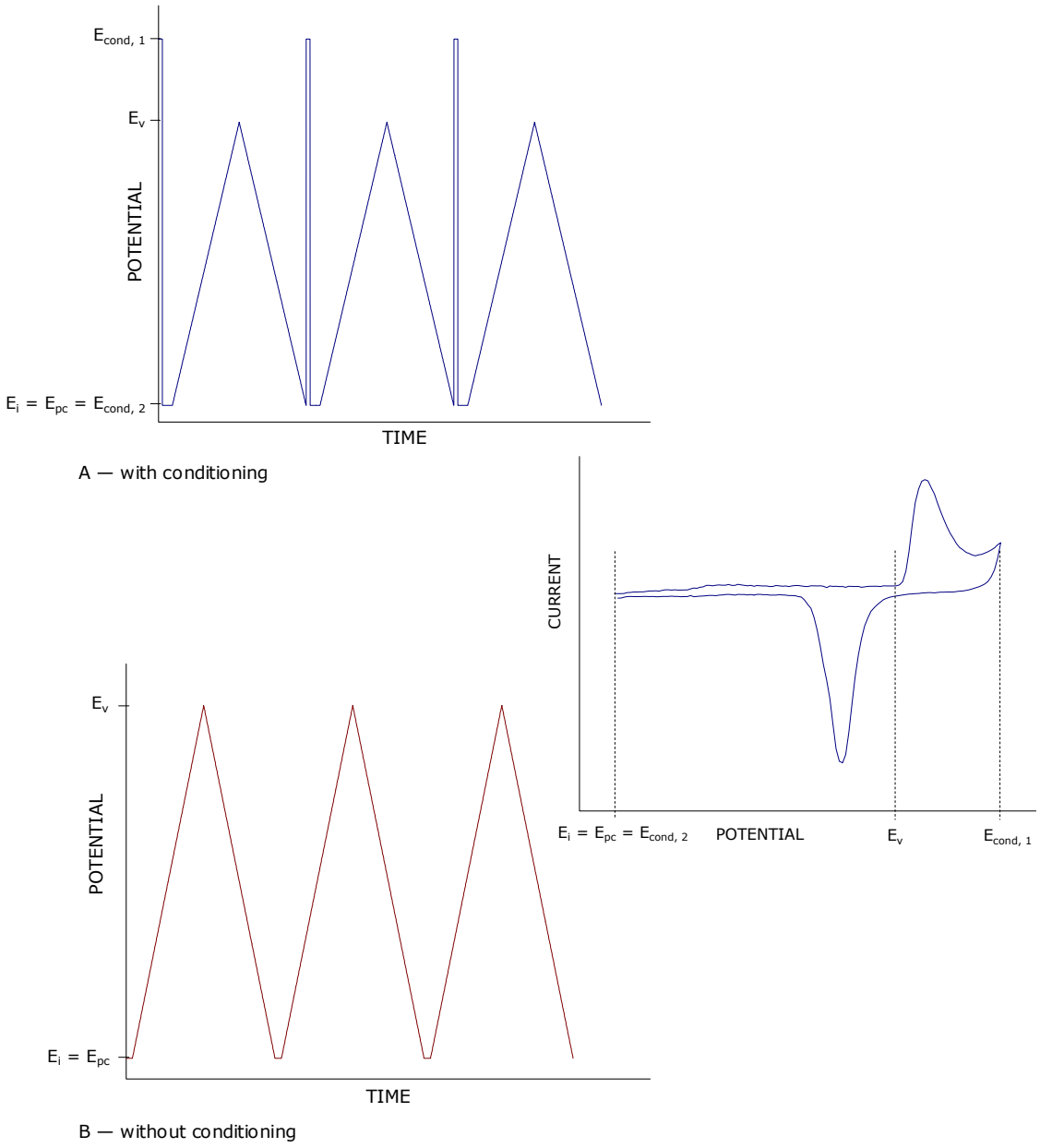

Figure 3.7 Generic potential waveforms for repetitive cyclic voltammetry, with (**A**) and without (**B**) electrode conditioning (not to scale). The inset (to the right) shows typical choices of the initial, vertex, preconcentration and conditioning potentials superimposed on a cyclic voltammogram (at Au). Note that the CV scan portion of the potential waveform does not extend into the potential region of oxide formation in either case.

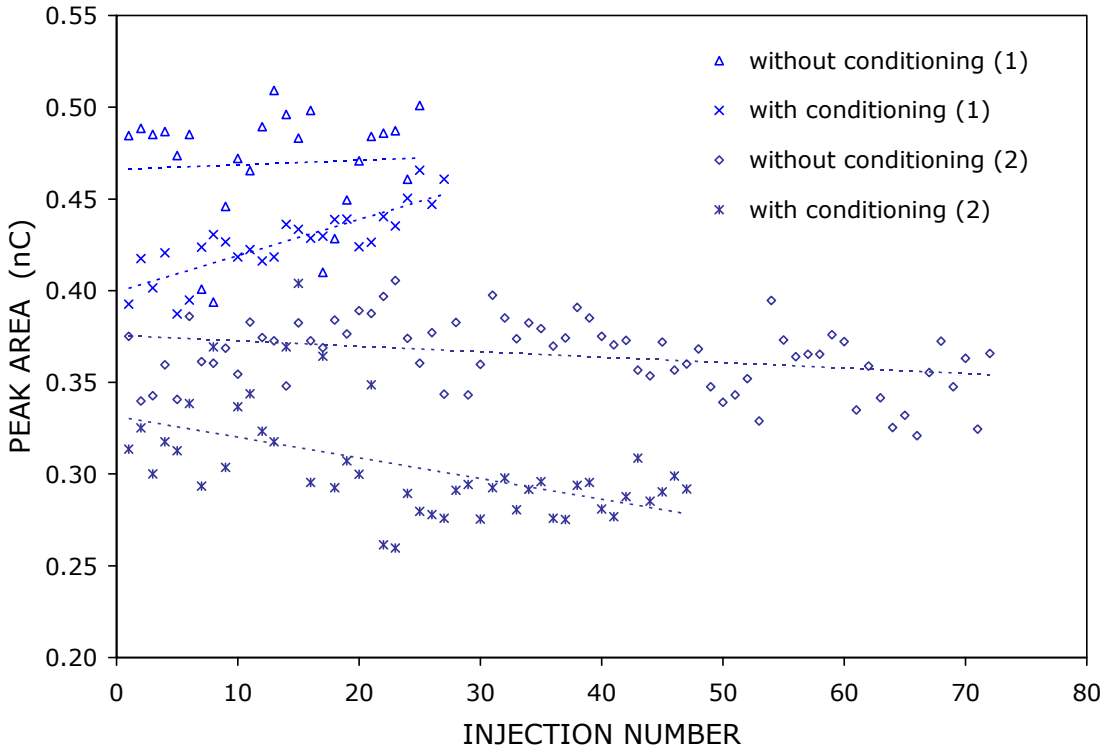

Figure 3.8 Repeated injections of 10^{-5} mol/L Pb^{2+} under flow injection conditions in 1 mol/L CH_3COOH. Initial potential, $E_i = -500$ mV; vertex potential, $E_v = 1200$ mV; preconcentration potential, $E_{pc} = -500$ mV; sweep rate 100 V/s; preconcentration time 0.3 s. Electrode conditioning pulses were applied for 20 ms at 1700 mV, followed by 20 ms at −600 mV (for the series with conditioning only). Working electrode 50 μm Au; Ag|AgCl reference. Integration (for generation of the signal) was done in the range between 0 and 300 mV.

	WITH CONDITIONING		WITHOUT CONDITIONING	
	TRIAL 1	TRIAL 2	TRIAL 1	TRIAL 2
STANDARD DEVIATION	*0.019*	*0.030*	*0.031*	*0.019*
AVERAGE	*0.43*	*0.30*	*0.47*	*0.36*
RSD	*4.4*	*9.9*	*6.7*	*5.2*
*STANDARD DEVIATION	*0.018*	*0.035*	*0.031*	*0.017*
*AVERAGE	*0.42*	*0.32*	*0.47*	*0.37*
*RSD	*4.2*	*10.9*	*6.7*	*4.7*

*over first 25 injections only

Table 3.1 A summary of the analysis of the data depicted in Figure 3.8: relative standard deviation of two independent trials involving stability of the response of an Au electrode to injections of 10^{-5} mol/L Pb^{2+} (repetitive cyclic voltammetry detection; potential waveforms with and without conditioning).

signal relative to the results without conditioning is apparent, rather than any enhancement of response.

The results of these two attempts to investigate the effects of electrode conditioning in terms of the stability of the electrode response are inconclusive. However, there is not expected to be any benefit in the inclusion of conditioning pulses in the detection waveform, since the electrode is scanned over a significant potential range (as discussed in Section 3.2.2). The inclusion of conditioning pulses in amperometric detection would, however, be expected to be more beneficial, since there is no electrode cycling.

3.3 SCOPE OF REPETITIVE CYCLIC VOLTAMMETRY DETECTION OF METALS AT GOLD

3.3.1 Detection of Various Metals at Gold using Repetitive Cyclic Voltammetry (RCV)

The following results exhibit the versatility of the electrochemical detection of metals at Au using repetitive cyclic voltammetry (described in Section 2.3.4). Typical results from flow-injection experiments involving the detection of metals (as aqueous ions) are depicted in Figure 3.9, which shows the response of Au to solutions containing Cu^{2+}, Ni^{2+}, Zn^{2+} and Pb^{2+} in 1 mol/L acetic acid (pH ~ 2.4) under flow-injection conditions. The cyclic voltammograms shown include both the CV without metal present in solution and the progressive response of the electrode to the injection of the metal-containing solution over the time of a single injection (these CVs are superimposed).

In 0.5 mol/L CH_3COOH and 0.5 mol/L CH_3COONa (pH ~ 4.6) responses were obtained for Co^{2+}, Mn^{2+} and Ni^{2+} (see Figure 3.10). The observed peaks for Co^{2+} and Mn^{2+} were not visible in acetic acid. Both Co^{2+} and Mn^{2+} exhibit underpotential deposition peaks at very negative potentials (see Figure 3.10 A, B and C). The negative potential range accessible at gold is limited by the onset of reduction of the hydronium ions present in solution. A likely explanation for the absence of a response for Co^{2+} and Mn^{2+} in acetic acid is that as the pH is lowered, more hydronium ions are present, and hydrogen generation occurs before a potential negative enough for deposition of Co^{2+} or Mn^{2+} can be reached.

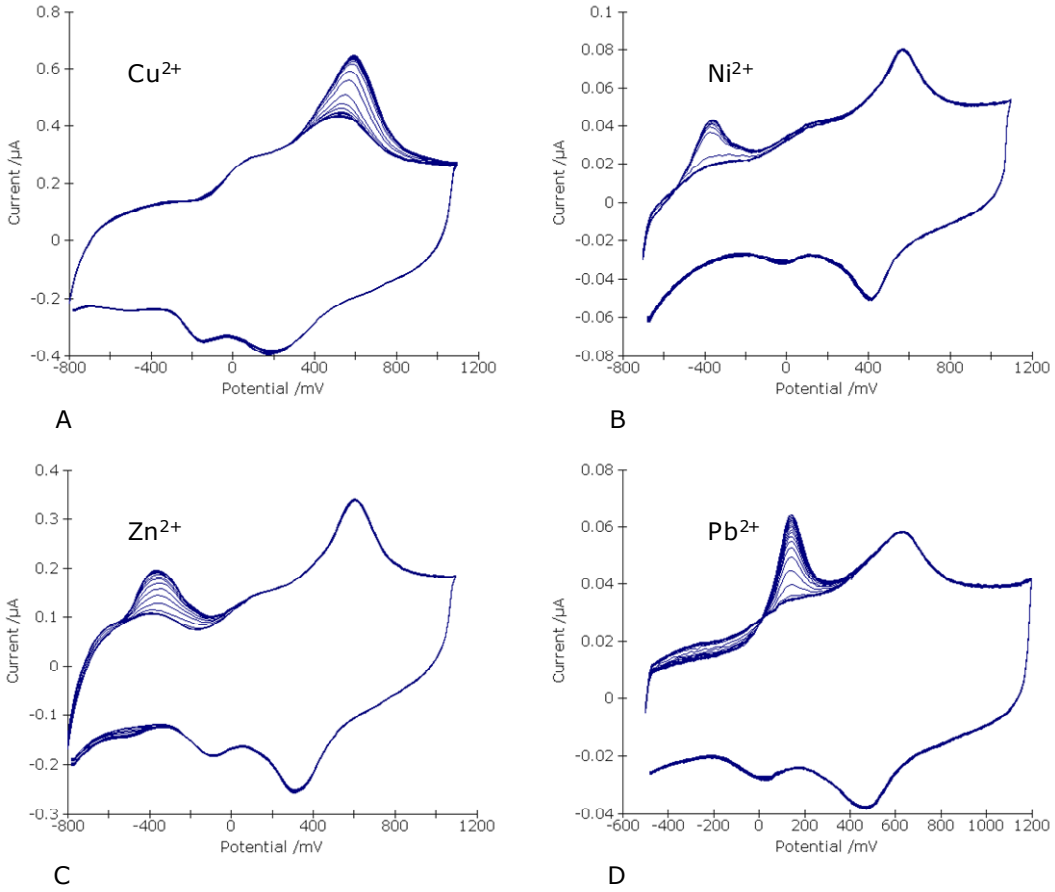

Figure 3.9 Results for the detection of metals by RCV using flow-injection analysis. All experiments were done in 1 mol/L CH_3COOH at a 50-μm Au working electrode and Ag|AgCl reference electrode. The sweep rate was 100 V/s and the preconcentration time 0.3 s. **A**: 4×10^{-5} mol/L Cu^{2+}; **B**: 6×10^{-6} mol/L Ni^{2+}; **C**: 5×10^{-5} mol/L Zn^{2+}; **D**: 1×10^{-5} mol/L Pb^{2+}.

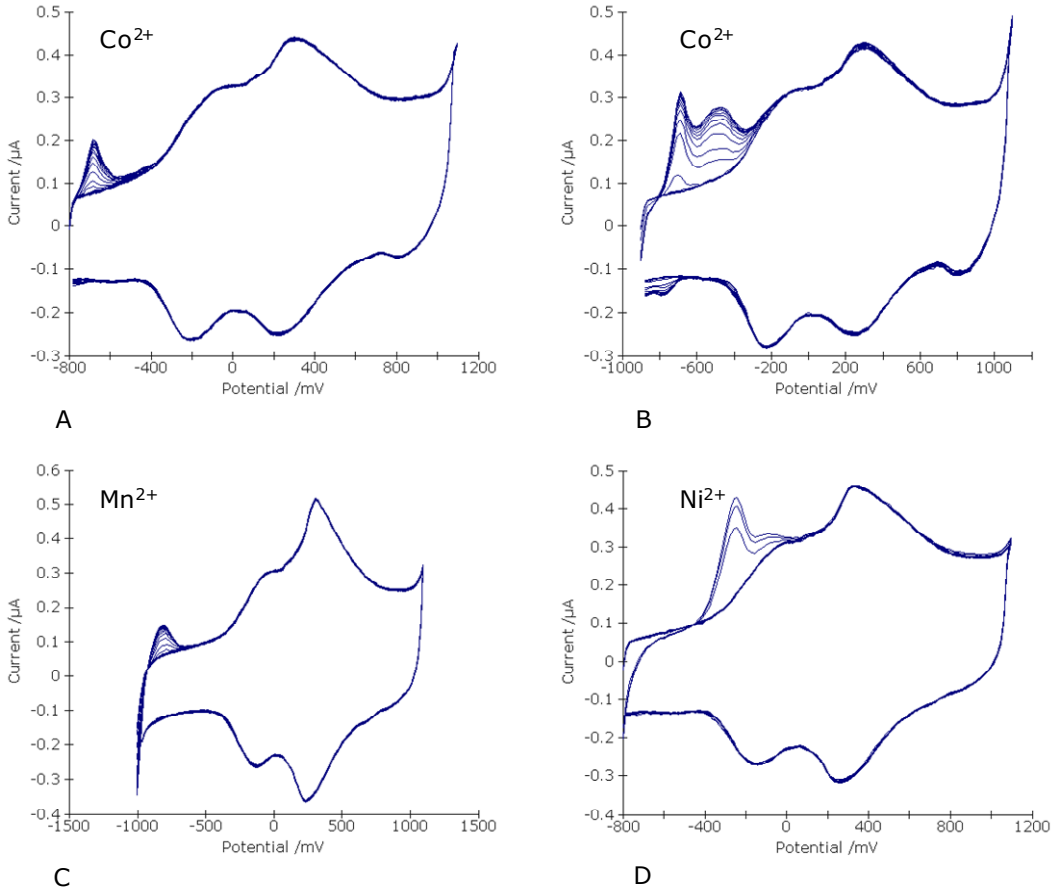

Figure 3.10 Results for the detection of metals by RCV using flow-injection analysis. All experiments were done in 0.5 mol/L CH_3COOH and 0.5 mol/L CH_3COONa at a 50-μm Au working electrode and Ag|AgCl reference electrode. The sweep rate was 100 V/s and the preconcentration time 0.3 s. **A**: 5×10^{-5} mol/L Co^{2+}; **B**: 1.5×10^{-4} mol/L Co^{2+}; **C**: 7×10^{-5} mol/L Mn^{2+}; **D**: 1×10^{-4} mol/L Ni^{2+}.

The appearance of the response for a particular metal can change quite dramatically with concentration, as shown by the inclusion of results for two different concentrations of Co^{2+} (Figure 3.10 A and B). Results for several other metals are not shown: in particular, the detection of Cd^{2+} and Tl^{+} was possible both in acetic acid and acetic acid/sodium acetate solutions. In addition, detection of As was possible in the form of AsO_2^- (results are shown in Figure 3.11).

As illustrated by these results, there is an impressive array of metals that are easily detected using repetitive cyclic voltammetry at gold over the potential range of approximately −800 to 1200 mV vs. Ag|AgCl, negative of the region for oxide formation. The intended application of RCV detection at gold is in CE systems where metals are separated before reaching the detector: however, consideration of these results suggests that simultaneous detection of certain combinations of metals (without separation) would also be possible, given sufficient peak separation in the potential domain.

Particularly interesting and somewhat unexpected is the possibility of the analysis of manganese at gold (Figure 3.10 C). Manganese is difficult to detect at mercury due to limited solubility and the large reduction potential required. Although the use of boron-doped diamond has been reported for detection of manganese [82] the determination of manganese using anodic stripping voltammetry at polycrystalline gold electrodes provides another alternative.

3.3.2 Calibration Curves and Detection Limits of Metals at Au using Flow-Injection Analysis (FIA) and RCV Detection

As mentioned previously, the response in RCV detection is generated by integration over a user-specified potential region (see Section 2.3.4 and [78]) . Selection of a potential range depends on the metal of interest, since (as seen in the previous section) each metal exhibits a characteristic potential-dependent response.

The selection of a potential range for generation of the response can have unexpected consequences, as illustrated in Figure 3.12. This figure depicts two possible integration regions for the analysis of the calibration curve data (bottom left). The background-subtracted cyclic voltammograms (bottom right) show two peaks for Ni^{2+} in the potential domain. The top of Figure 3.12 shows calibration curves generated using

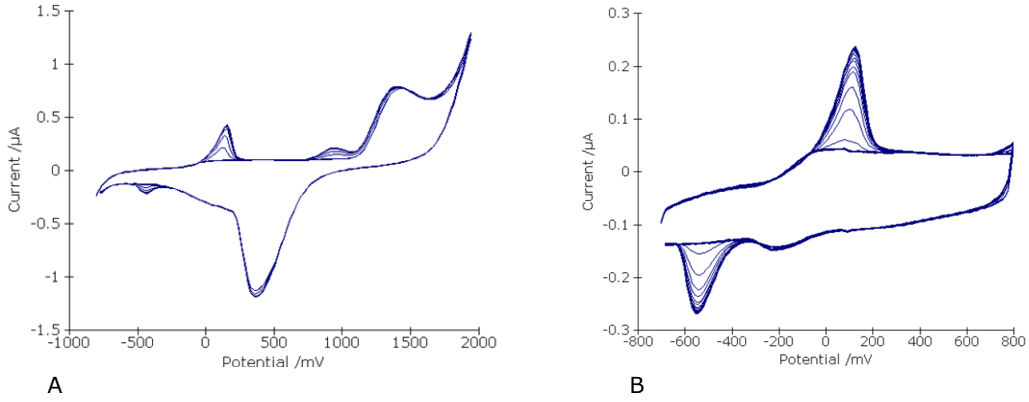

Figure 3.11 Results for detection of AsO_2^- by RCV under flow-injection analysis conditions. 50 μm Au working electrode; Ag|AgCl reference electrode; preconcentration time 0.3 s. **A**: 8×10^{-5} mol/L AsO_2^- (1 mol/L CH_3COOH); sweep rate 20 V/s; **B**: 1×10^{-5} mol/L AsO_2^- (1 mol/L CH_3COOH); sweep rate 40 V/s.

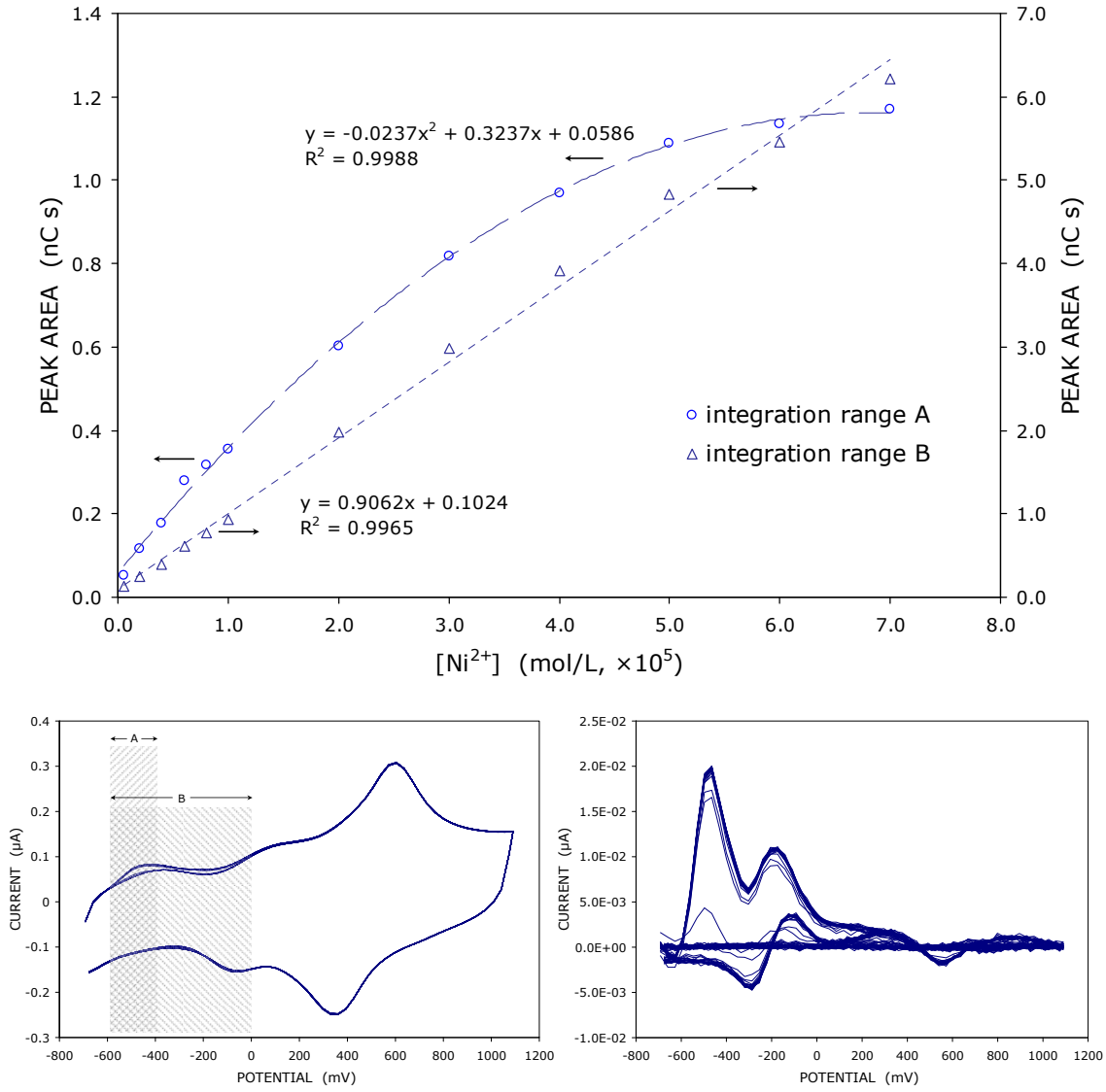

Figure 3.12 Calibration curves for Ni^{2+} in 1 mol/L CH_3COOH (FIA): 50 μm Au working electrode; Ag|AgCl reference; sweep rate 100 V/s; preconcentration 0.3 s at −700 mV; initial potential −700 mV; vertex potential 1100 mV; conditioning pulses of 1800 mV and −700 mV (20 ms at each). The top figure includes calibration curves generated from the same runs, but for integration ranges of −600 to −400 mV (**A**) and −600 to 0 mV (**B**). The two potential regions are indicated in the shaded regions on the bottom left, which shows overlapping cyclic voltammograms for one injection of 6×10^{-6} mol/L Ni^{2+}. The same cyclic voltammograms, this time with the background subtracted, are included on the bottom right.

the same data set, but analyzed with integration over the two different potential regions depicted in the bottom left of Figure 3.12. These two calibration curves are obviously quite different: there is a leveling-off of the first curve (integration over −600 to −400 mV) at higher concentrations, whereas the second curve (integration from −600 to 0 mV) is much more linear. The detection limits for Ni^{2+} (determined as discussed below) for both integration ranges are not appreciably different: 8×10^{-8} mol/L for integration over −600 to −400 mV and 5×10^{-8} mol/L for integration from −600 to 0 mV. A linear response is observed over a larger concentration region for the wider integration range since integration over −600 to −400 mV does not include the entire response of the electrode to the Ni at the electrode surface.

Calibration curves were done for various metals (in 1 mol/L CH_3COOH or 0.5 mol/L CH_3COOH / 0.5 mol/L CH_3COONa) and are shown below in Figure 3.13. Deviation from linearity at relatively low concentrations is obvious in most cases. At polycrystalline electrodes, multiple UPD peaks are observed at increasing surface coverage (as an example, see the response for Co^{2+} in Figure 3.10 A and B). For this reason, the calibration curves are strongly dependant on the integration range used to calculate the response ΔQ (as defined by Equation 2.1 in Section 2.3.4). Non-linearity can (to a certain extent, as discussed above) be corrected by use of a wider potential range, thus encompassing more of the changes due to the adsorption of the metal at higher concentrations. However, higher selectivity can be achieved by selection of a narrow integration range. For capillary electrophoresis, a wide integration range for generation of the response is preferred initially since this gives a response for a wide range of analytes: if necessary, the data can be reanalyzed using the appropriate integration range to give a better response for any one particular analyte.

Since the underpotential deposition of metals on gold is a surface process, it is expected that the response will be proportional to the surface coverage of the metal at the electrode. If enough time is available for the surface coverage of the metal to reach equilibrium, an adsorption isotherm such as the Langmuir isotherm can be used to explain the shape of the calibration curves. When the thermodynamics of adsorption dictate the electrode coverage, a linear calibration curve is expected only for very small surface coverages (<5%) and the electrode will be saturated as the analyte fills the

adsorption sites and coverage reaches a full monolayer. However, this is a limiting case. If no equilibrium is reached on the timescale of the experiment, the electrode coverage may be controlled by either the rate of mass transport to the electrode or kinetics of the interfacial adsorption step [78]. In the former case (i.e. electrode coverage dependant on mass transport) a linear calibration curve is expected only up to the point when full electrode coverage occurs during the preconcentration period. To elucidate to what extent each of these factors (thermodynamics of adsorption, rate of mass transport and/or kinetics) contributes to the shape of the calibration curve for a particular metal under specific experimental conditions – including, but not limited to, sweep rate, concentration, preconcentration time and deposition potential – simulation of the system under consideration would be helpful.

From a purely analytical perspective, useful quantitative information can be obtained from a calibration curve regardless of the concentration dependence of the response. Also, for RCV detection, experimental conditions (particularly the preconcentration time and integration range) can be adjusted to obtain a reasonably linear response over a considerable concentration range.

Detection limits of the metals depicted in Figure 3.13 were calculated using Equation 3.1, where s_b is the standard deviation of the blank.

$$c_{dl} = \frac{3s_b}{m} \tag{3.1}$$

Under the above conditions and using the data points from the lower concentrations (linear portion) of each calibration curve to calculate the slope m (see Figure 3.13) the following detection limits were obtained: Mn^{2+}, 2×10^{-6} mol/L; Co^{2+}, 6×10^{-7} mol/L; Pb^{2+}, 3×10^{-7} mol/L; Cu^{2+}, 3×10^{-7} mol/L; and AsO_2^-, 6×10^{-8} mol/L. These are not particularly impressive, but conditions were not optimized for individual metals (for instance, a sweep rate of 100 V/s was used in most cases, whereas it is known that metals exhibit optimal responses at different sweep rates [10]).

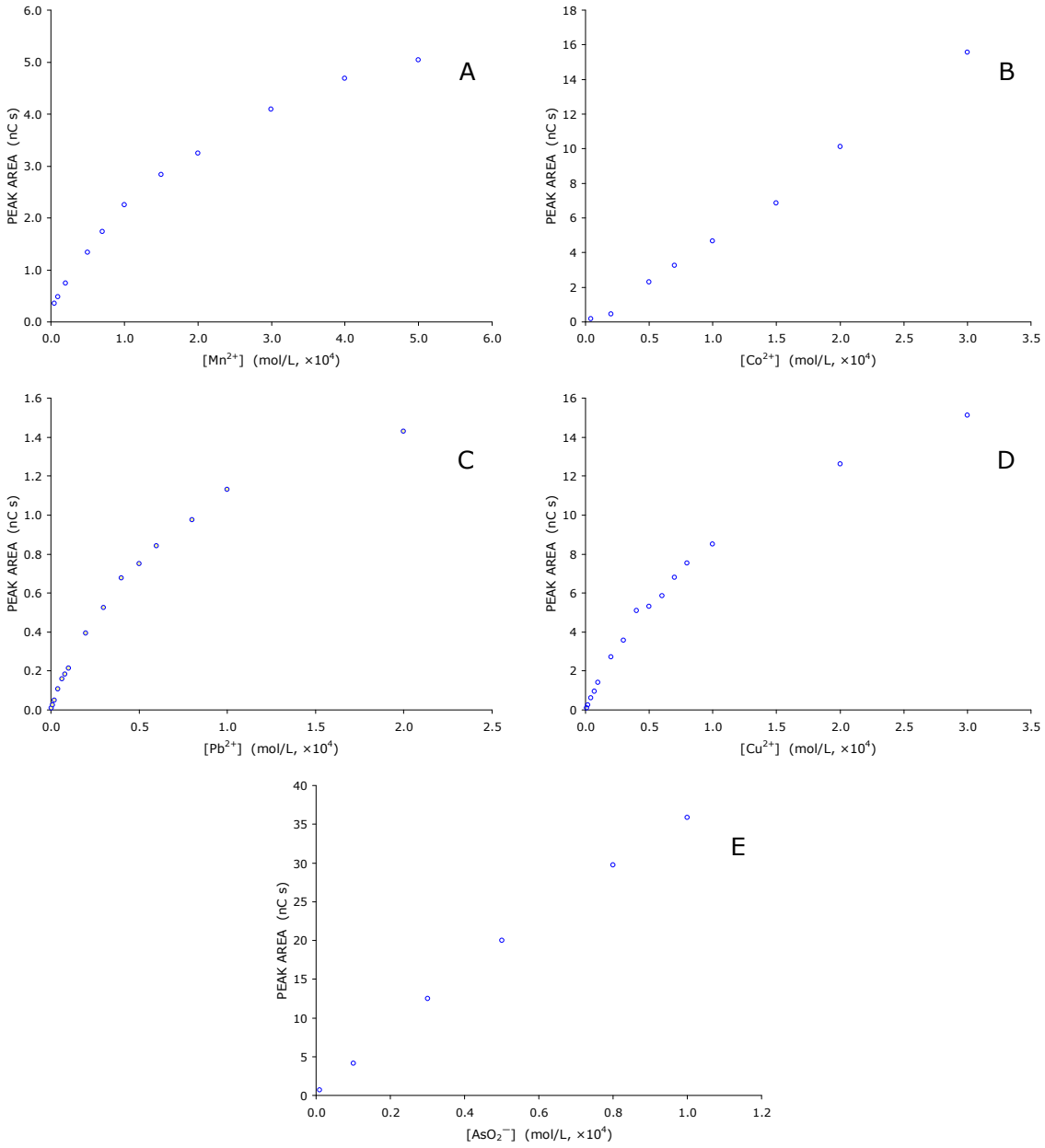

Figure 3.13 Calibration curves for (**A–E**): Mn^{2+}, Co^{2+}, Pb^{2+}, Cu^{2+} and AsO_2^-; 50 μm Au working electrode; Ag|AgCl reference. **A, B**: 0.5 mol/L CH_3COOH and 0.5 mol/L CH_3COONa background electrolyte; sweep rate 100 V/s; preconcentration time 0.3 s; **C, D**: background electrolyte 1 mol/L CH_3COOH; sweep rate 100 V/s; preconcentration time 0.3 s.

Figure 3.13 *(see previous page)*

A: Mn^{2+}; E_i = −1000 mV; E_v = 1100 mV; E_{pc} = −1000 mV; $E_{cond,\ 1}$ = 1500 mV; $E_{cond,\ 2}$ = −1000 mV; integration between −900 and 0 mV.

B: Co^{2+}; E_i = −900 mV; E_v = 1100 mV; E_{pc} = −900 mV; $E_{cond,\ 1}$ = 1500 mV; $E_{cond,\ 2}$ = −900 mV; integration between −800 and 0 mV.

C: Pb^{2+}; E_i = −600 mV; E_v = 1000 mV; E_{pc} = −600 mV; $E_{cond,\ 1}$ = 1700 mV; $E_{cond,\ 2}$ = −600 mV; integration between 0 and 200 mV.

D: Cu^{2+}; E_i = −800 mV; E_v = 1100 mV; E_{pc} = −800 mV; $E_{cond,\ 1}$ = 1700 mV; $E_{cond,\ 2}$ = −800 mV; integration between 400 and 700 mV.

E: AsO_2^-; background electrolyte 0.05 mol/L H_3PO_4; sweep rate of 50 V/s; E_i = −600 mV; E_v = 1800 mV; E_{pc} = −600 mV; no conditioning applied; integration between 100 and 1100 mV.

3.4 UNDERPOTENTIAL DEPOSITION – ANODIC STRIPPING VOLTAMMETRY

3.4.1 Gold as a Substrate for Anodic Stripping Voltammetry

As discussed in Chapter 1, gold is a feasible alternative to mercury for determination of metals by stripping analysis (Section 1.1.2) and is becoming more common in recent years. However, at the time of this work, there was – to our knowledge – no published work regarding the performance of stripping voltammetry at gold.

Several slightly different approaches to stripping voltammetry were taken in this work. For the results presented here, stripping analysis was performed using background subtraction under flow injection conditions. The background current was generated in the presence of analyte, but with a negligible preconcentration time – i.e. there was no switching of solutions. However, rather than collecting one cyclic voltammogram with significant preconcentration and one without, an experiment very similar to repetitive cyclic voltammetry was devised: the electrode was cycled continuously, with a complete cyclic voltammogram stored for every cycle; then, electrode cycling was stopped with the preconcentration potential applied for some time; finally, the cycling was started again. In this way, the first cyclic voltammogram recorded after the pause for preconcentration is the actual "stripping" step of the analysis; however, a whole series of cyclic voltammograms is collected both before and after preconcentration.

The results of this approach are illustrated in Figures 3.14 and 3.15. In Figure 3.14, a single continuous cyclic voltammetry stripping experiment is shown for the detection of 5×10^{-8} mol/L Pb^{2+} on gold. The response shown in the inset is calculated in the same manner as described in Section 2.3.4, over a user-specified integration potential. Figure 3.15 shows a calibration curve generated from similar data for a range of concentrations. Under these conditions, the detection limit for Pb^{2+} was 2×10^{-10} mol/L. Although not exhaustive, these preliminary results illustrate the feasibility of the use of gold as a substrate for stripping voltammetry.

The stripping experiment shown in Figure 3.14 also reinforces the discussion earlier (see Section 3.2.2) of the lack of interference from impurities during scanning electrochemical detection. It is obvious from this data that the metal – which in this case

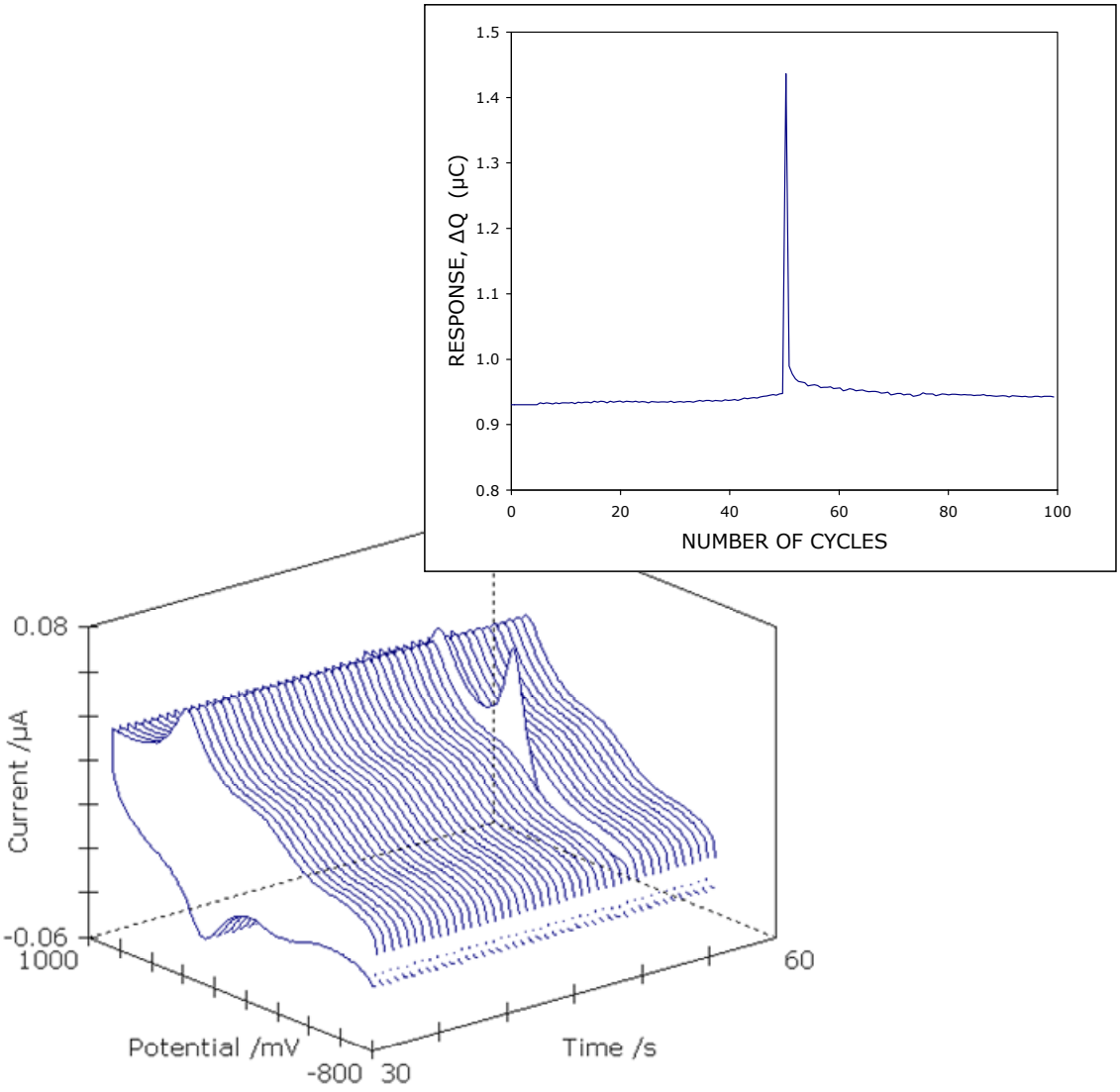

Figure 3.14 A single continuous cyclic voltammetry stripping experiment for 5×10^{-8} mol/L Pb^{2+} in 1 mol/L CH_3COOH at an Au ultramicroelectrode (25 μm diameter). The sweep rate was 40 V/s, and preconcentration was done at −700 mV (vs. Ag|AgCl) for 100 s. Initial potential −700 mV, vertex potential 1000 mV, preconcentration time (between scans except for stripping step) 0.5 s.

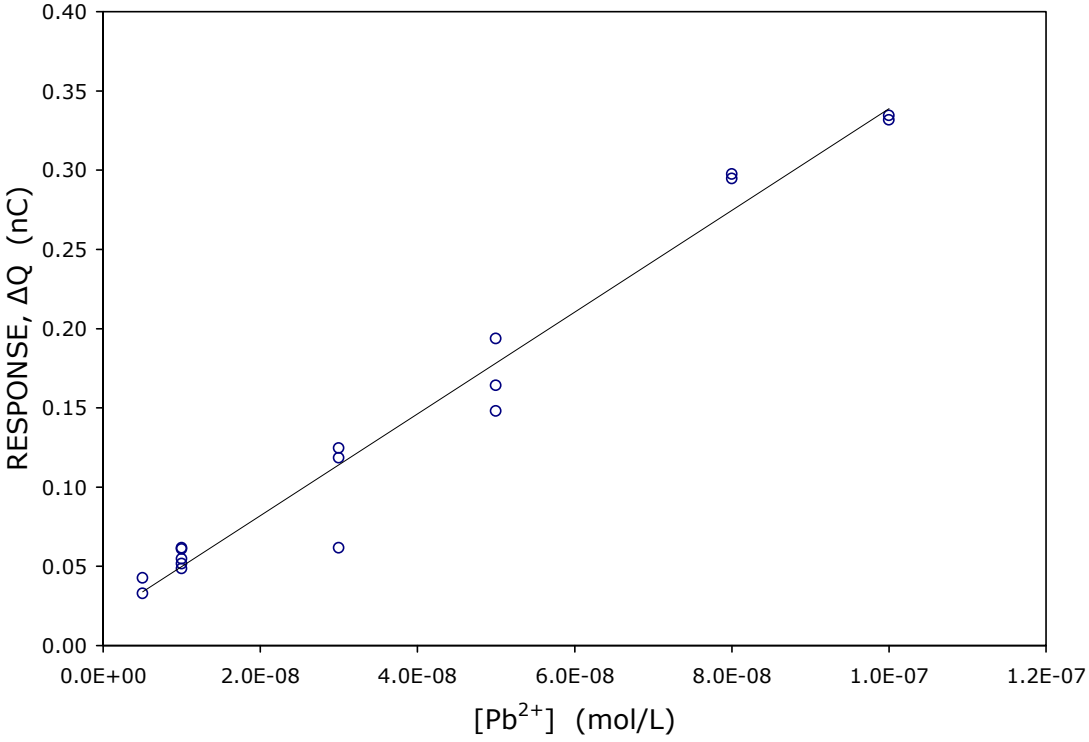

Figure 3.15 Calibration curve for Pb^{2+} in 1 M CH_3COOH under flow-injection conditions, using continuous cyclic voltammetry stripping detection at Au (25 μm in diameter). Sweep rate 40 V/s, preconcentration at −700 mV (vs. Ag|AgCl) for 100 s.

was accumulated on the electrode surface for 100 s – can be removed from the electrode almost completely in one cycle, even if that cycle lasts for 85 ms and only a portion of the cycle included potentials at which desorption (stripping) of the metal is possible. Deposition of lead would be expected to take place in the negative region of the applied potential waveform, i.e. from −700 to 0 mV, and also when the preelectrolysis potential is applied (500 ms). Thus, one can calculate the time of one potential waveform during which accumulation of lead is possible (τ_{ads}) – which, for these experimental conditions would be 53.5 ms. Similarly, the time available during one potential scan for desorption, τ_{des}, is 5 ms. The ratio $\tau_{ads}/\ \tau_{des}$ is 10.7, yet the desorption of the metal is essentially complete within one potential cycle. This is a clear indication of the effectiveness of potential scanning techniques in eliminating possible electrode contamination.

3.4.2 Effect of Sweep Rate on Determination of Metals at Gold by ASV

The variation of Faradaic and background currents with sweep rate is of interest in performing stripping analysis at gold. Cyclic voltammograms (forward scan only) for 5×10^{-7} mol/L Pb^{2+},Cu^{2+} and Cd^{2+} in 1 mol/L CH_3COOH taken at sweep rates between 1 V/s and 100 V/s are shown in Figure 3.16. A response for Cd^{2+} is not visible at any sweep rate. The peaks for both Pb^{2+} and Cu^{2+}, while not obvious at 1 V/s, are better defined as the sweep rate increases.

Figure 3.17 shows the variation of signal to noise ratio with sweep rate for 2×10^{-7} mol/L Pb^{2+} in 1 mol/L CH_3COOH at gold. From this graph it is clear that both the Faradaic current (due to Pb^{2+}) and background currents increase with increasing sweep rate, although not at the same rate.

An examination of the relationship between signal-to-noise ratio and sweep rate for the type of stripping experiment described in the previous section (Section 3.4.1) was done, since noise levels also vary with sweep rate. Results are shown in Figure 3.18 for the variation of signal-to-noise ratio with sweep rate (for 2×10^{-7} mol/L Pb^{2+}). In this case, the signal-to-noise ratio increases with sweep rate but levels off by about 70 V/s. Sweep rates above 90 V/s were not investigated.

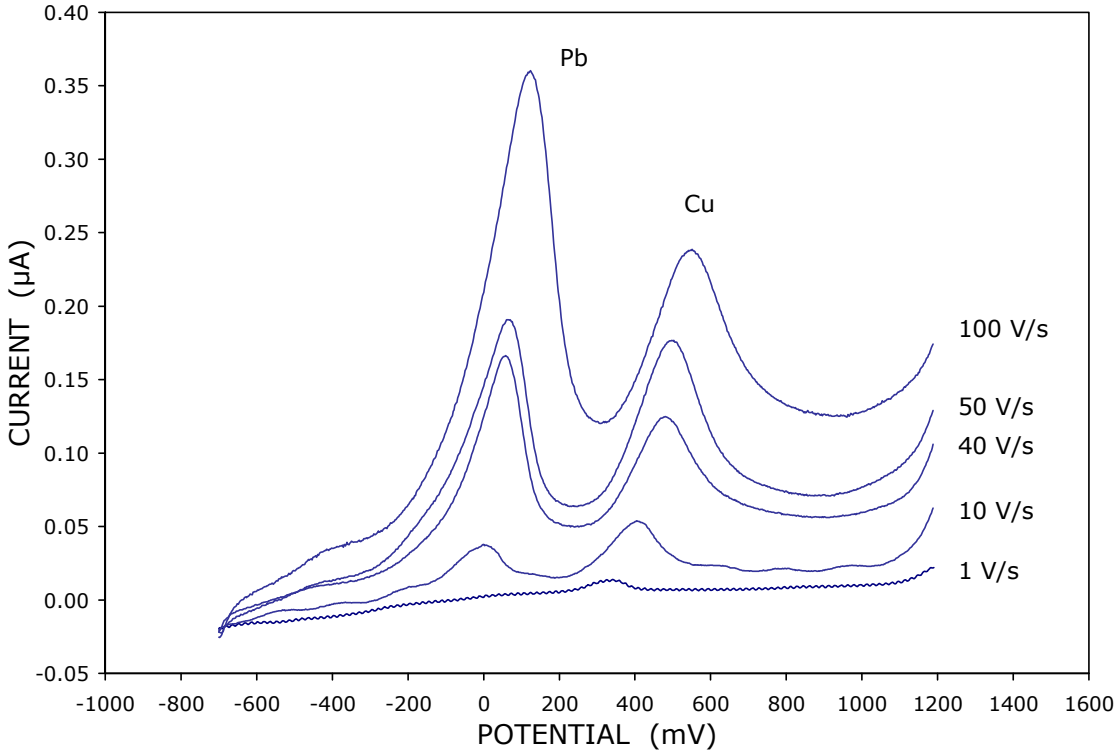

Figure 3.16 Variation of stripping peaks with sweep rate: a series of cyclic voltammograms at a 25-μm Au electrode of 5×10^{-7} mol/L Pb^{2+},Cu^{2+} and Cd^{2+} in 1 mol/L CH_3COOH (solution not stirred). The initial potential was −700 mV and final potential was 1200 mV. The potential applied between experiments was 0 mV.

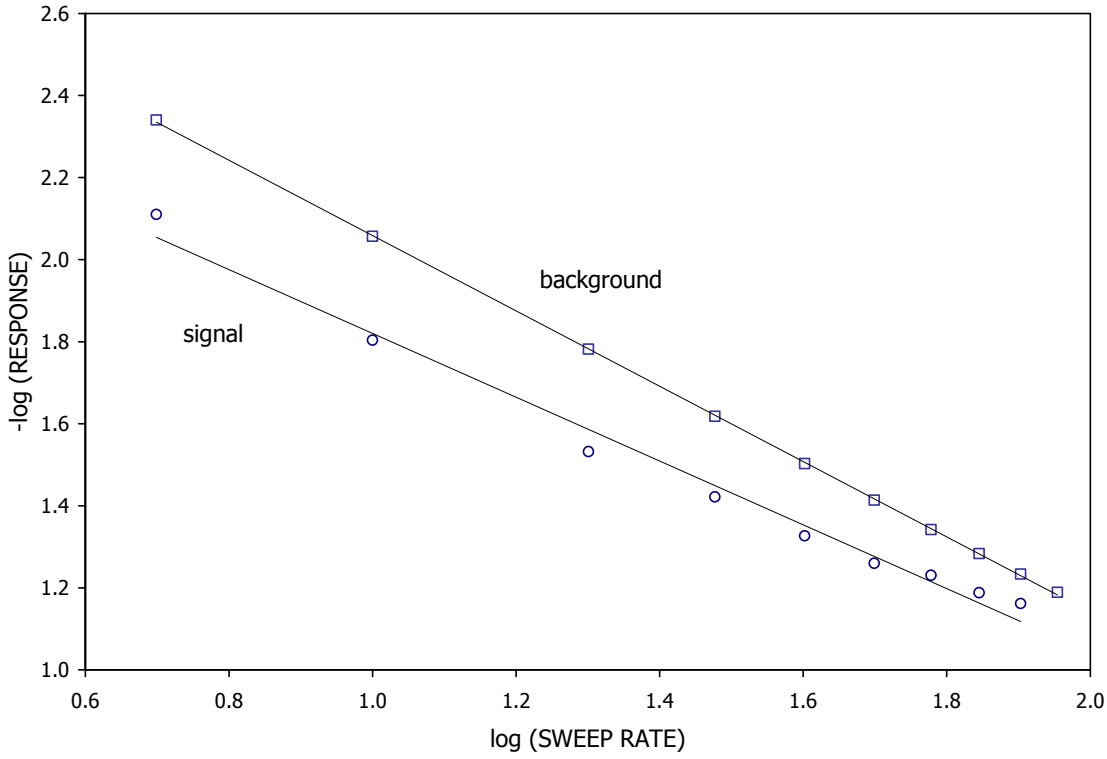

Figure 3.17 Negative log of response (peak current, μA) vs. log of sweep rate for stripping experiments of 2×10^{-7} mol/L Pb^{2+} in 1 mol/L CH_3COOH supporting electrolyte at a 25-μm Au electrode. Initial potential −550 mV, vertex potential 1050 mV, final potential −550 mV, various sweep rates. Preelectrolysis time 50 s.

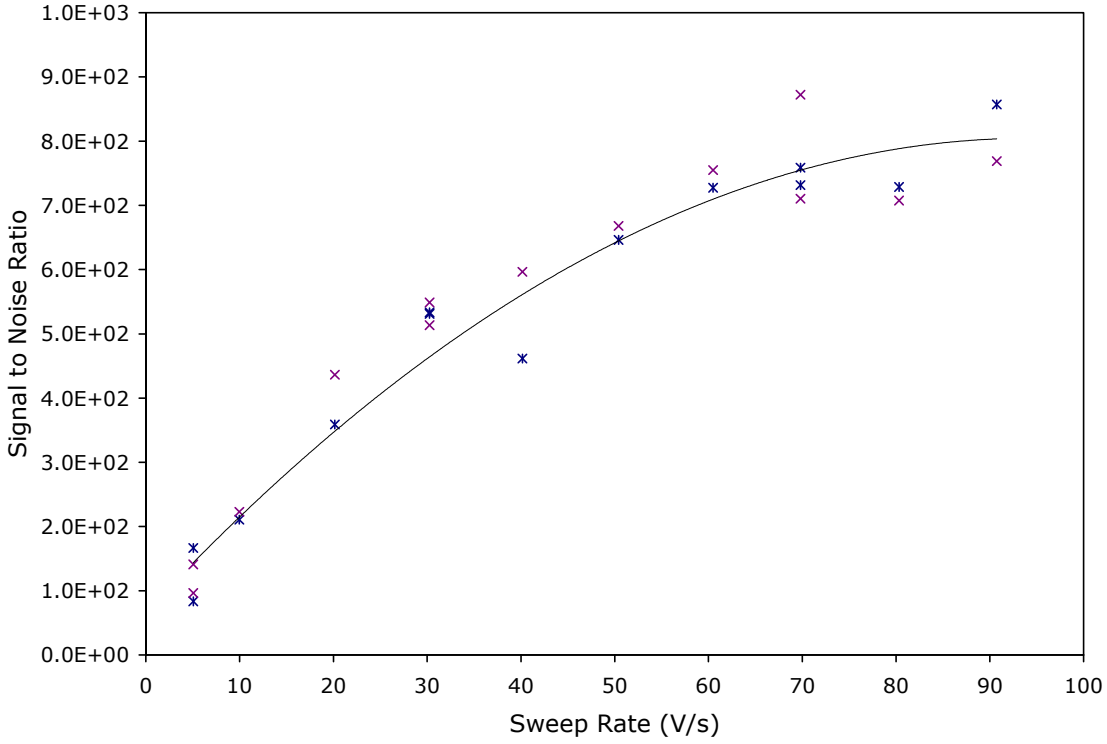

Figure 3.18 Continuous cyclic voltammetry stripping experiments for 2×10^{-7} mol/L Pb^{2+} in 1 mol/L CH_3COOH at a 25-μm Au working electrode. Initial potential −600 mV, vertex potential 1100 mV, rest potential −600 mV, preelectrolysis time (during scanning only) 0.2 s, preelectrolysis time before stripping 100 s.

3.5 CONCLUSIONS

The stability of gold ultramicroelectrodes under conditions of RCV was examined. In acidic solution, the electrodes can be used for detection of metals for over 24 hours: the scanning of the electrode into the oxide formation region is not necessary for stable detection. Furthermore, the inclusion of potential "conditioning" pulses (into the region of oxide formation) is of limited value, as scanning alone is effective in preventing adsorption of impurities.

Many metal ions can be detected using RCV at gold, including Tl^{+}, Co^{2+}, Ni^{2+}, Zn^{2+}, Cd^{2+}, Cu^{2+}, Pb^{2+} and Mn^{2+}. For Co^{2+}, Ni^{2+} and Mn^{2+} detection must take place at a higher pH (for instance, in acetic acid/sodium acetate, pH ~4.6) due to interference from the onset of hydrogen formation in more acidic solution. Nevertheless, detection limits (under flow-injection conditions) for several metals were determined: for Mn^{2+}, 2×10^{-6} mol/L; Co^{2+}, 6×10^{-7} mol/L; Pb^{2+}, 3×10^{-7} mol/L; Cu^{2+}, 3×10^{-7} mol/L; and AsO_2^{-}, 6×10^{-8} mol/L. As illustrated by the example of Ni^{2+}, the shape of the calibration curve can be strongly dependant on the potential region of the CV curve chosen for generation of the response.

Since the underlying process of UPD is the basis for accumulation of metals at the electrode surface during both repetitive cyclic voltammetry and UPD-ASV, it is reasonable to expect that any of the above-listed metals could be determined using a form of stripping analysis at polycrystalline gold. As an example of this possibility, a calibration curve was generated for the UPD-ASV analysis of Pb^{2+} at gold in acetic acid solution. The detection limit was 2×10^{-10} mol/L. Polycrystalline gold shows considerable promise in providing an alternative to mercury as a substrate for the detection of metals using anodic stripping voltammetry, although the preconcentration of the metal is limited somewhat by saturation of available adsorption sites at the surface. Also interesting is that Mn^{2+}, which can not be detected at mercury, can potentially be detected at gold.

CHAPTER 4: KINETICS OF UPD PROCESSES

4.1 FORWARD

Previous investigations of the detection of various metals by repetitive cyclic voltammetry indicate that different trends exist for the dependence of response (as CV charge, in coulombs) on sweep rate (see Reference [10]). The authors speculate that these different patterns are associated with changes in the rate of the charge-transfer step relative to the rate of mass transport [10]. A maximum signal-to-noise ratio (over the elution of a CE peak) was reported for sweep rates of 150−350 V/s for analytes with fast charge-transfer kinetics (i.e. Tl^{+} and Pb^{2+}) [10]. Furthermore, a cursory examination of cyclic voltammograms obtained at Au in the presence of metals reveals that the charge transfer process associated with metal deposition are very fast – the cyclic voltammograms showed reversible behaviour at scan rates of up to 10^3 V/s (the upper limit accessible in the "normal" CV mode of the data acquisition software).

It is obvious that the conditions for detection should be those under which the sensitivity of the method is maximized: in this case, higher sweep rates are advantageous, since the sensitivity of the method (apparently) increases with sweep rate (for metals such as Tl^{+} and Pb^{2+} [10]). From this point of view alone – i.e. determination of the optimal sweep rate for detection – it is an interesting proposition to study the effect of sweep rates beyond the range previously investigated. However, the possibility of measuring the rates of adsorption processes of metals at a foreign metal substrate is also of interest in itself.

As discussed in the Introduction (Section 1.1), the characteristics of ultramicroelectrodes (small ohmic drop, enhanced mass transport and low time constant) make them ideal for the determination of kinetics of fast electrode processes. However, UMEs are also more susceptible to minute imperfections or flaws in their construction that can cause systematic errors in determinations of charge-transfer kinetics [14]. The

meaningful measurement of kinetic parameters of surface processes is only possible with due consideration of the quality of the electrode, since these processes occur at the electrode/solution interface and thus are extremely sensitive to the state of the electrode surface (see Section 1.2.1). Surface crystallography, the adsorption of impurities, or slight imperfections in the electrode can all have a pronounced effect on the measured kinetic parameters. Polycrystalline gold disc electrodes were used throughout this work: this is convenient in terms of ease of electrode preparation, in contrast with the complicated processes involved in preparation of single crystal electrodes.

4.2 DETERMINATION OF THE KINETICS OF UPD OF METALS AT POLYCRYSTALLINE GOLD ELECTRODES

4.2.1 Treatment of Data and Experimental Considerations

At the high sweep rates necessary for the determination of the kinetics of the interfacial adsorption step of the UPD process, the noise levels in the cyclic voltammograms were quite high (Figure 4.1). This is expected, considering the high bandwidth required for these experiments. Furthermore, although the data acquisition system was capable of collecting data at these frequencies, the experimental system is not yet optimized for analytical applications. This problem can be circumvented by use of either FFT low-pass filtration or linear averaging of the raw data after background subtraction, as depicted in Figure 4.1 C and D.

As explained in Section 2.6.3, a simulation program was used to generate cyclic voltammograms with the input of kinetic parameters: background-subtracted experimental cyclic voltammograms served as data sets of "target" cyclic voltammograms to later be matched by the simulation program. For each metal/electrolyte system, a number of scan rates were used to generate a complete set of experimental cyclic voltammograms. Certain parameters – temperature, sweep rate, initial and final potential, electrode area and the bulk concentration of metal in solution – were set within the simulation to match actual experimental conditions as closely as possible. These were kept constant for the simulation of each system. However, the kinetic parameters – including initial coverage, rate constant (k_s), symmetry factor (α) and electrosorption valency (γ) – were varied until, using the *same* kinetic parameters, a

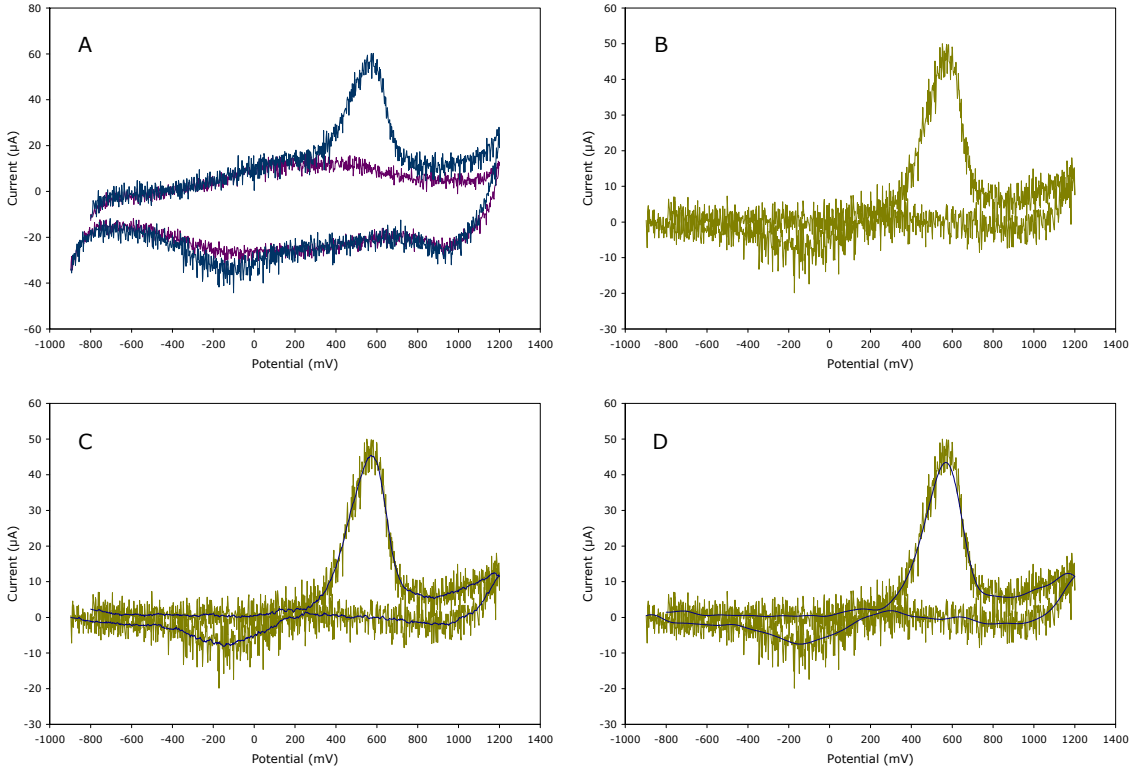

Figure 4.1 Removal of noise in cyclic voltammograms used for the determination of kinetics: **A** (top left) shows the cyclic voltammogram at a 25-μm Au electrode for 2×10^{-5} mol/L Cu^{2+} in 1 M $HClO_4$ (sweep rate 15800 V/s; preconcentration time 1 s; $E_i = -800$ V, $E_v = 1200$ V, and $E_f = -900$ V) as well as the blank. The background-subtracted current is plotted in **B**. In **C** and **D**, the results of application of low-pass FFT filtration (**C**) and linear averaging over 30 points (**D**) are shown, superimposed on top of the raw background-subtracted data from **B**.

reasonably close match between an *entire set* of experimental and simulated cyclic voltammograms was achieved. In this way, a set of experimental CVs for a system, taken over a range of sweep rates, were matched with a set of simulated CVs, and the kinetic parameters used to match the entire set were specific to that system.

Reasonably good agreement between experimental and simulated curves was possible with the judicious choice of simulation parameters. Figure 4.2 illustrates one particular instance: the fit between experimental and simulated data cyclic voltammograms obtained for a single cyclic voltammogram for Cu^{2+} (both experimental and simulation parameters are given in the legend). However, in some cases it was difficult to make out the smaller adsorption peak in the reverse scan, due to a combination of broadness of the peak and the noise levels. The choice of experimental conditions, particularly the preconcentration potential at which the electrode is held during deposition, is very important if the cyclic voltammograms are to yield any useful information.

Figure 4.3 illustrates this problem: two sets of cyclic voltammograms for the underpotential deposition of Cd^{2+} are shown, both in perchloric acid. In Figure 4.3 A, the preconcentration potential was −700 mV (vs. Ag|AgCl reference), whereas in Figure 4.3 B the electrode is held at a less negative potential (−500 mV) before the cyclic voltammetry scan. The difference is obvious: considerable broadening of the dissolution peak and loss of peak symmetry (as depicted in Figure 4.3 A) at a deposition potential of −700 mV. It may be that monolayer coverage of the electrode surface is exceeded, with adsorption of the excess at sites on top of the Cd monolayer causing the broadening. Another possibility is the formation of intermetallic compounds between gold and cadmium as the surface concentration of cadmium increases. Whatever the explanation, the curves shown in Figure 4.3 A are unsuitable for determination of kinetics.

4.2.2 Variation in Peak Separation with Sweep Rate

A comparison of the variation of peak separation with sweep rate for experimental and simulated cyclic voltammograms is shown in Figure 4.4. The experimental data in this figure is based on the analysis of cyclic voltammograms collected at different sweep rates and surface coverages (by using different preelectrolysis times) for the UPD of Cu^{2+} in 1 M H_2SO_4. For each cyclic voltammogram – both experimental and simulated –

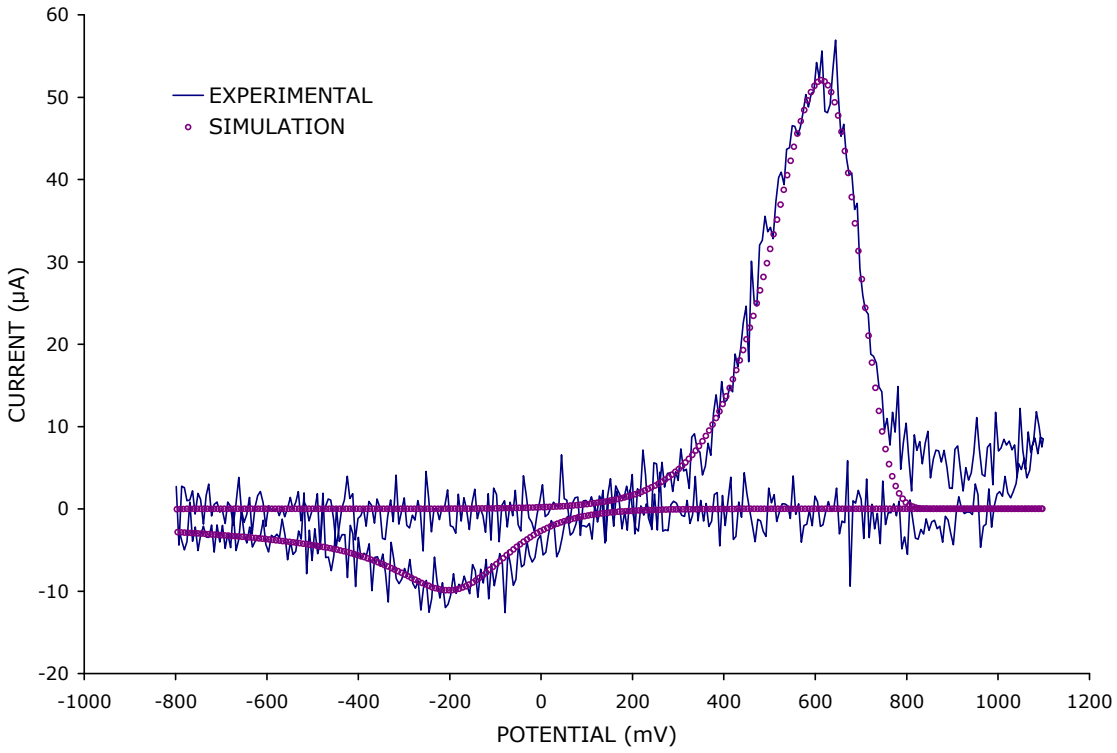

Figure 4.2 Fit between experimental (background-subtracted) and simulated cyclic voltammograms. The background-subtracted CV shown is for 2×10^{-5} mol/L Cu^{2+} in 1 mol/L M H_2SO_4 at a 25-μm Au electrode (Pt auxiliary; Ag|AgCl reference). The sweep rate was 29700 V/s; preconcentration time 2 s; E_i = −800 mV and $E_v = E_{pc}$ = 1100 mV. The parameters for the simulated CV were as follows: electrosorption valency 0.6; rate constant 4.0×10^4 s^{-1}; initial coverage 0.7; and symmetry factor 0.55.

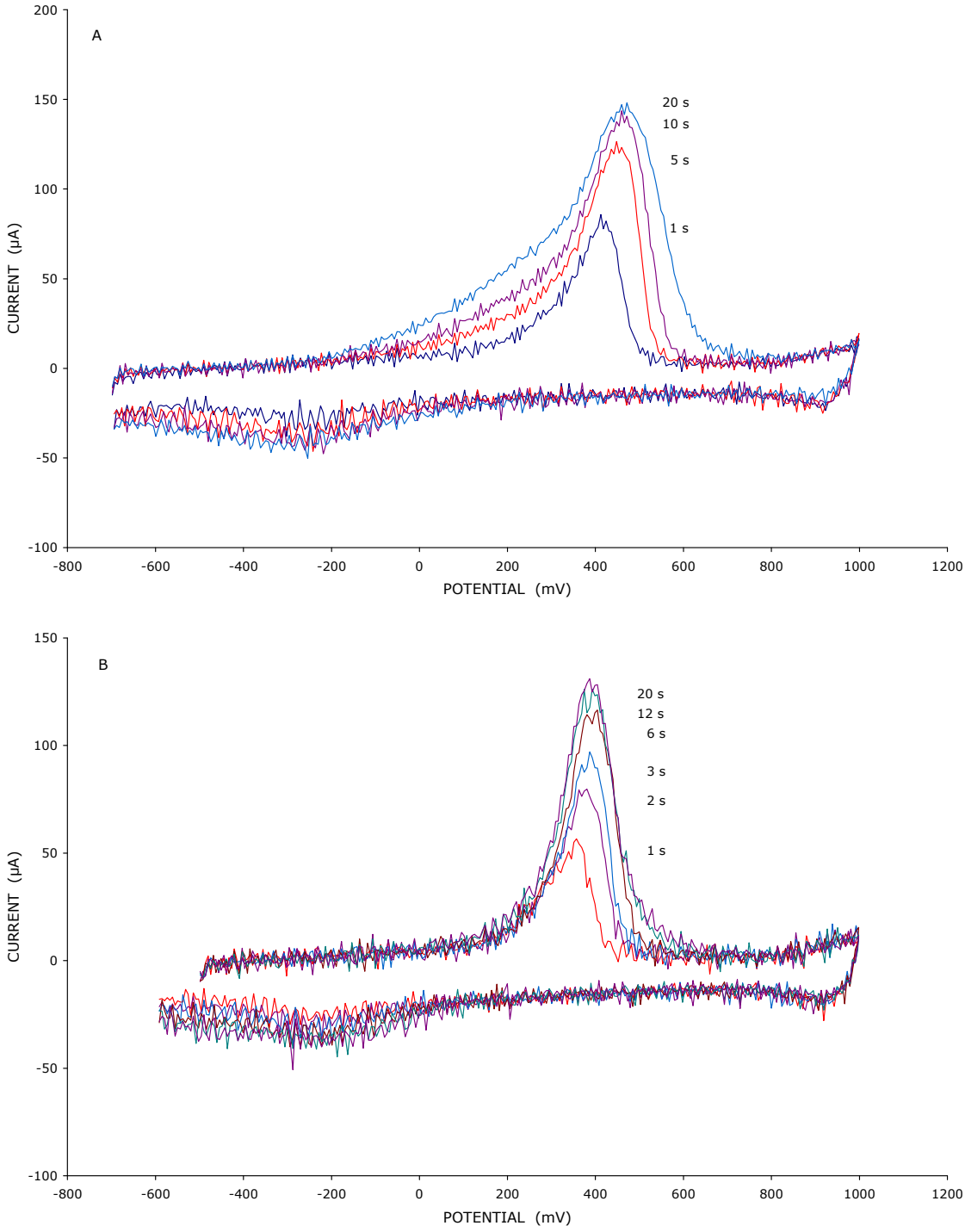

Figure 4.3 Variation in deposition potential (and preconcentration time) for 2×10^{-5} mol/L Cd^{2+} in 1 M $HClO_4$, sweep rate 19800 V/s. For **A**: deposition/initial potential −700 mV, vertex potential 1000 mV, final potential −700 mV; **B**: deposition/initial potential −500 mV, vertex potential 1000 mV and final potential −600 mV.

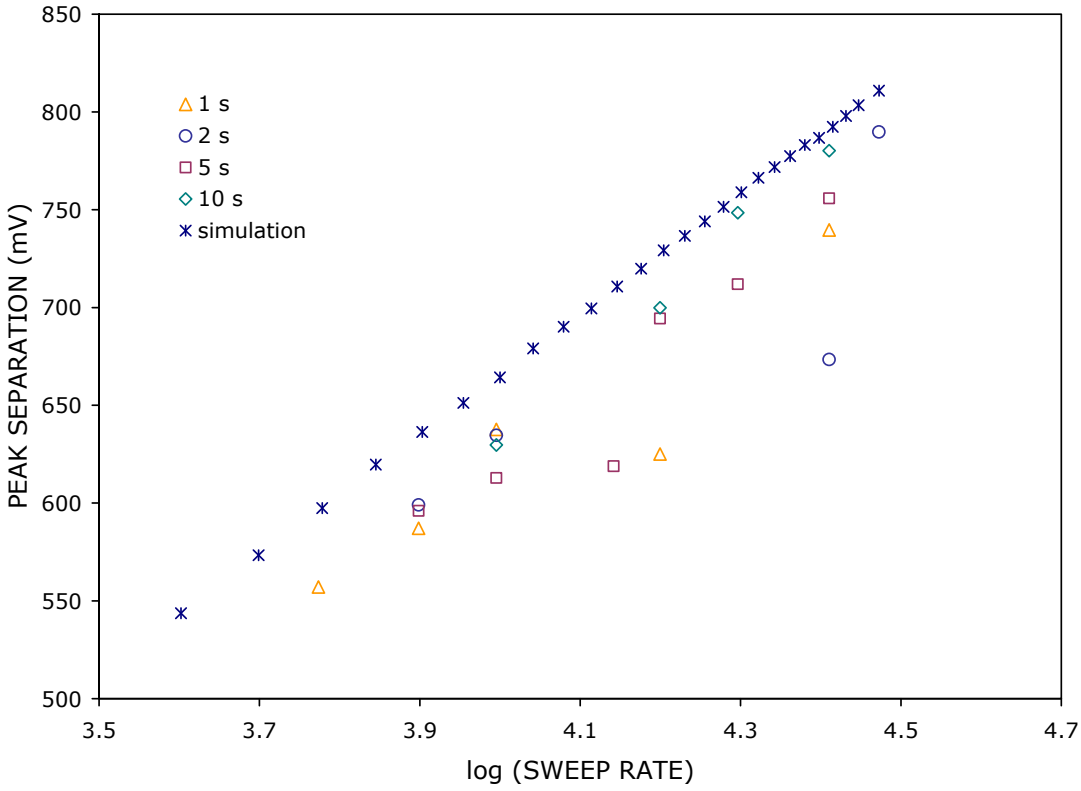

Figure 4.4 Comparison of experimental and simulated data for the variation of peak separation with log of sweep rate for different surface coverages (by variation of preelectrolysis time). Experimental conditions: 2×10^{-5} mol/L Cu^{2+}; background electrolyte 1 mol/L H_2SO_4, 25-μm Au working electrode, Ag|AgCl reference electrode.

the separation between the adsorption/desorption peaks in the cyclic voltammogram was determined and plotted as a function of the log of sweep rate. The experimental data follows the same trend as the simulated data – with the exception of a few outlying points. However, the values of peak separation determined from analysis of the experimental cyclic voltammograms were consistently lower than the values obtained from analysis of the simulated CVs. This is likely due to the choice of separation parameters in the simulation, the rate constant in particular. Another possible factor contributing to the discrepancy could be the way in which peak separation was determined from the experimental data (in this case, the cyclic voltammograms were not filtered before analysis).

4.2.3 Summary of Kinetic Parameters for the UPD of Cu and Pb at Au

The kinetic parameters, including rate constants, used to match simulated CV curves to experimental data sets for the systems studied (Cu in both $HClO_4$ and H_2SO_4, and Pb in H_2SO_4) are summarized in Table 4.1. The experimental data sets consist of background-subtracted cyclic voltammograms obtained at a variety of sweep rates: each data set contains cyclic voltammograms for at least five different sweep rates. The parameters recorded in Table 4.1 – including the rate constant (k_s), symmetry factor (α), and electrosorption valency (γ) – were used in the simulation program to match an entire series of experimental CVs.

Two independent sets of experimental data for the underpotential deposition of Cu on polycrystalline gold were analyzed in both $HClO_4$ and H_2SO_4 as a check for the consistency of the method of determining kinetic parameters using this method. The values of the rate constants determined from analysis of two independent experimental data sets for the Cu/H_2SO_4 system were 3.2×10^4 s^{-1} and 4.0×10^4 s^{-1} (see Table 1) – which, while not entirely in agreement, are at least of the same order of magnitude. Similarly, the CV-matching of two sets of experimental cyclic voltammograms for the Cu/$HClO_4$ system resulted in rate constants of 1.6×10^4 s^{-1} and 6×10^3 s^{-1}. Since the fitting of the experimental data with simulated cyclic voltammograms is essentially a process of trial and error, this ability to generate kinetic parameters that are generally consistent from independent sets of experimental data was encouraging. Still, the kinetic parameters given in this work should be regarded only as a reasonable first estimate.

METAL / ELECTROLYTE	RATE CONSTANT, k_s ($\times 10^3$ s^{-1})	SYMMETRY FACTOR, α	ELECTROSORPTION VALENCY, γ
Cu / H_2SO_4	*40*	*0.55*	*0.60*
	32	*0.47*	*0.67*
Cu / $HClO_4$	*16*	*0.44*	*0.65*
	6	*0.54*	*0.71*
Pb / H_2SO_4	*400*	*0.67*	*0.74*

Table 4.1 Summary of kinetic parameters for various metal/electrolyte combinations obtained from matching of experimental CV curves with simulated data. Two independent sets of experimental data were analyzed for the Cu / $HClO_4$ and Cu / H_2SO_4 systems: both sets of kinetic parameters used to match the experimental data sets are presented here for comparison.

Unfortunately, since there are very few experimental determinations of the kinetics of adsorption of metals at metal electrodes previously reported it is not possible to compare these with literature values.

According to the data presented in Table 4.1, the process of adsorption of Cu on gold in H_2SO_4 is faster than Cu adsorption in $HClO_4$ by a factor of approximately two. The variation in rate constants observed for different compositions of background electrolyte is not surprising, considering that the anions present in solution are known to play a significant role in the UPD process [83, 84]. Coadsorption between anions and metal ions also occurs: one example of many is the coadsorption of Cu^{2+}/SO_4^{2-}, Cu^{2+}/Cl^- and Cu^{2+}/Br^- on gold [83]. It may be that coadsorption of SO_4^{2-} with Cu^{2+} somehow facilitates the adsorption process.

The data presented here would also suggest that the rate of UPD of Pb on gold is much larger than the rate of Cu UPD (4.0×10^5 s^{-1} vs. 3.6×10^4 s^{-1}). The reason behind this is not fully understood.

4.2.4 Discrepancies in Electrosorption Valency

In all the systems studied, the electrosorption valency term used to fit the experimental curves was significantly less than what would be expected for a fully discharged metal deposited on the electrode surface (see Table 4.1), and also less than experimentally determined values of electrosorption valency (e.g. 1.4 for Cu^{2+} in $HClO_4$ at an Au(111) surface [36]). It is important to stress that the values that appear in Table 1 are not measured quantities, but chosen arbitrarily to fit the experimental data. However, assuming that these values accurately depict the situation during adsorption, this would seem to support a model including partial charge transfer during the initial adsorption step, as discussed earlier (see Section 4.1) and in Reference [37].

The values of electrosorption valency given in the literature are determined from experiments on a much longer time scale than the experiments presented in this work. For example, work done by Shi and Lipkowski measuring the total charge density of an Au(111) electrode during Cu UPD from an electrolyte containing bromide led the authors to conclude that the Cu UPD reaction does not involve a partial charge transfer mechanism [38]. However, these measurements were done at equilibrium, and thus it is very difficult to apply these conclusions to work done on a much shorter time scale. The

values obtained from the existing literature may reflect the overall transfer of electrons from the metal to the substrate. On the time scale of these experiments, however, there remains a slight possibility that only partial electron transfer occurs, in which case a lower value for the electrosorption valency is reasonable.

Another strong possibility is that the values of electrosorption valency presented in Table 4.1 are artificially low, due to the broadening of the stripping peaks in the experimental cyclic voltammograms on the polycrystalline gold electrodes. The stripping peaks at single crystal electrodes are sharp and well-defined, whereas the polycrystalline electrodes have an irregular surface structure, with different crystal faces exposed and many different adsorption sites, resulting in the broadening of the peaks. The broad peaks of these experimental CVs are impossible to match in the simulation program without low values of the electrosorption valency parameter. This latter explanation seems quite likely, especially given the limitations of the simulation program used in this work. The simulation was initially developed for modeling of adsorption processes at Hg. In this model, Hg is assumed to be atomically smooth, and an assumption regarding the homogeneity of adsorption sites is reasonable. However, the situation at polycrystalline gold is far more complex: on polycrystalline gold, a variety of exposed crystal faces, steps and terraces exist, resulting in nonequivalence of possible adsorption sites. This leads to peaks which are much broader than at either Hg or a single-crystal electrode. The simulation ideally should involve a range of adsorption energies (a Gaussian distribution) to account for the deposition of metal ions at non-equivalent sites on the substrate.

4.3 CONCLUSION

An attempt was made to measure the kinetics of adsorption of metals at polycrystalline gold by matching of experimental and simulated cyclic voltammograms. Rate constants of interfacial adsorption were estimated to be 3.6×10^4 s^{-1} for Cu in H_2SO_4, 1.1×10^4 s^{-1} for Cu in $HClO_4$, and 4.0×10^5 s^{-1} for Pb in H_2SO_4. The electrosorption valency parameter caused some difficulty: it was difficult to match the experimental stripping peak widths with simulated curves using values of the electrosorption valency close to the charge on the metal ions. The values of the electrosorption valency parameter arising from simulation of this kinetics data would, taken by themselves, seem to indicate partial

electron transfer during the adsorption step. However, these low electrosorption valencies are far more likely an artifact due to the simulation program, which was developed for systems in which the adsorption sites are homogeneous.

CHAPTER 5: CAPILLARY ELECTROPHORESIS & ELECTROPHORETIC EXTRACTION

5.1 FORWARD

This chapter presents the results of experiments involving capillary electrophoresis and certain modifications and extensions to conventional capillary electrophoresis. As discussed earlier, CE is a powerful analytical tool for separations: however, improvements in sensitivity are important if it is to be applied to environmental samples such as soils and/or natural waters. Furthermore, the application of CE/ECD to the determination of metals in soil samples may require several sample preparation steps – including filtration and/or ultracentrifugation – to remove any sediment and/or particles from the solution before analysis.

If a method could be devised in which particles present in an aqueous soil extract did not interfere with analysis, this would eliminate the need for extensive sample pretreatment. In addition, dynamic equilibria involving metals and colloids in solution could be investigated more readily if particles were not removed from the solution before analysis: thus, such a method could be useful in studies of bioavailability. Other possible applications for the determination of metals in solutions containing particles are analysis of waste from chemical mechanical planarization processes [85] (which involve the use of slurries of alumina or silica particles to polish the surface of silicon chips) or on-line monitoring of metal species in effluent streams during industrial processes.

The method that has been developed during the course of this work is known as electrophoretic extraction. Again, the rationale behind the development of this technique is the presumed advantage associated with the elimination of particle-removal steps from the sample prior to analysis. The results of initial experiments with this technique are presented in Section 5.3: however, results involving capillary electrophoresis of metals with repetitive cyclic voltammetry detection are presented first.

5.2 CAPILLARY ELECTROPHORESIS EXPERIMENTS

5.2.1 CE of Metals with Detection by RCV

Previously reported separations of metal ions by CE using fast cyclic voltammetry detection at gold were done in a background electrolyte containing creatinine and α-hydroxyisobutyric acid (HIBA) at a pH of 4.8: using this electrolyte, the separation of Tl^{+}, Co^{2+}, Ni^{2+}, Zn^{2+}, Cd^{2+}, and Pb^{2+} was possible [10]. However, in the creatinine/HIBA-based background electrolyte, no response was observed for Cu^{2+}. It is very likely that complexation of the Cu^{2+} with the organic components of the background electrolyte interfered with detection. For this reason, the use of organic components such as creatinine or HIBA in the background electrolyte was avoided in this work. Separations were generally done in acetic acid, phosphoric acid, or a buffer composed of acetic acid and ammonium acetate. While the optimization of separation conditions for capillary electrophoresis was not the focus of this work – i.e. conditions were chosen for simplicity in terms of detection rather than separation – in most cases baseline resolution of the metals was achieved.

The separation of 2×10^{-5} mol/L Pb^{2+}, Cu^{2+} and Cd^{2+} in 1 mol/L CH_3COOH is shown in Figure 5.1 as an example of a capillary electrophoresis experiment using repetitive cyclic voltammetry detection. There is a slight drift in the background response initially but this stabilizes with time. The three metal ions are separated within 200 s. The inset (Figure 5.1) shows the background-subtracted cyclic voltammograms over the elution of the three peaks. Although the sweep rate in this instance was relatively slow – only 20 V/s – the peaks are well-defined. Using data from this separation, the detection limit for Cu^{2+} was estimated to be 3×10^{-7} mol/L, whereas detection limits for both Pb^{2+} and Cd^{2+} under these conditions are about 2×10^{-7} mol/L.

Figure 5.2 shows the separation of 1×10^{-4} mol/L Tl^{+}, Cd^{2+}, Cu^{2+}, Pb^{2+}, Zn^{2+}, Ni^{2+} and Co^{2+} and 2×10^{-4} mol/L Mn^{2+} in 0.01 mol/L acetic acid with 0.01 mol/L ammonium acetate (pH ~ 4.6). In this case, baseline resolution is achieved for all metal ions except manganese and cobalt, which coelute. While this electropherogram illustrates the wide range of metals that can be analyzed using repetitive cyclic voltammetry detection at gold, the sensitivity of the method is relatively poor: certainly the analysis of metals in natural samples at low levels is not possible.

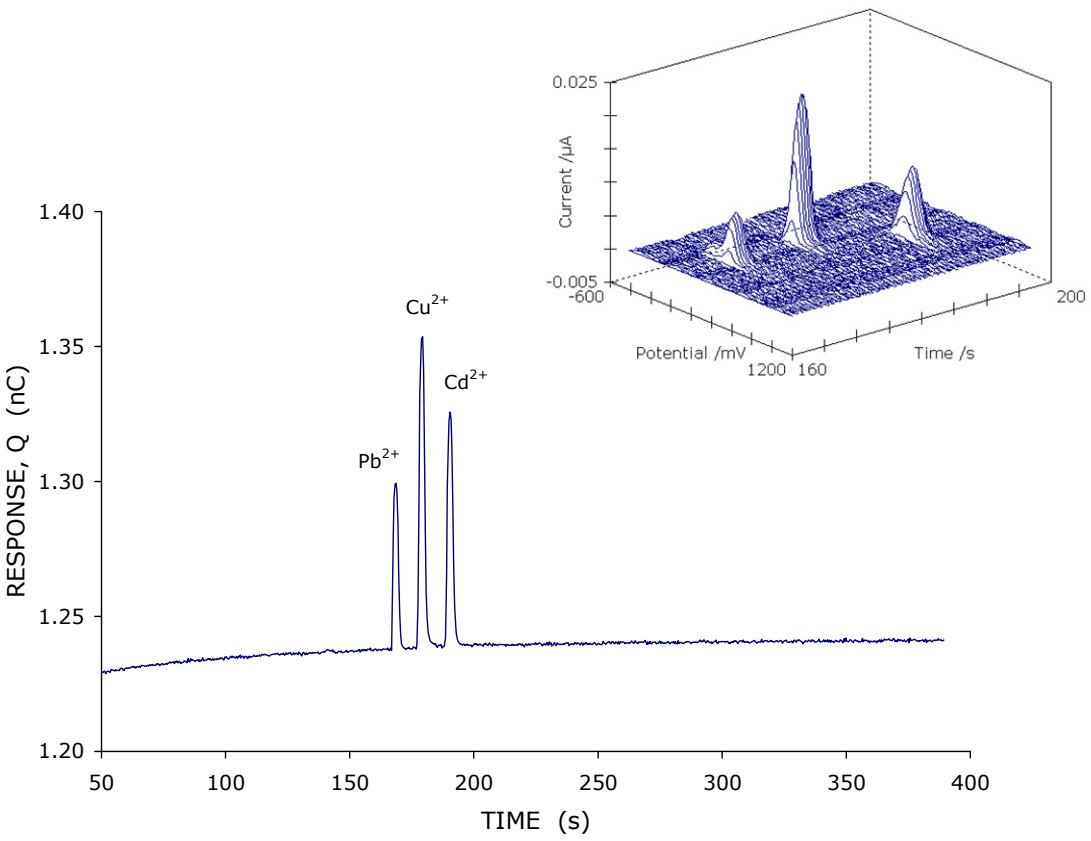

Figure 5.1 Electropherogram of 2×10^{-5} mol/L Pb^{2+}, Cu^{2+} and Cd^{2+} in 1 mol/L CH_3COOH. Electrokinetic injection at 10 kV for 5 s; separation voltage 20 kV; 40 cm capillary with internal diameter of 20 μm. Detection was done at a 25-μm Au electrode with a sweep rate of 20 V/s; initial and rest potential −500 mV, final potential 1100 mV; preconcentration time 0.22 s; offset potential 280 mV; integration over the region of −200 to 800 mV.

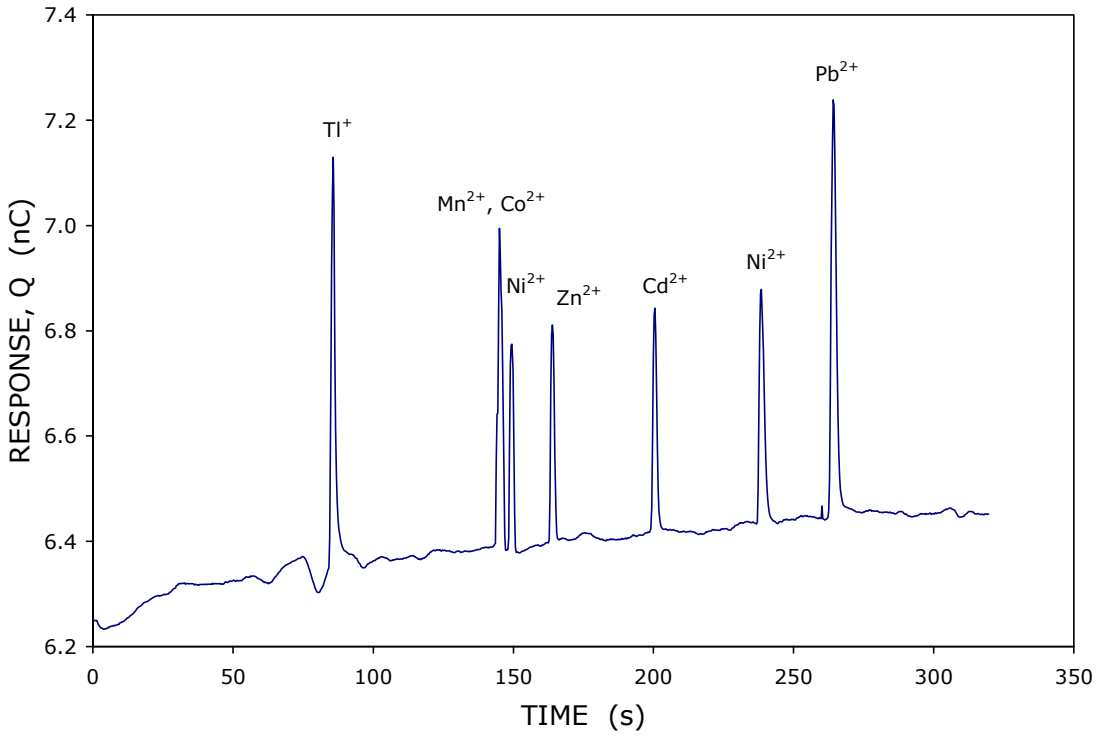

Figure 5.2 Electropherogram showing the separation of Tl^{+}, Cd^{2+}, Cu^{2+}, Pb^{2+}, Zn^{2+}, Ni^{2+}, Mn^{2+} and Co^{2+}. The concentration of each metal was 1×10^{-4} mol/L (except Mn^{2+} which was 2×10^{-4} mol/L). Injection was done at 3 kV for 10 s; the background electrolyte was 0.01 mol/L acetic acid and 0.01 mol/L ammonium acetate (pH ~ 4.6). The separation capillary was 40 cm (internal diameter 20 μm) and the separation voltage was 15 kV. RCV detection was done using the following parameters: sweep rate 50 V/s, preconcentration time of 0.2 s; initial and rest potentials −800 mV, vertex 1100 mV, offset 450 mV. The integration range was from −700 to 800 mV.

5.2.2 Enhancement of Sensitivity in CE

5.2.2.1 Detection-End Stacking

Figure 5.3 shows the results of a series of CE experiments involving the injection of a sample solution of three different metal ions (5×10^{-5} mol/L Tl^{+}, Ni^{2+} and Cd^{2+}) from a solution of 0.01 mol/L H_3PO_4 and 0.01 mol/L KH_2PO_4, with the same solution filling the capillary. The concentration of the solution in the reservoir *at the detection end only* was increased for subsequent runs – with concentrations ranging between 0.05 mol/L H_3PO_4 / 0.05 mol/L KH_2PO_4 to 1 mol/L H_3PO_4 / 1 mol/L KH_2PO_4 (pH ~ 2.1) – without any change to the solution filling the capillary and the injection-end reservoir.

With the increasing concentration of background electrolyte solution in the detection cell, considerable enhancement of the CE peaks was observed. The peak heights of all three metals increased by a factor of approximately 4 when the solution filling the detection reservoir was changed from 0.01 mol/L H_3PO_4 / 0.01 mol/L KH_2PO_4 to 0.2 mol/L H_3PO_4 / 0.2 mol/L KH_2PO_4 (with a solution of 0.01 mol/L H_3PO_4 / 0.01 mol/L KH_2PO_4 still filling the separation capillary). This is shown more clearly in Figure 5.4.

It seems reasonable to hypothesize that this phenomena is the same that occurs during sample stacking (see Section 1.3.3): a conductivity gradient exists at the detection end of the capillary, since the concentration of the solution at the capillary outlet is higher than the concentration of the solution filling the capillary. If the observed increase in response is indeed due to stacking of the analyte at the detection end, the enhancement of the response should be proportional to the increase in conductivity of the background electrolyte in the detection reservoir. The conductivity of the H_3PO_4 / KH_2PO_4 solution does not vary linearly with concentration: however, the conductivity of a solution of phosphoric acid (a weak acid) should be roughly proportional to the square root of the concentration [86]. A plot of peak area versus the square root of the concentration of H_3PO_4 and KH_2PO_4 at the detection end is shown in Figure 5.5. While not entirely linear, this data does support the idea of the observed increase in response being related to conductivity differences, as in sample stacking.

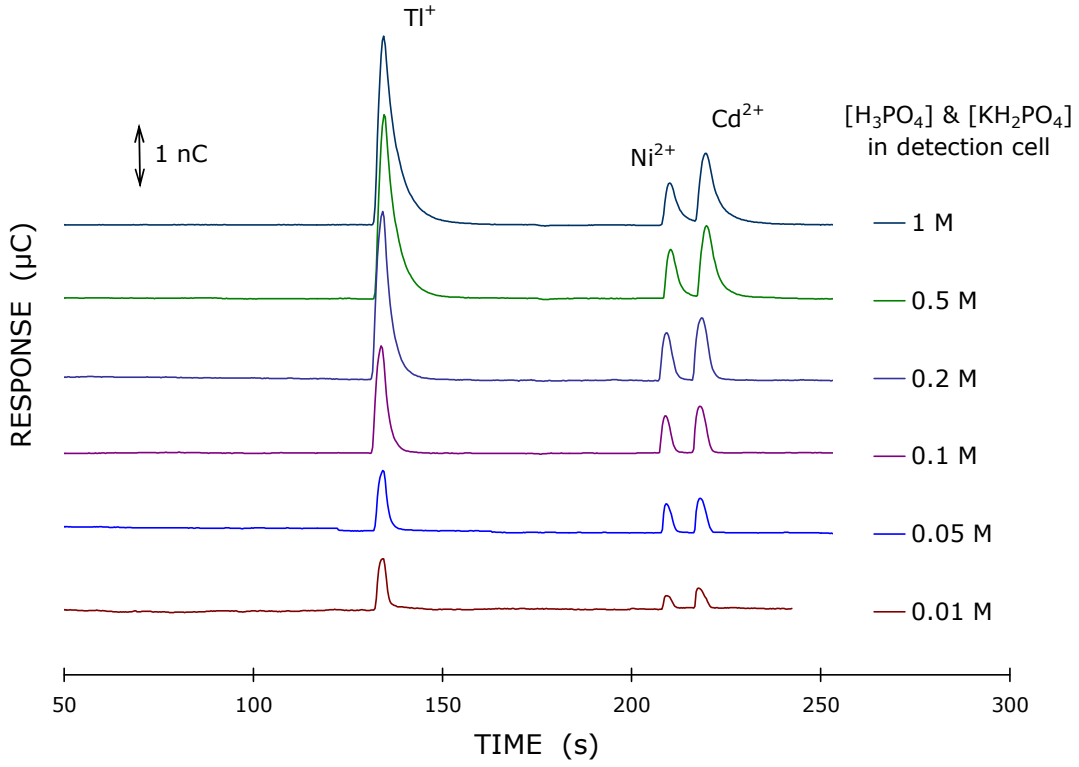

Figure 5.3 A series of experiments showing the enhanced response associated with increasing the concentration of background electrolyte of the solution at the detection end of the capillary (relative to the solution filling the capillary). The sample solution contained 5×10^{-5} mol/L Tl^{+}, Ni^{2+} and Cd^{2+} in 0.01 mol/L H_3PO_4 and 0.01 mol/L KH_2PO_4 and was injected at 3 kV for 10 s. Detection was done at a 25-μm Au electrode (sweep rate 50 V/s); and separation involved a 40-cm capillary, with 20-μm internal diameter and a separation voltage 15 kV. The concentration of H_3PO_4 and KH_2PO_4 at the detection end is shown to the right of each electropherogram in the graph.

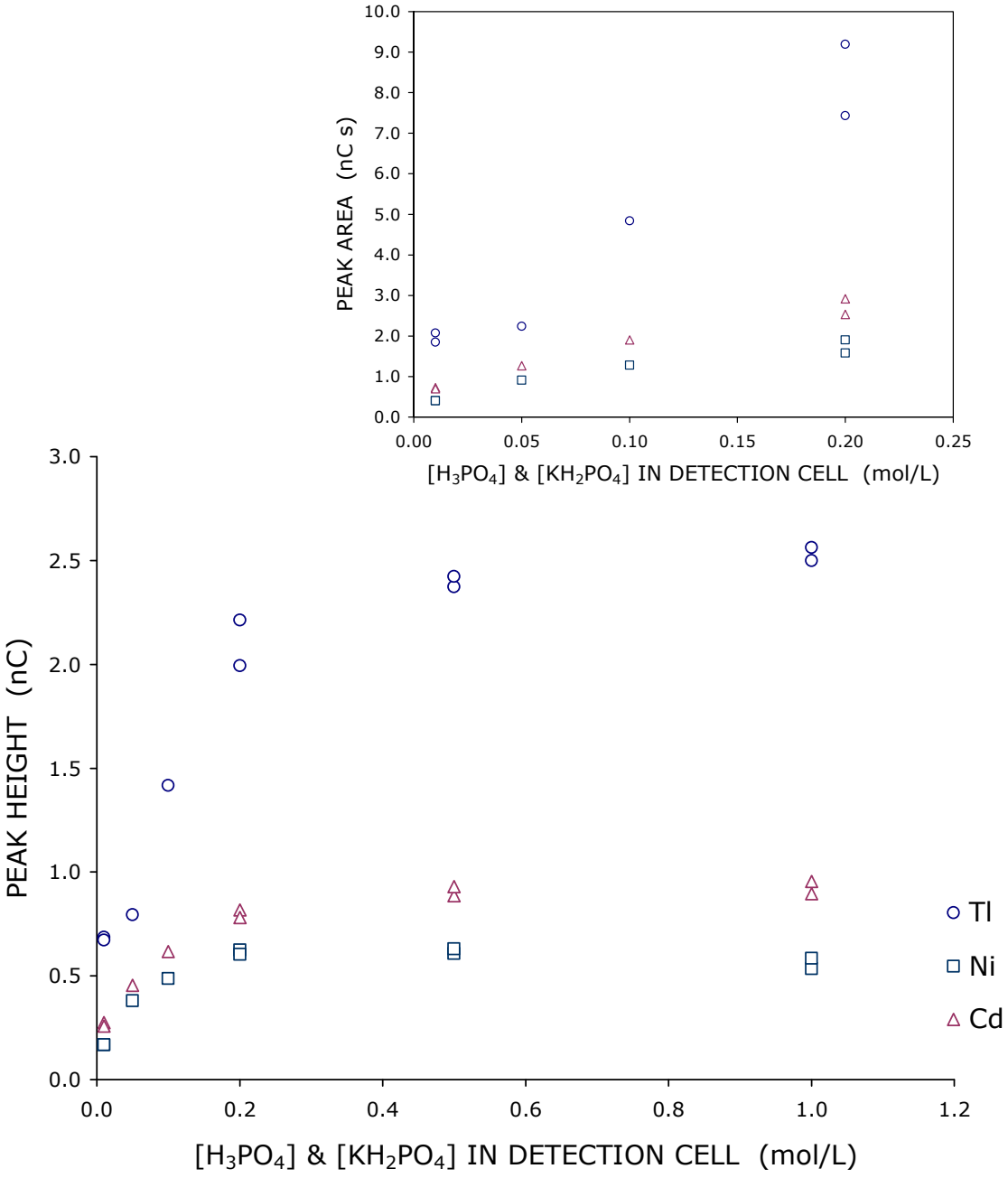

Figure 5.4 Analysis of electropherograms shown in Figure 5.3: the peak height vs. concentration of H_3PO_4 and KH_2PO_4 for Tl^+, Ni^{2+}, and Cd^{2+} (legend to right of graph). The inset shows the peak area as a function of concentration of H_3PO_4 and KH_2PO_4.

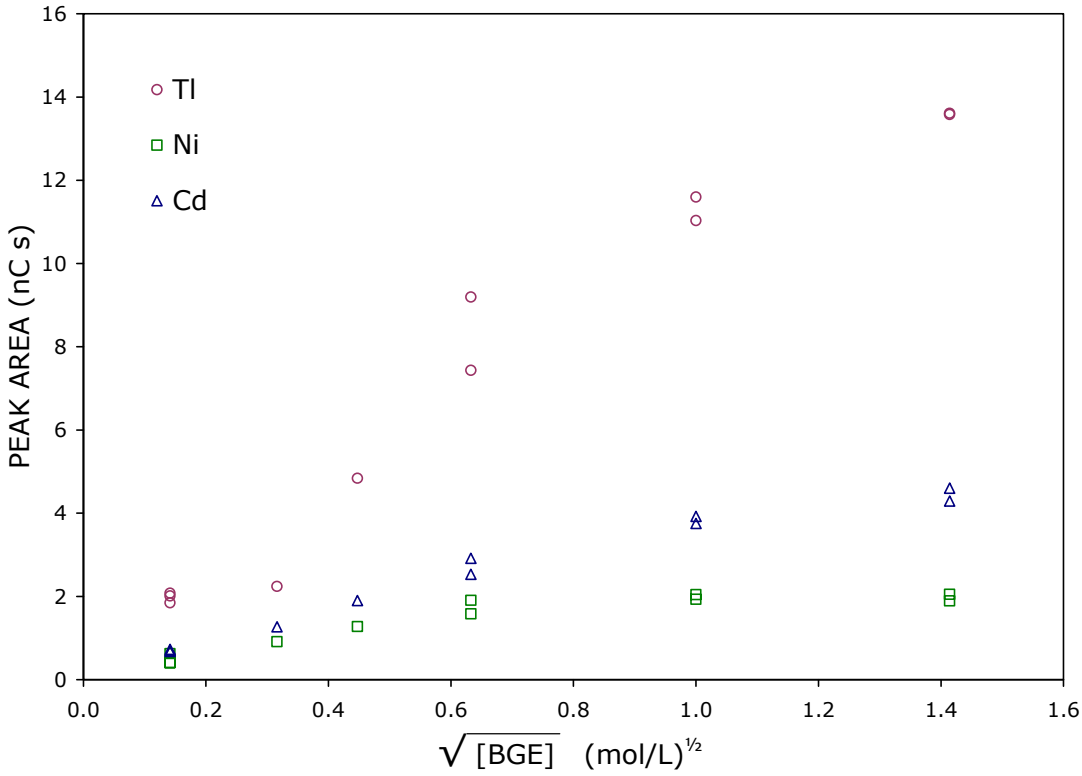

Figure 5.5 Analysis of data shown in Figure 5.3: peak area vs. the square root of the total concentration of H_3PO_4 and KH_2PO_4 at the detection end of the capillary.

The observed enhancement of the peaks in the electropherogram with increasing concentration of BGE at the detection end (as in Figure 5.3) is highly dependent on the positioning of the electrode at the end of the capillary. In related experiments (not shown) the electrode was moved away from the capillary along the capillary axis. When the concentration of the detection-end solution was increased, the peaks for Ni^{2+} and Cd^{2+} diminished, while there was still a slight increase for the peak area Tl^{+}. Another experiment resulted in a dramatic increase in the peak size for Tl^{+} with no response for the other two metals. This may be attributable to poor positioning of the detection electrode with respect to the capillary. Once the metal exits the capillary, transport of the metal to the electrode is based on diffusion and the electric field at the capillary exit, which extends into the solution to a certain extent (depending on the conditions, including the conductivity of the solution in the detection cell and applied voltage). Complex formation between Ni^{2+} and Cd^{2+} and $H_2PO_4^{-}$ and/or HPO_4^{2-} is also likely to play a role. Computer modeling of stacking effects occurring at the detection end, while complex, would be helpful.

While the phenomena of stacking is well known and commonly used for enhancement of sensitivity during introduction of sample onto the capillary (with many variations) the use of stacking at the detection end of the capillary is underutilized, and to our knowledge has not been reported in the literature. Under optimized conditions, it could be an extremely simple way of improving detection limits for end-column detection in capillary electrophoresis.

5.3 ELECTROPHORETIC EXTRACTION

Electrophoretic extraction is a novel technique designed to take advantage of the differences in the electrophoretic mobilities of analyte ions (in this case metal ions) and colloidal particles (soil and/or other particles) present in solution. The mobility of an ion in an electrical field is significantly larger than the mobility of a colloidal particle under the same conditions. Thus, when an electrical field is applied to a solution containing both analyte ions and colloidal particles, the analyte ions will reach the cathode (or anode, depending on their charge) in a much shorter time than the colloids.

To prevent particles from entering the capillary, electrophoretic extraction involves the application of positive pressure to the capillary outlet, resulting in the bulk

movement of solution towards the injection end of the capillary. The application of pressure in a CE system for certain purposes (other than for hydrodynamic injection) is not completely unheard of. Electroosmotic flow is commonly measured by monitoring the time of migration of a neutral marker: however, under conditions of low electroosmotic flow – for instance, when the EOF has been deliberately suppressed by modification of the capillary – this method is not practical. This is due to the prohibitively long time required for the elution of the marker [87, 88]. Several methods have been reported whereby residual electroosmotic flow is determined by use of pressure to force a neutral marker through the capillary [87, 88]. Flow-injection systems interfaced with capillary electrophoresis also exist, and are another example of the use of pressure in CE systems [89-92].

Ideally, electrophoretic extraction should result in a steady-state situation being established, providing a constant flux of analyte ions to the detection end. The migration of analyte ions to the detection end occurs under application of a potential field, against the same hydrodynamic flow of solution that prevents particles from entering the capillary. The applied pressure must be regulated in some way to prevent colloidal particles in the solution from entering the capillary when the separation potential is applied. The migration time of the analyte will obviously be longer than for the situation in which there is no hydrodynamic flow of solution opposing the movement of the analyte to the capillary outlet. The hydrodynamic flow must not be greater than the migration of the ions in the applied potential field: otherwise, no analyte will reach the capillary outlet.

No separation of analytes occurs in electrophoretic extraction in its original conception. Any metal in the analyte solution eventually reaches the electrode, at a time characterized by the electrophoretic mobility of that particular metal (provided the electrophoretic mobility is high enough to overcome the hydrodynamic flow). Some selectivity is retained by virtue of the different potentials at which the stripping peaks are observed; that is, the determination of several metals simultaneously is still possible if the peaks are sufficiently separated in the potential domain.

Electrophoretic extraction could be used to in combination with anodic stripping voltammetry. The only difference would be the means of mass transport operative

during preconcentration. Rather than stirring or the use of a rotating electrode, analyte ions are transported from the sample solution to the electrode surface under the influence of the potential field applied across the capillary. Significant preconcentration of the analyte at the electrode surface is possible, without the analysis being carried out in the sample itself, and without the need for extensive sample preparation.

It should be noted that the application of positive pressure causes a small amount of the background electrolyte to leach from the end of the capillary into the sample solution. The amount of solution flowing into the solution at the injection end is small enough that the composition of the sample solution should not change considerably, given a sufficient volume of background electrolyte in the detection cell. Also, the electroosmotic flow would not be expected to remain constant throughout the duration of an electrophoretic extraction experiment, since analyte ions would eventually be present throughout the entire capillary, and their presence would alter the double-layer structure at the capillary wall. This effect, however, is unimportant in that it would cause only a slight (perhaps unnoticeable) variation in the time required for the analyte ions to reach the detection electrode.

5.3.1 Initial Experimentation

The rate of ion migration in the electrophoretic extraction experiment can be divided into three components: the electrophoretic mobility of the ion, the electroosmotic flow, and the gravitational flow of the solution. This is expressed mathematically as follows:

$$\frac{L}{\tau} = v_{ep} + v_{eo} - S \tag{5.1}$$

where L is the length of the capillary, τ is time, v_{eo} is the electroosmotic flow, v_{ep} is the electrophoretic velocity of the analyte and S is the gravitational flow rate (in the direction opposite to ion migration). Since both the electroosmotic flow and the velocity of the analyte are proportional to the applied electrical field, Equation 5.1 can be written as

$$\frac{L}{\tau} = E(\mu_{ep} + \mu_{eo}) - S \tag{5.2}$$

where E is the applied voltage gradient (in V/cm), μ_{ep} is the electrophoretic mobility of the analyte, and μ_{eo} is the electroosmotic flow. Finally, substituting for the gravitational flow rate, S (see Section 1.3.1) and dividing by the length of the capillary gives a more useful form (Equation 5.3):

$$\frac{1}{\tau} = \frac{E\left(\mu_{ep} + \mu_{eo}\right) - kr_c^{\,2}}{L} \tag{5.3}$$

where k is a constant and r_c is the internal radius of the capillary.

Consideration of Equation 5.3 reveals that a plot of the reciprocal migration time of an analyte (in this case Pb^{2+}) against applied voltage for a particular capillary internal radius should result in a linear relationship. The graph in Figure 5.6 illustrates this relationship for four capillaries with internal radii of 15, 20, 25 and 50 μm. Linear dependence of the reciprocal migration time with voltage is observed for all capillary sizes, as expected. In addition, the negative intercept of each line is shown as a function of the square of capillary radius in Figure 5.7. This relationship is also linear, as expected for hydrodynamic flow.

No particles were present in solution for these experiments, but they do illustrate that crude regulation of the hydrodynamic flow is possible simply by varying the internal diameter of the capillary. Furthermore, it is obvious that the analyte (Pb^{2+}) still reaches the detection end of the capillary in the presence of an opposing bulk flow of solution.

5.3.2 Electrophoretic Extraction with Preconcentration by Stacking

Figures 5.8 and 5.9 show the results of several experiments involving electrophoretic extraction with repetitive cyclic voltammetry detection performed at a gold ultramicroelectrode. Figure 5.8 illustrates a series of experiments done with the capillary in a vertical orientation, and the injection end of the capillary immersed in a solution containing 2×10^{-6} mol/L Pb^{2+} in (a) background electrolyte (1 mol/L CH_3COOH), (b) 0.1 mol/L CH_3COOH, (c) 0.01 mol/L CH_3COOH, and (d) water. This set of experiments is an example of stacking: as the difference in conductivities between the injection solution and the solution filling the capillary increases, there is a corresponding enhancement of the signal. Furthermore, the same enhancement of signal due to stacking

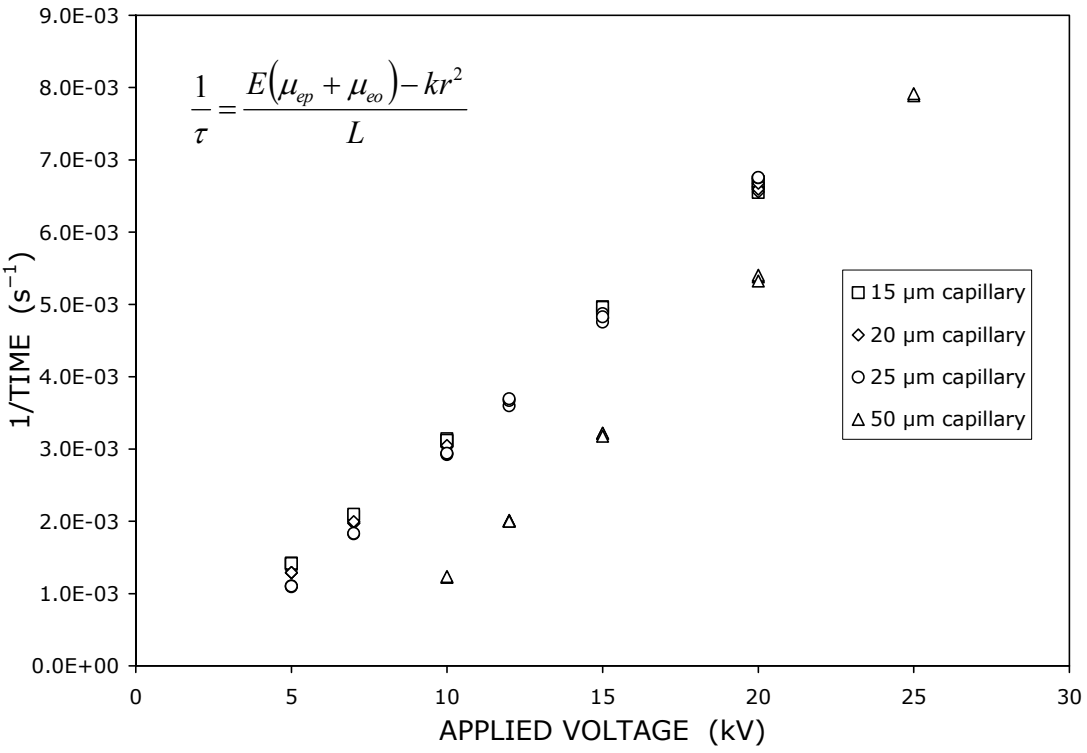

Figure 5.6 The reciprocal migration time of 1×10^{-5} mol/L Pb^{2+} (1 mol/L CH_3COOH) as a function of applied voltage for various capillary internal diameters (see legend). All capillaries were 40 cm long and oriented vertically.

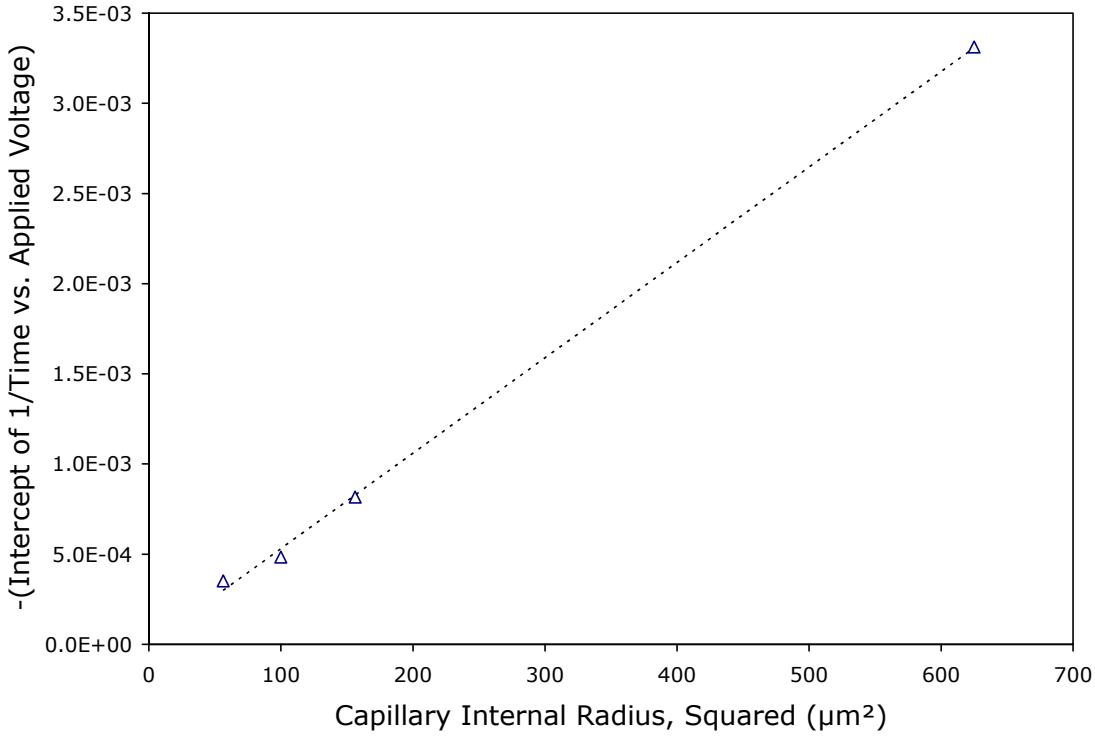

Figure 5.7 The negative intercept of the linear relationships in Figure 5.6, plotted as a function of the square of the capillary internal radius.

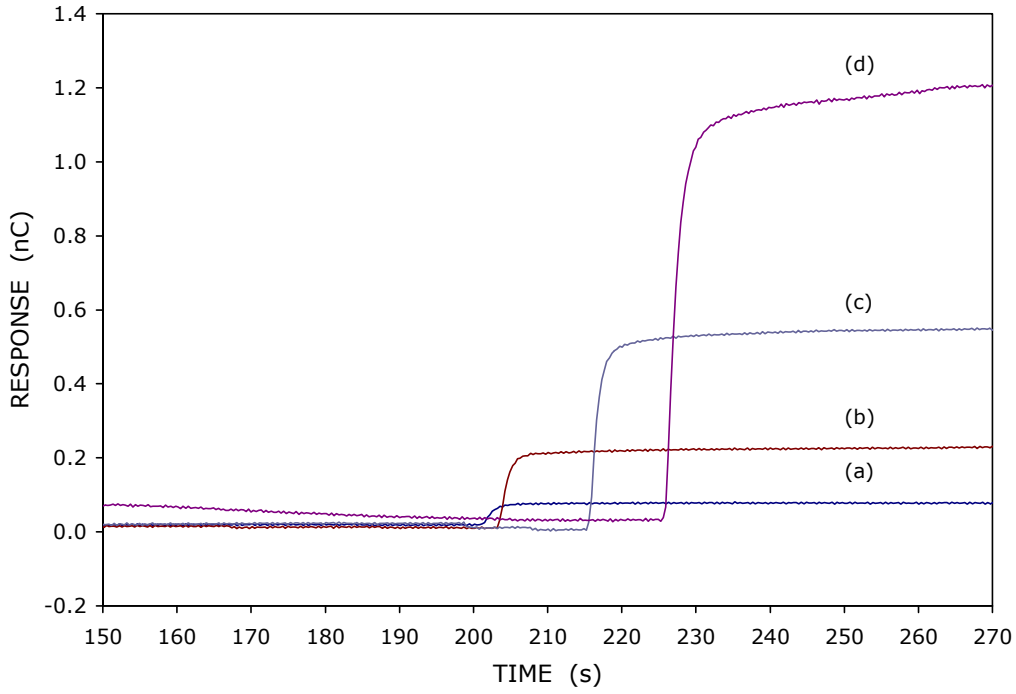

Figure 5.8 Electrophoretic extraction experiment, with detection of Pb^{2+} using repetitive cyclic voltammetry at a 25 μm Au electrode (sweep rate 200 V/s). Injection of 2×10^{-6} mol/L Pb^{2+} from (a) background electrolyte (1 mol/L CH_3COOH); (b) 0.1 mol/L CH_3COOH; (c) 0.01 mol/L CH_3COOH; and (d) water. No particles were added to these solutions. The capillary used was 40 cm long, and had an internal diameter of 20 μm. The difference in height between the injection and detection ends of the capillary was 40 cm.

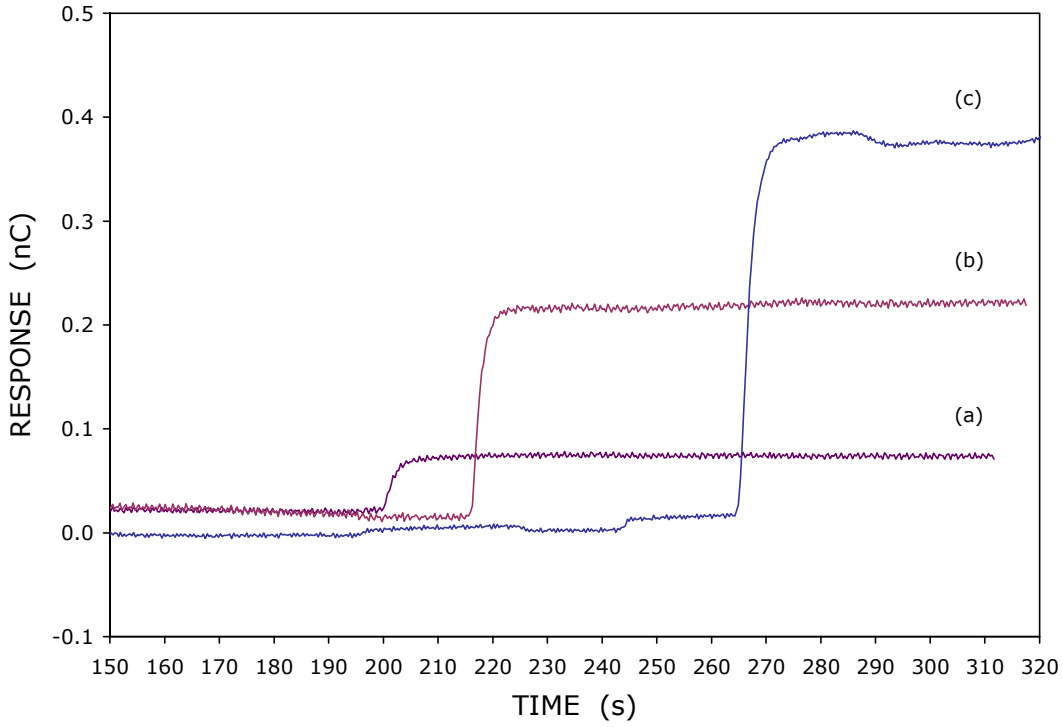

Figure 5.9 Electrophoretic extraction experiment, with injection of 2×10^{-6} mol/L Pb^{2+} from (a) background electrolyte (1 mol/L CH_3COOH); (b) 0.1 mol/L CH_3COOH; and (c) 0.01 mol/L CH_3COOH. All sample solutions contained alumina particles. Other conditions were identical to those in Figure 5.8.

occurs even when particles (alumina was used for initial experimentation) are present in solution, as shown in Figure 5.9.

It should be noted that the CE experiments in this work discussed previously (see Section 5.2.1) involved detection-end stacking (Section 5.2.2.1): in that case, the enhancement of the response was observed with an increase in the conductivity of background electrolyte (relative to the solution filling the capillary) at the *detection* end (see Figure 5.3). In Figures 5.8 and 5.9, enhancement of the response occurs as a result of stacking at the *injection* end and coincides with a decrease in conductivity of the sample solution. However, in both cases, the analyte ions undergo stacking as they move from a region of lower conductivity to a region of higher conductivity, and the enhancement of the response is proportional to the difference in conductivity between the two solutions.

A comparison of the magnitudes of the signals (in Figure 5.8) for samples injected from 1 mol/L CH_3COOH and water reveals that the signal increases by a factor of about 20. This is a significant gain in sensitivity, but falls short of some literature values reported for signal enhancement by stacking in capillary electrophoresis. In some cases where stacking was employed, enhancement of the response by a factor of up to $\sim 10^3$ was reported [93, 94]. The much lower enhancement observed here can be explained as follows. The signal enhancement possible as a result of stacking is limited by the conductivity difference between the background electrolyte and the sample solution. In this case, the background electrolyte is CH_3COOH, a weak acid, with low conductivity, so the conductivity difference between the sample and the background electrolyte is relatively small, and a low enhancement of the signal is the result. The situation is further complicated by the existence of a mixing zone at the end of the capillary, arising from the flow of the background electrolyte into the sample solution. Rather than having two distinct concentration zones, the background electrolyte (high conductivity) and the sample (low conductivity) there will be a concentration gradient present at the exit of the capillary, where some convective mixing of the background electrolyte and sample solution occurs. The stacking of the analyte will thus depend on the conductivity difference across this mixing zone. This situation is complex, and for a more complete investigation of the effects of this on signal enhancement due to stacking, computer

modeling to simulate the mixing zone and the stacking of the analyte across this mixing zone would be useful.

The conductivity of a weak acid such as CH_3COOH is roughly proportional to the square root of its concentration [86]. Since the increase in response under stacking conditions is directly proportional to the conductivity difference between the background electrolyte and the sample solution, the reciprocal response should increase linearly with the conductivity of the BGE solution. A plot of the reciprocal response (to injections of 2×10^{-6} mol/L Pb^{2+}) plotted as a function of the square root of the concentration of background electrolyte of the sample solution is given in Figure 5.10 (the data presented in this graph is derived from the experimental data shown in Figures 5.8 and 5.9). It is clear that the relationship between reciprocal response and the square root of the concentration of the background electrolyte is almost linear in both cases (with and without alumina particles present).

The results above indicate that there is at least some enhancement of the signal possible when there is a conductivity difference between the sample and electrolyte solutions. Moreover, the presence of alumina particles in the sample solution does not interfere with signal enhancement due to stacking (as indicated by Figures 5.8–5.10).

More enhancement of the response using stacking would be possible with the use of a more conductive solution as the background electrolyte, such as a strong acid. Initial electrophoretic extraction experiments were actually performed in nitric acid solutions (results not shown). However, the response obtained in such experiments was not constant with time: instead of a steady-state situation being established, with a constant flux of analyte ions reaching the detection end of the capillary, the system was unstable. This was attributed to changes in the solution filling the capillary when a strong acid is used as the background electrolyte.

For a system such as nitric acid, with a low conductivity sample present at the injection end and the voltage applied continuously, the background electrolyte (flowing from the detection compartment) initially fills the capillary. However, it is expected that cations from the sample solution begin to migrate up the capillary under the influence of the applied voltage. This eventually causes a change in the composition of the electrolyte inside the capillary, since the amount of background electrolyte flowing into

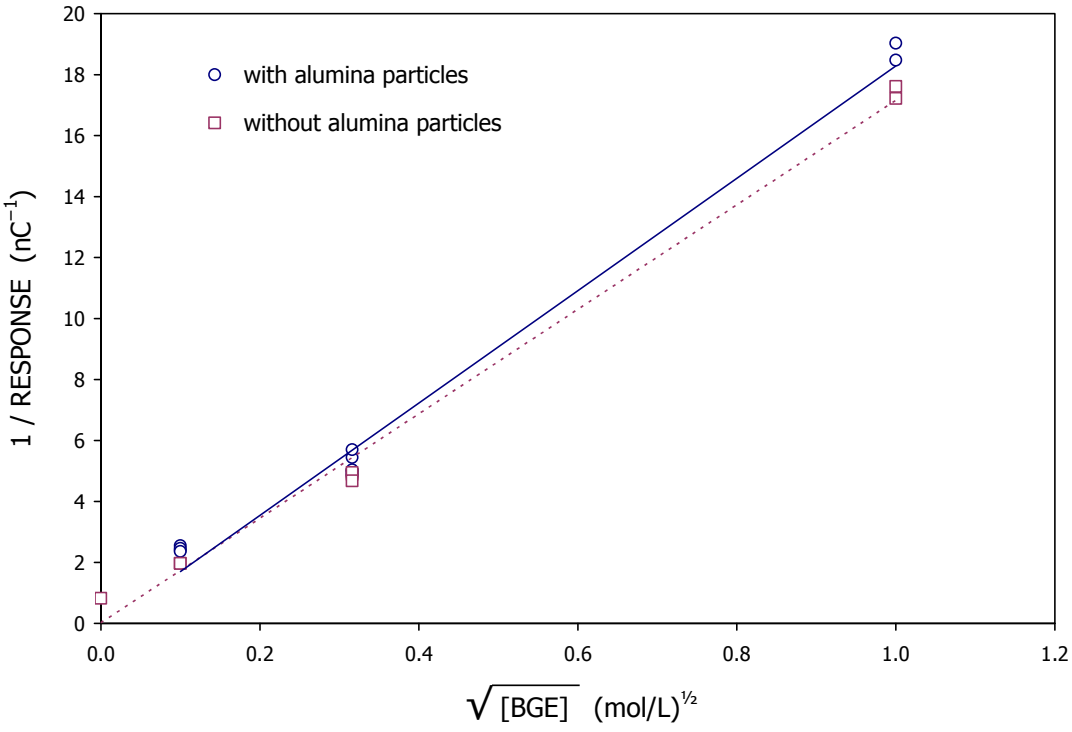

Figure 5.10 Plot of the reciprocal response versus square root of concentration of CH_3COOH. The data in this graph is derived from the data shown in Figures 5.8 and 5.9.

the capillary is not sufficient to keep the composition of the solution inside the capillary constant. There is a gradual replacement of protons from the nitric acid with the cations present in the sample solution. This problem is minimized by the use of a weak acid (in these experiments, acetic acid) as the electrolyte solution, since there is undissociated acid present to act as a reserve source of protons across the length of the capillary. Again, computer modeling of this effect would be helpful. Another plausible contribution to the instability in electrophoretic extraction experiments using nitric acid is Joule heating (see Section 1.3.1) due to the comparatively high conductivity of nitric acid.

5.3.3 Possible Modifications to Electrophoretic Extraction

A major problem with the original electrophoretic extraction experiments is the loss of selectivity due to the lack of a separation. Analysis of the analyte ions directly from the original particle-containing sample is possible, as demonstrated in previously (see Section 5.3.2). However, this is at the expense of selectivity: all analytes present in the solution will reach the detection electrode and be deposited at the electrode surface. Any selectivity thus rests entirely in the possibility of sufficient separation of metals in the potential domain (as in anodic stripping voltammetry) to permit analysis of both metals simultaneously. This lack of selectivity of the electrophoretic extraction method can be overcome with modifications to allow the combination of the electrophoretic extraction with a separation step. Numerous variations could be devised: however, two will be described below.

One possible modification involves the use of a T-junction to connect two capillaries at right angles to each other (see Figure 5.11). In the electrophoretic extraction/preconcentration step, potential is applied across the vertical part of the capillary. As in the simple electrophoretic extraction experiment, the analyte ions will migrate towards the cathode, filling the vertical part of the capillary, with the colloidal particles remaining in the sample solution. After this step is complete, the electrodes are switched so that the potential is applied at the top of the capillary, and the detection end of the separation column is grounded. In this way, the analyte ions in the solution filling the vertical section of the capillary (above the capillary junction) are forced to migrate into the separation capillary. After this, the separation proceeds as usual. The volume of

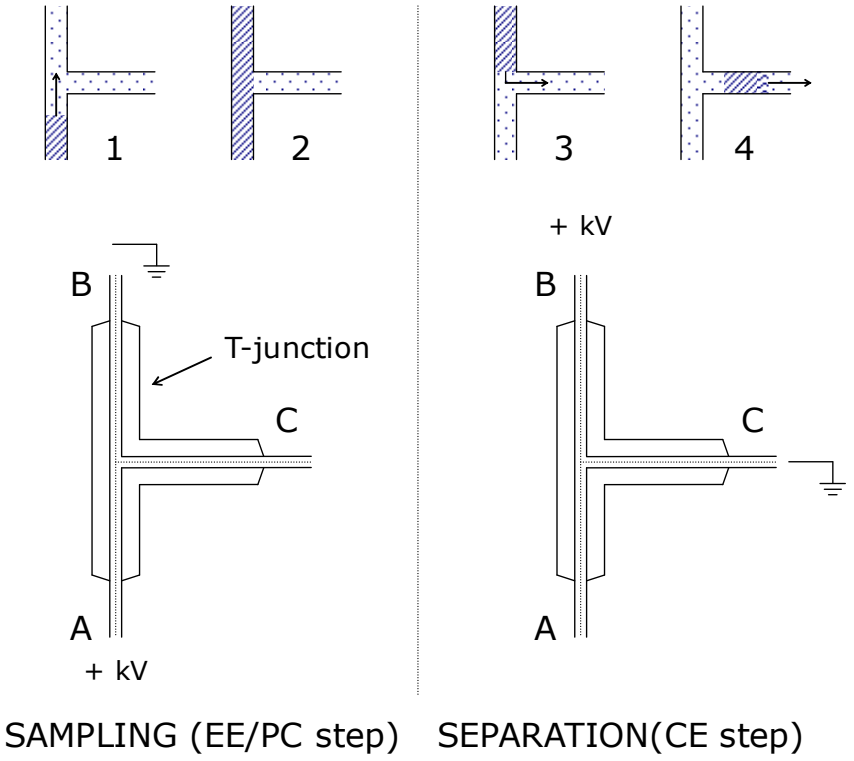

Figure 5.11 Schematic of electrophoretic extraction and injection using a T-junction.

sample injected in this method is equal to the volume of the (vertically-positioned) electrophoretic extraction capillary that is above the junction between it and the separation capillary. Although this method was tried, the results (not shown) were not useful, due to the high injection volume and poor resolution.

Another modification involves the pressure injection of a sample plug from a solution containing particles and the subsequent separation by capillary electrophoresis with a backflow. The hydrodynamic flow during separation results in the exclusion (from the separation capillary) of any particles introduced during sample injection. In theory, it should be possible using this technique to sample ions directly from particle-containing solutions. The sample plug may contain some particulate matter: however, this would be removed by the backpressure during the separation, while the applied voltage would result in the migration of the sample ions towards the detection end. Any loss of the sample ions due to the flow of a portion of the sample plug from the capillary during the first moments of the separation would need to be minimized by the appropriate choice of conditions. This technique also bears some resemblance to techniques described in the literature for removal of sample plugs after stacking procedures: however, as mentioned previously, in most cases capillary electrophoresis is not performed under conditions involving laminar flow.

5.4 CONCLUSIONS

The separation of Tl^+, Cd^{2+}, Cu^{2+}, Pb^{2+}, Zn^{2+}, Ni^{2+}, Mn^{2+} and Co^{2+} in 0.01 mol/L ammonium acetate, 0.01 mol/L acetic acid with detection by RCV at a gold ultramicroelectrode was achieved within 5 minutes (Mn^{2+} and Co^{2+} coelute). Detection limits were estimated for the separation of Cu^{2+}, Pb^{2+} and Cd^{2+} in 1 mol/L CH_3COOH: for Cu^{2+} the detection limit is 3×10^{-7} mol/L, and for both Pb^{2+} and Cd^{2+}, the detection limit is 2×10^{-7} mol/L.

Electrophoretic extraction offers promise as a novel technique to determine metals directly from particle-containing solutions. The premise behind this method – that analyte ions still reach the detector with the application of backpressure during the experiment, whereas interference from particles is prevented – was investigated and found to be reasonable. Further modifications are envisioned which would allow this idea to be developed: one such technique is a modified injection from a T-junction, and

another is the separation of metal ions with backpressure. Preconcentration during electrophoretic extraction experiments may take place both at the electrode surface and as a result of the stacking phenomena observed in capillary electrophoresis.

CHAPTER 6: CONCLUSIONS AND FUTURE WORK

6.1 SUMMARY

A variety of metal ions can be detected using repetitive cyclic voltammetry at gold in the potential range of about −800 to 1200 mV vs. Ag|AgCl (negative of the region for oxide formation). These include Cd^{2+}, Tl^{+}, Cu^{2+}, Ni^{2+}, Zn^{2+}, Pb^{2+} and Ni^{2+}, which can easily be detected in 1 mol/L acetic acid (pH ~ 2.4) or 0.5 mol/L CH_3COOH, 0.5 mol/L CH_3COONa (pH ~ 4.6). In addition, Co^{2+} and Mn^{2+} can be determined in acetic acid/sodium acetate at a pH of about 4.6, but not in acetic acid solutions due to interference at negative potentials from the reduction of hydronium ion at the lower pH. Particularly interesting is the possibility of the analysis of manganese at gold: manganese is difficult to detect at mercury due to limited solubility and the large potential required for the reduction of Mn^{2+}.

The underpotential deposition of Cu was used to investigate the stability of Au electrodes in both acidic and basic solutions during repetitive cyclic voltammetry detection. Although the lifetime of gold ultramicroelectrodes was found to be limited under scanning conditions in 0.5 mol/L sodium borate, in acidic solution (1 mol/L CH_3COOH) a gold electrode was used for detection over a period of more than 30 hours (RSD of 0.09). A comparison between scanning over the entire potential range at Au versus scanning limited to the region before oxide formation was done, but no appreciable difference in results was observed when relative standard deviations were considered. The possibility of improving electrode response using electrode conditioning – i.e. by inclusion of a series of potential pulses before the CV scan – was also investigated, but offered no significant advantage.

Polycrystalline gold was found to be a suitable substrate for the determination of metals by anodic stripping voltammetry. In this mode of stripping analysis, metals are accumulated on the electrode surface by underpotential deposition processes during the

preconcentration step. All the metals that can be detected using repetitive cyclic voltammetry (listed above) could potentially be analyzed using underpotential deposition anodic stripping voltammetry at polycrystalline gold, including manganese.

The kinetics of underpotential deposition was examined by matching simulated cyclic voltammograms to experimental background-subtracted cyclic voltammograms. Reasonably good agreement between experimental and simulated curves was possible with the judicious choice of simulation parameters: experimental data sets consisted of cyclic voltammograms collected at a variety of sweep rates for each compound. A rate constant of 3.6×10^4 s^{-1} was determined for the underpotential deposition of copper in sulphuric acid, and 1.1×10^4 s^{-1} for copper in perchloric acid, suggesting that sulfate may facilitate the underpotential deposition of copper on gold. The rate determined for the UPD of lead at polycrystalline gold (4.0×10^5 s^{-1}) is an order of magnitude larger than the rate for copper UPD (3.6×10^4 s^{-1}). The values of electrosorption valency used in the simulation to fit the experimental data were significantly less than values for a fully discharged metal at the electrode surface, and also less than experimentally determined values: this is likely due to a shortcoming in the simulation, in which all adsorption sites are treated as equivalent.

Repetitive cyclic voltammetry was again applied to the detection of metals separated by capillary electrophoresis. Separation of Tl^+, Cd^{2+}, Cu^{2+}, Pb^{2+}, Zn^{2+}, Ni^{2+}, Co^{2+} and Mn^{2+} was achieved in 0.01 mol/L acetic acid with 0.01 mol/L ammonium acetate (pH ~ 4.6; Co^{2+} and Mn^{2+} coelute). Different methods were examined to improve sensitivity, including stacking. While various forms of stacking are commonly exploited at the injection end, in this work it is shown that detection-end stacking is also useful for signal enhancement: as the conductivity of the electrolyte filling the detection cell is increased relative to the solution filling the capillary, the same phenomena occurs as that exploited during sample injection. For example, signal enhancement by a factor of 4 was attained for 5×10^{-5} mol/L Tl^+, Ni^{2+} and Cd^{2+} by simply switching the solution in the detection cell from the background electrolyte (0.01 mol/L H_3PO_4 / 0.01 mol/L KH_2PO_4) to 0.2 mol/L H_3PO_4 / 0.2 mol/L KH_2PO_4. This effect was shown to be related to the conductivity difference between the capillary and detection-end solutions.

A novel technique was investigated for the analysis of particle-containing solutions. Electrophoretic extraction is designed to take advantage of differences in the electrophoretic mobilities of analyte ions and colloidal particles (soil and/or other particles) present in solution. To prevent particles from entering the capillary, electrophoretic extraction involves the application of positive pressure to the capillary outlet, resulting in the bulk movement of solution towards the injection end of the capillary while the separation voltage is applied. Various modes of this technique are possible. One mode of operation involves continuous extraction of analyte ions from a particle-containing solution, with a constant flux of ions being deposited at an electrode for determination by stripping analysis. Another conceivable option is to perform regular capillary electrophoresis with constant back-pressure during the separation. Plots of the reciprocal migration time of a test analyte (Pb^{2+}) against applied voltage for different capillary radii reveal a linear relationship, as expected. Sample stacking can also be exploited for signal enhancement in electrophoretic extraction experiments.

6.2 FUTURE WORK

A method for the construction of single-crystal Au ultramicroelectrodes has been described [95, 96] involving the preparation of Au(100) and Au(111) electrodes from crystals grown in a silicate gel. The availability of such single-crystal Au ultramicroelectrodes opens several possibilities for further research. Use of single-crystal electrodes may improve the sensitivity of the detection method described in this work. Furthermore, the use of single-crystal electrodes would simplify the determination of kinetics of underpotential deposition for reasons already discussed.

The values of kinetic parameters presented in this work should only be regarded as a first approximation: very little is actually known about the kinetics of the interfacial adsorption step of the underpotential deposition of metals. Further study is needed to ascertain whether the low values of electrosorption valency obtained through simulation of kinetics are an artifact due to limitations in the simulation program or actually reflect partial electron transfer. The simulation program used throughout this work was developed specifically for adsorption at Hg surfaces, which are homogeneous [80]: further refinement of the simulation to take into account the heterogeneity of polycrystalline gold would clarify the situation.

It would be beneficial to have a method whereby the positioning of the electrode could be entirely automated. One obvious possibility would be to use a three-dimensional micromanipulator interfaced to a computer, along with software to precisely control the position of the electrode with respect to the end of the separation capillary. This can be achieved by monitoring the potential shift of the working electrode at the end of the capillary (when the separation potential is applied), and adjusting the electrode position accordingly. A micropositioner/computer interface has already been developed in this lab [97, 98] for scanning electrochemical microscopy (SECM) experiments. This system would simply require some adaptation for use in a CE experiment.

During CE experiments, a non-uniform electric field exists at the end of the capillary due to the separation voltage. Running a scanning experiment (similar to SECM) with the detection electrode as a probing tip would allow the electric field at the end of the capillary to be mapped in three dimensions. This could be applied in the development of a system for automated positioning based on the magnitude of the potential shift observed at the detection electrode. An increased understanding of the spatial dependence of the electric field at the detection end would also clarify the existence of any limitations to application of electrochemical detection to capillary electrophoresis under certain conditions.

Microfluidic devices (micro-total analysis systems or "lab-on-a-chip" devices [94-103]) provide many interesting options for the expansion of this research. The positioning of an ultramicroelectrode at the end of the separation capillary for electrochemical detection is not trivial: it requires time and skill. At the same time, the Au UMEs used in this work have a reasonably long lifetime (over 24 hours). The use of microfabricated disposable lab-on-a-chip devices would circumvent the problem of electrode positioning and cleaning entirely, since the ultramicroelectrode would be produced with the device. Also, certain experiments investigated throughout the course of this research (i.e. electrophoretic extraction experiments and variants) would be more easily performed on a lab-on-a-chip device developed specifically for this purpose, rather than the rather cumbersome experimental setups described in this work.

APPENDIX A: CONTROL OF HIGH VOLTAGE POWER SUPPLY

The power supply used for the majority of the experiments described in this thesis is a Spellman CZE1000R, which has a maximum output of ±30 kV. Two modes of operation are possible with this instrument: it may be controlled manually or by use of a computer interface. Control of the high voltage power supply with the computer is attractive for several reasons. First, data acquisition for electrochemical detection is done entirely through the computer, and it is convenient to have the power supply also controlled by the computer. For instance, with computer control of both data acquisition and separation voltage allows detection to be started automatically a controlled time after the voltage is applied. More importantly, computer-controlled separation voltage allows for accurately timed electrokinetic injection, increasing reproducibility compared to the rather crude method of switch and stopwatch. Finally, interfacing of the high voltage power supply also leads to the possibility (with further modifications) of a completely automated system for sampling, separation and detection.

Control of the output voltage of the Spellman CZE1000R by computer is accomplished as follows: in the manual mode, a jumper is present over pins 2 and 3 (internal voltage control) and pins 11 and 12 (reference voltage), as shown in Figure A.1. For external control, these jumpers are removed and replaced with two signals: one (0–10 V) to specify the output voltage (pin 3), and a second (>3 V) that to enable the voltage output (pin 12). All that is necessary, then, is the control of two lines from the computer, one with an output of 0–10 V through a DA converter, to send the appropriate voltage for the desired output voltage, and an "enable" line of more than 3 V that can be either high or low (on or off). This is depicted in Figure A.2. When both of these outputs carry a voltage, the output of the high voltage power supply will be proportional to the voltage on the regulatory line. If either the regulatory line or enable line has a voltage of

0 V, the high voltage power supply will not output a voltage. Thus, switching the high voltage power supply on or off is as simple as controlling the enable line (with the other line always set to some non-zero voltage). In addition, accurate electrokinetic injection is easily accomplished by use of a timer on the computer: all that is necessary is a timing subroutine in the software and user-defined inputs for injection time and voltage.

A microcontroller (Burr-Brown, PIC16C73B) with programmable memory was used to control the two voltage lines to the high-voltage power supply. Programming was done using a compiler (PICBasic) specifically designed for these types of chips, along with a manufacturer-supplied device to encode the program on the chip memory (the memory of the chip is erased by exposure to UV light). The program encoded on the chip is executed whenever the power supply is switched on. Each of the eight pins on the chip can be set for either output or input, and to either high (+5 V) or low (0 V) logic independently of the other pins on the chip. This chip was incorporated into an electronic circuit containing an analog-to-digital converter (Burr-Brown, ADS7841), a digital-to-analog converter (DAC7615), and an operational amplifier. An analog-to-digital converter is included for monitoring the separation current.

The subroutines developed for control of the high voltage power supply and electrokinetic injection were incorporated into the MicroVoltammetry software. A screenshot of the graphical user interface is shown in Figure A.3.

PIN	FUNCTION
1	10 V reference
2	internal voltage control
3	voltage program input
4	internal current control
5	current program input
6	signal common
7	voltage test point
8	current test point
9	external interlock
10	external interlock
11	10 V reference
12	enable
13	spare
14	spare

Figure A.1 A diagram showing the layout of the pins of the Spellman CZE1000R. In the default mode the jumpers are in the position shown. To control the high voltage power supply using the computer, pins 3 (voltage input) and 12 (enable – 10 V) are used. Pins 9 and 10 are connected to the interlock on the safety box.

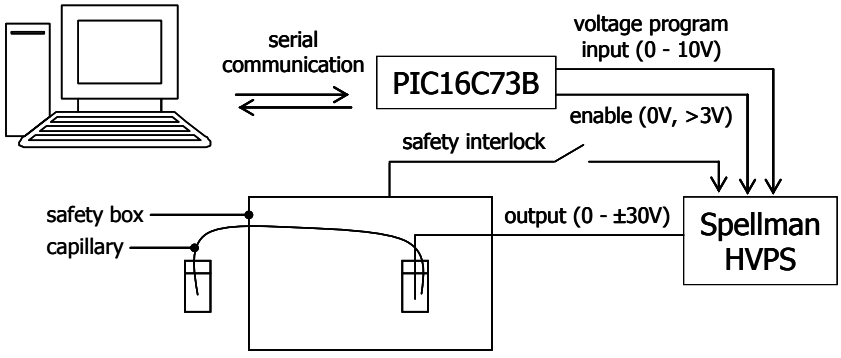

Figure A.2 A diagram of the interface between the high voltage power supply and the computer.

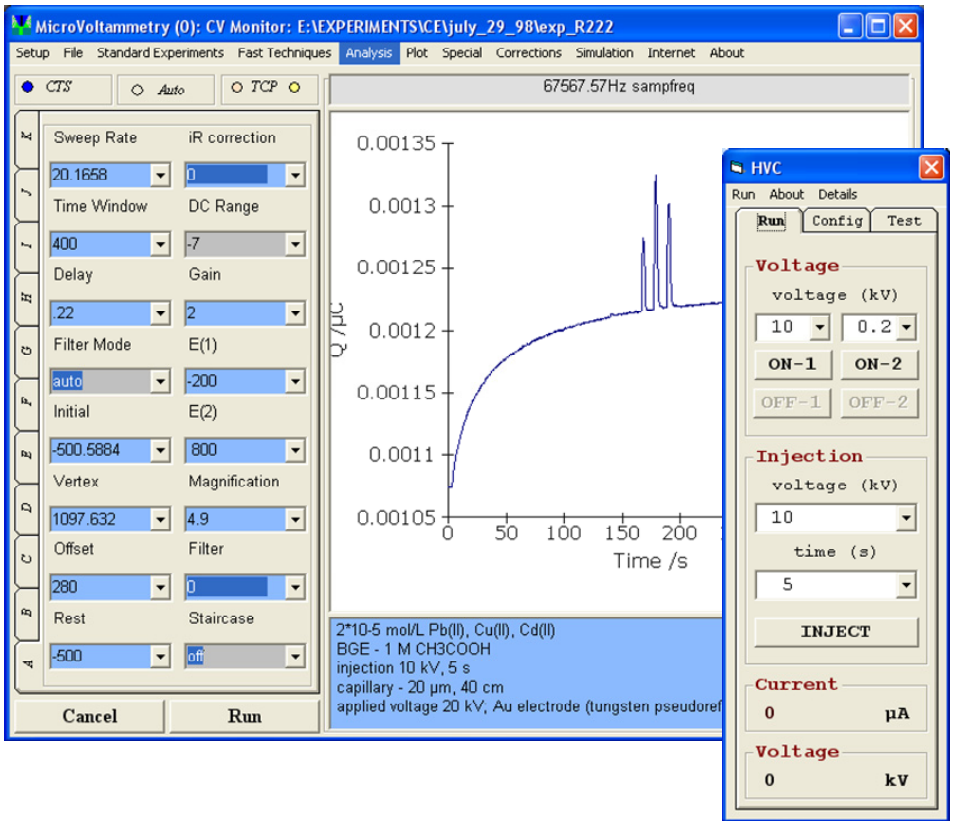

Figure A.3 Screenshot of the MicvoVoltammetry software in CV Monitor mode, used for detection in capillary electrophoresis. The high voltage power control window is included to the right. The offset potential in this case is 280 mV.

REFERENCES

[1] H. L. Needleman, Environmental Research 84:20 (2000).
[2] D. C. Bellinger, Pediatrics 113:1016 (2004).
[3] J. Doull, C. D. Klaassen, M. O. Amdur, and Editors, Casarett and Doull's Toxicology: The Basic Science of Poisons. 2nd Ed, 1980.
[4] T. R. Crompton, Determination of Metals and Anions in Soils, Sediments and Sludges, 2001.
[5] R. N. P. Farrow and G. F. Lewis, Analytical Proceedings 25:157 (1988).
[6] T. S. West, H. W. Nuernberg, and Editors, The Determination of Trace Metals in Natural Waters, 1988.
[7] L. Y. Kheifets and A. E. Vasyukov, Journal of Analytical Chemistry (Translation of Zhurnal Analiticheskoi Khimii) 51:432 (1996).
[8] R. Zhu, S. M. Macfie, and Z. Ding, Journal of Experimental Botany 56:2831 (2005).
[9] W. Lu and R. M. Cassidy, Analytical Chemistry 65:1649 (1993).
[10] J. Wen, A. Baranski, and R. Cassidy, Analytical Chemistry 70:2504 (1998).
[11] J. Heinze, Angewandte Chemie 105:1327 (1993).
[12] R. M. Wightman and D. O. Wipf, Accounts of Chemical Research 23:64 (1990).
[13] D. O. Wipf and R. M. Wightman, Analytical Chemistry 60:2460 (1988).
[14] A. S. Baranski, Journal of Electroanalytical Chemistry and Interfacial Electrochemistry 307:287 (1991).
[15] J. Wang, Stripping Analysis: Principles, Instrumentation, and Applications, 1985.
[16] M. Esteban and E. Casassas, TrAC, Trends in Analytical Chemistry 13:110 (1994).
[17] E. Kirowa-Eisner, Y. Bonfil, D. Tzur, and E. Gileadi, Journal of Electroanalytical Chemistry 552:171 (2003).
[18] A. S. Baranski and H. Quon, Analytical Chemistry 58:407 (1986).
[19] G. Herzog and D. W. M. Arrigan, TrAC, Trends in Analytical Chemistry 24:208 (2005).
[20] Y. Bonfil, M. Brand, and E. Kirowa-Eisner, Analytica Chimica Acta 387:85 (1999).
[21] Y. Bonfil, M. Brand, and E. Kirowa-Eisner, Analytica Chimica Acta 424:65 (2000).
[22] Y. Bonfil and E. Kirowa-Eisner, Analytica Chimica Acta 457:285 (2002).
[23] Y. Bonfil, M. Brand, and E. Kirowa-Eisner, Analytica Chimica Acta 464:99 (2002).
[24] M. Brand, I. Eshkenazi, and E. Kirowa-Eisner, Analytical Chemistry 69:4660 (1997).
[25] Y. Bonfil, M. Brand, and E. Kirowa-Eisner, Electroanalysis 15:1369 (2003).
[26] P. Salauen and C. M. G. van den Berg, Analytical Chemistry 78:5052 (2006).
[27] B. Krasnodebska-Ostrega and J. Piekarska, Electroanalysis 17:815 (2005).
[28] V. Beni, V. I. Ogurtsov, N. V. Bakunin, D. W. M. Arrigan, and M. Hill, Analytica Chimica Acta 552:190 (2005).
[29] G. Herzog and D. W. M. Arrigan, Analytical Chemistry 75:319 (2003).
[30] J. Wang and H. D. Dewald, Analytical Chemistry 56:156 (1984).
[31] G. A. East and E. P. Marinho, Biological Trace Element Research 103:261 (2005).
[32] B. Krasnodebska-Ostrega, E. Stryjewska, and J. Golimowski, Chemia Analityczna (Warsaw, Poland) 50:807 (2005).
[33] J. Xia, W. Wei, Y. Hu, H. Tao, and L. Wu, Analytical Sciences 20:1037 (2004).

[34] Y. Bonfil, M. Brand, and E. Kirowa-Eisner, Reviews in Analytical Chemistry 19:201 (2000).
[35] A. Aramata, Modern Aspects of Electrochemistry 31:181 (1997).
[36] M. R. Deakin and O. Melroy, Journal of Electroanalytical Chemistry and Interfacial Electrochemistry 239:321 (1988).
[37] G. Salie and K. Bartels, Electrochimica Acta 39:1057 (1994).
[38] Z. Shi and J. Lipkowski, Journal of Physical Chemistry 99:4170 (1995).
[39] X. H. Xia, L. Nagle, R. Schuster, O. M. Magnussen, and R. J. Behm, Physical Chemistry Chemical Physics 2:4387 (2000).
[40] M. H. Hoelzle, U. Retter, and D. M. Kolb, Journal of Electroanalytical Chemistry 371:101 (1994).
[41] H. M. Widmer, Chimia 43:134 (1989).
[42] J. W. Jorgenson and K. D. Lukacs, Analytical Chemistry 53:1298 (1981).
[43] A. G. Ewing, R. A. Wallingford, and T. M. Olefirowicz, Analytical Chemistry 61:292A (1989).
[44] H. J. Issaq, Journal of Liquid Chromatography & Related Technologies 25:1153 (2002).
[45] H. J. Issaq, Electrophoresis 21:1921 (2000).
[46] R. A. Wallingford and A. G. Ewing, Analytical Chemistry 60:1972 (1988).
[47] P. D. Grossman, Capillary Electrophor.:3 (1992).
[48] S. C. Beale, Analytical Chemistry 70:279R (1998).
[49] G. W. Castellan, Physical Chemistry – 3rd Edition, 1983.
[50] M. Urbanek, L. Krivankova, and P. Bocek, Electrophoresis 24:466 (2003).
[51] W. R. Vandaveer, S. A. Pasas, R. S. Martin, and S. M. Lunte, Electrophoresis 23:3667 (2002).
[52] R. S. Keynton, T. J. Roussel, M. M. Crain, D. J. Jackson, D. B. Franco, J. F. Naber, K. M. Walsh, and R. P. Baldwin, Analytica Chimica Acta 507:95 (2004).
[53] J. L. Beckers and P. Bocek, Electrophoresis 21:2747 (2000).
[54] R.-L. Chien, Electrophoresis 24:486 (2003).
[55] J. Tanyanyiwa, S. Leuthardt, and C. Hauser Peter, Electrophoresis 23:3659 (2002).
[56] K. Swinney and D. J. Bornhop, Electrophoresis 21:1239 (2000).
[57] F.-M. Matysik, Electroanalysis 12:1349 (2000).
[58] B. Huang, L. Zhang, J.-J. Li, and J.-K. Cheng, Analytical Chemistry 68:2366 (1996).
[59] C. A. Monnig and R. T. Kennedy, Analytical Chemistry 66:280R (1994).
[60] R. A. Wallingford and A. G. Ewing, Analytical Chemistry 59:1762 (1987).
[61] L. A. Holland and A. M. Leigh, Electrophoresis 23:3649 (2002).
[62] G. C. Gerhardt, R. M. Cassidy, and A. S. Baranski, Analytical Chemistry 70:2167 (1998).
[63] G. C. Gerhardt, R. M. Cassidy, and A. S. Baranski, Analytical Chemistry 72:908 (2000).
[64] K. Uchiyama, H. Nakajima, and T. Hobo, Analytical and Bioanalytical Chemistry 379:375 (2004).
[65] A. T. Woolley, K. Lao, A. N. Glazer, and R. A. Mathies, Analytical Chemistry 70:684 (1998).
[66] W. Lu, R. M. Cassidy, and A. S. Baranski, Journal of Chromatography 640:433 (1993).
[67] M. Zhong and S. M. Lunte, Analytical Chemistry 68:2488 (1996).
[68] M.-C. Chen and H.-J. Huang, Analytical Chemistry 67:4010 (1995).
[69] A. M. Fermier, M. L. Gostkowski, and L. A. Colon, Analytical Chemistry 68:1661 (1996).
[70] P. D. Voegel, W. Zhou, and R. P. Baldwin, Analytical Chemistry 69:951 (1997).
[71] S. Sloss and A. G. Ewing, Analytical Chemistry 65:577 (1993).
[72] J. Ye and R. P. Baldwin, Analytical Chemistry 65:3525 (1993).
[73] S. Park, S. M. Lunte, and C. E. Lunte, Analytical Chemistry 67:911 (1995).
[74] S. Park and C. E. Lunte, Analytical Chemistry 67:4366 (1995).

[75] X. Huang, R. N. Zare, S. Sloss, and A. G. Ewing, Analytical Chemistry 63:189 (1991).
[76] W. Lu and R. M. Cassidy, Analytical Chemistry 66:200 (1994).
[77] T. J. O'Shea, R. D. Greenhagen, S. M. Lunte, C. E. Lunte, M. R. Smyth, D. M. Radzik, and N. Watanabe, Journal of Chromatography 593:305 (1992).
[78] A. S. Baranski and P. Norouzi, Canadian Journal of Chemistry 75:1736 (1997).
[79] A. J. Bard and L. R. Faulkner, Electrochemical Methods: Fundamentals and Applications, 1982.
[80] A. S. Baranski and A. Moyana, Langmuir 12:3295 (1996).
[81] D. S. Austin, J. A. Polta, T. Z. Polta, A. P. C. Tang, T. D. Cabelka, and D. C. Johnson, Journal of Electroanalytical Chemistry and Interfacial Electrochemistry 168:227 (1984).
[82] C. E. Banks, J. Kruusma, R. R. Moore, P. Tomcik, J. Peters, J. Davis, S. Komorsky-Lovric, and R. G. Compton, Talanta 65:423 (2005).
[83] Z. Shi, S. Wu, and J. Lipkowski, Electrochimica Acta 40:9 (1995).
[84] H. D. Abruna, J. M. Feliu, J. D. Brock, L. J. Buller, E. Herrero, J. Li, R. Gomez, and A. Finnefrock, Electrochimica Acta 43:2899 (1998).
[85] D. K. Watts, N. Kimura, and M. Tsujimura, New Trends in Electrochemical Technology 3:437 (2005).
[86] A. Hamnett, C. H. Hamann, and W. Vielstich, Electrochemistry, 1997.
[87] J. E. Sandoval and S.-M. Chen, Analytical Chemistry 68:2771 (1996).
[88] S. V. Ermakov, L. Capelli, and P. G. Righetti, Journal of Chromatography, A 744:55 (1996).
[89] B. Karlberg and P. Kuban, Journal of Flow Injection Analysis 17:5 (2000).
[90] P. Kuban and B. Karlberg, Analytica Chimica Acta 404:19 (2000).
[91] P. Kuban, R. Pirmohammadi, and B. Karlberg, Analytica Chimica Acta 378:55 (1999).
[92] P. Kuban and B. Karlberg, Trends in Analytical Chemistry 17:34 (1998).
[93] Z. K. Shihabi, Journal of Chromatography, A 902:107 (2000).
[94] P. Kuban, M. Berg, C. Garcia, and B. Karlberg, Journal of Chromatography, A 912:163 (2001).
[95] V. Komanicky and W. R. Fawcett, Angewandte Chemie, International Edition 40:563 (2001).
[96] V. Komanicky and W. R. Fawcett, Electrochimica Acta 49:1185 (2004).
[97] P. M. Diakowski and A. S. Baranski, Electrochimica Acta 52:854 (2006).
[98] A. S. Baranski and P. M. Diakowski, Journal of Solid State Electrochemistry 8:683 (2004).
[99] N. A. Polson and M. A. Hayes, Analytical Chemistry 73:312A (2001).
[100] K. B. Mogensen, H. Klank, and J. P. Kutter, Electrophoresis 25:3498 (2004).
[101] J. Evenhuis Christopher, M. Guijt Rosanne, M. Macka, and P. R. Haddad, Electrophoresis 25:3602 (2004).
[102] D. Erickson and D. Li, Analytica Chimica Acta 507:11 (2004).
[103] W. R. Vandaveer, S. A. Pasas, R. S. Martin, and S. M. Lunte, Electrophoresis 23:3667 (2002).